The Role of the Cellular Membrane Environment in Mediating Fibrillization and Toxicity of Islet Amyloid Polypeptide

Helder Carmen

Brasenose College

University of Oxford

A thesis submitted for the degree of

Doctor of Philosophy

Trinity 2016

This thesis is dedicated to
Aileen

Acknowledgements

I would firstly like to thank Prof. David Vaux for the opportunity to be part of his group - it has been a very stimulating and enjoyable experience. I would also like to thank all of the members of the Vaux group, past and present, for their support during the last four years. I would like to thank Letty, Chongsoo, Marek, Sameer, Ivan, Alex and Daina for their continued support during my research and for making the lab a fun place to be during the challenges of research. I would like to thank Niall Moon for synthesizing the probe used for experiments described in the thesis. I would like to thank my Mum, Dad and sister for supporting me not only during my years in Oxford but also during my education up to this point, without which I might never have contemplated undertaking a DPhil. Finally I would like to thank my wonderful wife for being so amazing and supportive throughout. Without her I'm sure I would not have been able to complete the work and write up of this thesis.

Abstract

Islet amyloid polypeptide (IAPP) is a peptide that is produced by the beta cells in the pancreas. A misfolded, aggregated form of this peptide is associated with Type 2 Diabetes and is found as large fibrils in pancreata, intimately associated with the islet architecture. The role of these fibrils is though to be benign in terms of membrane damage. However, smaller oligomers that assemble en-route to becoming fibrils are thought to be toxic to cells. In addition, the assembly of the peptide into amyloid is known to be accelerated by lipid and the assembly process itself has been shown to cause damage to cell and artificial lipid membranes. The environment in which Islet amyloid polypeptide is produced is in secretory granules that are highly regulated, and various environmental factors have been shown to affect assembly of IAPP into fibrils. The work presented in this thesis looks at two important factors from these granules, zinc and pH, and their effect on the interaction of this peptide with the membrane. Using lipid membrane mimetics, I have shown a novel function of membrane fusion for human IAPP and in addition show that this function can be modulated by zinc. I have also investigated the consequences for membrane at the molecular scale using environment-sensitive fluorophores that report on lipid order and viscosity. Finally, I show that depending on the lipid composition and the pH, hIAPP and rIAPP can increase the order of lipid membranes.

Name: Helder Carmen

Department: Sir William Dunn School of Pathology

College: Brasenose College

word count: 40,000

Contents

List of Figures

List of Tables

Abbreviations

BMI body mass index

CCP cell crossing peptide

CGRP calcitonin gene-related peptide

Cont control

CPE Carboxypeptidase E

CD circular dichroism

dH_2O distilled water

DiI 1,1-dioctadecyl-3,3,3,3-tetramethylindocarbocyanine

DiO 3,3'-Dioctadecyloxacarbocyanine perchlorate

D.I.T data integration time

DMEM Dulbecco's Modified Eagle's Medium

DMSO dimethyl sulfoxide

DPA diplonic acid

DPH 1,6-Diphenyl-1,3,5-hexatriene

DPPC 1,2-dipalmitoyl-sn-glycero-3-phosphocholine

DPPS 1,2-Dipalmitoyl-sn-glycero-3-phosphoserine

DLS dynamic light scattering

EM electron microscopy

FIFO first in first out

F:L Fluorophore:Lipid

FTLA finite track length adjustment

FRET Förster resonance energy transfer

GPMV giant plasma membrane vesicle

GUV giant unilamellar vesicle

H_2O_2 hydrogen peroxide

HEPES (4-(2-hydroxyethyl)-1-piperazineethanesulfonic acid

HFIP Hexafluoro-2-propanol

hIAPP human islet amyloid polypeptide

HPLC high pressure liquid chromatography

Hz Hertz

IAPP islet amyloid polypeptide

IFG impaired fasting glucose

IRF instrument response function

ISA International Society of Amyloidosis

laurdan 6-Dodecanoyl-N,N-dimethyl-2-naphthylamine

LUV large unilamellar vesicle

MS mass spectrometry

NaCl sodium chloride

NC nitrocellulose

NTA Nanoparticle Tracking Analysis

NMR nuclear magnetic resonance

PAM peptidylglycine monooxygenase

PC1/3 prohormone convertase 1/3

PC2 prohormone convertase 2

PC3 prohormone convertase 3

PC 2-Oleoyl-1-palmitoyl-sn-glycero-3-phosphocholine

PE Phosphatidylethanolamine

PC 2-Oleoyl-1-palmitoyl-sn-glycero-3-phosphocholine

PS 1-palmitoyl-2-oleoyl-sn-glycero-3-phospho-L-serine

PSD particle size distribution

r18 octadecyl rhodamine B chloride

rpm revolutions per minute

SEM standard error of the mean

$\boldsymbol{t_{\frac{1}{2}}}$ Time till half maximal intensity

T2D type 2 diabetes

Tb terbium

TbCl3 terbium chloride

TCSPC Time-correlated single-photon counting

TEM transmission electron microscopy

TFA trifluoroacetic acid

ThT Thioflavin T

TICT twisted intramolecular charge transfer

TMA-DPH N,N,N-Trimethyl-4-(6-phenyl-1,3,5-hexatrien-1-yl)phenylammonium p-toluenesulfonate

Trp tryptophan

UV ultraviolet

$ZnCl_2$ zinc chloride

Chapter 1

Introduction

1.1 IAPP as an amyloid peptide

1.1.1 Amyloid proteins

The presence of amyloid at post-mortem examinations has been described since the 17th century, with deposits, and associated changes to organs, noted via macroscopic and microscopic observation (Sipe and Cohen, 2000; Schier, 2010). In 1854 Rudolph Virchow conducted biochemical experiments and concluded that the substance was comprised of cellulose and coined the term amyloid, derived from the Latin amylum and the Greek amylon (reviewed by Cohen (1986)). A subsequent discourse regarding the nature of deposits took place with the research community unsure as to whether the main component of deposits consisted of starch, cellulose or protein. However, in 1859 Friedreich and Kekule (Cohen, 1986) demonstrated both the presence of protein, based on the high nitrogen content, and the apparent absence of carbohydrate in a mass of amyloid and attention was shifted to the study of amyloid first as a protein and later as a class of proteins, with a propensity to undergo changes in conformation that result in fibril formation (Sipe and Cohen, 2000).

Since the first description of amyloid, various systems have been employed for the classification of the deposits and their related syndromes and involved tissues. Based on the location of macroscopic abnormalities found in organs and tissues of patients and associated clinical syndromes, the amyloidoses were initially classified as primary, secondary or hereditary (Sipe and Cohen, 2000). Following the

realisation of the chemical diversity of amyloid and amyloidosis in mid-70s, it was suggested that classification should be based on chemical composition. The Nomenclature Committee of the International Society of Amyloidosis (ISA) met in 2014 and made recommendations for the nomenclature of amyloid fibril proteins and the clinical classification of the amyloidoses (Sipe et al., 2014). A sample of amyloid proteins that are part of this classification are reproduced in table 1.1. Of the listed diseases and associated amyloid proteins, perhaps the most familiar to general audiences is Alzheimer's disease and associated Aβ protein, with its devastating consequences first described in the early 20th century by Alois Alzheimer and the neurohistopathology currently under heavy investigation (Scheltens et al., 2016). Less famous is islet amyloid polypeptide (IAPP), which is found as part of amyloid plaques in the pancreata of type 2 diabetes (T2D) sufferers, and is discussed in the next section.

Fibril protein	**Precursor protein**	**Systemic and/or localised**	**Acquired or hereditary**	**Target organs**
AL	Immunoglobulin Light Chain	S, L	A, H	All organs except CNS
AH	Immunoglobulin Heavy Chain	S, L	A	All organs except CNS
AA	(Apo) Serum Amyloid A	S	A	All organs except CNS
ATTR	Transthyretin, wild type	S	A	Heart mainly in males, Ligaments, Tenosynovium
	Transthyretin, variants	S	H	PNS, ANS, heart, eye, leptomen
Aβ2M	β2-Microglobulin, wild type	L	A	Musculoskeletal System
	β2-Microglobulin, variant	S	H	ANS
AApoAI	Apolipoprotein A I, variants	S	H	Heart, liver, kidney, PNS, testis, larynx (C terminal variants), skin (C terminal variants)
AApoAII	Apolipoprotein A II, variants	S	H	Kidney
AApoAIV	Apolipoprotein A IV, wild type	S	A	Kidney medulla and systemic
Aβ	Aβ protein precursor, wild type	L	A	CNS
	Aβ protein precursor, variant	L	H	CNS
APrP	Prion protein, wild type	L	A	CJD, Fatal insomnia
	Prion protein variants	L	H	CJD, GSS syndrome, Fatal insomnia
ACal	(Pro)calcitonin	L	A	C-cell thyroid tumors
AIAPP	Islet Amyloid Polypeptide	L	A	Islets of Langerhans, Insulinomas
AANF	Atrial Natriuretic Factor	L	A	Cardiac atria
APro	Prolactin	L	A	Pituitary prolactinomas, aging pituitary

Table 1.1. A Selection of Amyloid proteins and associated proteins. The first letter A of each fibril protein name stands for Amyloid and its designation is intended to distinguish protein in this form from monomeric protein. Adapted from Sipe et al. (2014).

1.1.2 Brief history of IAPP as an amyloid

The first description of what is now known as IAPP was the result of gross analyses of pancreata from patients who had type 2 diabetes (T2D). The material found in the islets was first described as hyaline in nature due to its glassy appearance (Opie, 1901). It was not until much later that these deposits started to be described as amyloid due to use of histological stains previously used to identify amyloid in other diseases (Ahronheim, 1943). electron microscopy (EM) enabled clear visualisation of fibrillar structures protruding into cells of the islets of Langerhans (Westermark, 1973) (fig. 1.1).

However it wasn't until the 1980's that the main constituent of these amyloid deposits was ascribed to the 37 amino acid peptide IAPP, with a C-terminal amidated peptide found to be the major peptide in the plaque (Cooper et al., 1987; Westermark et al., 1987a). In addition it was confirmed, by a variety of methods and groups, that the peptide was a product of β-cells in the islets of the pancreas (Westermark et al., 1987a,b; Johnson et al., 1988; Lukinius et al., 1989; Westermark et al., 1993).

Work is ongoing in an attempt to establish the general rules governing assembly of the various soluble amyloid peptides into plaques, as well as the molecular details of assembly of intermediates. Amyloid peptides generally share the same kinetic pathway to plaque formation but establishing general rules for this process is complicated (fig. 1.2). Indeed, the complex landscape of structural dynamics and kinetics has made it difficult to identify exactly how amyloid contributes to pathology like that shown in figure 1.1. In fact in previous years the question of whether amyloid plaques serve a protective role has been considered (Lee et al., 2004; Castellani et al., 2009). However, the general position has become that the fibrils that bundle together to form plaques are themselves not the most toxic form of amyloid proteins but that the active assembly of intermediates to fibrils, and the intermediates themselves, are likely to be the main players in the pathology of T2D (Williams et al., 2011; Sokolov et al., 2006; Kayed et al., 2004; Meier et al., 2006).

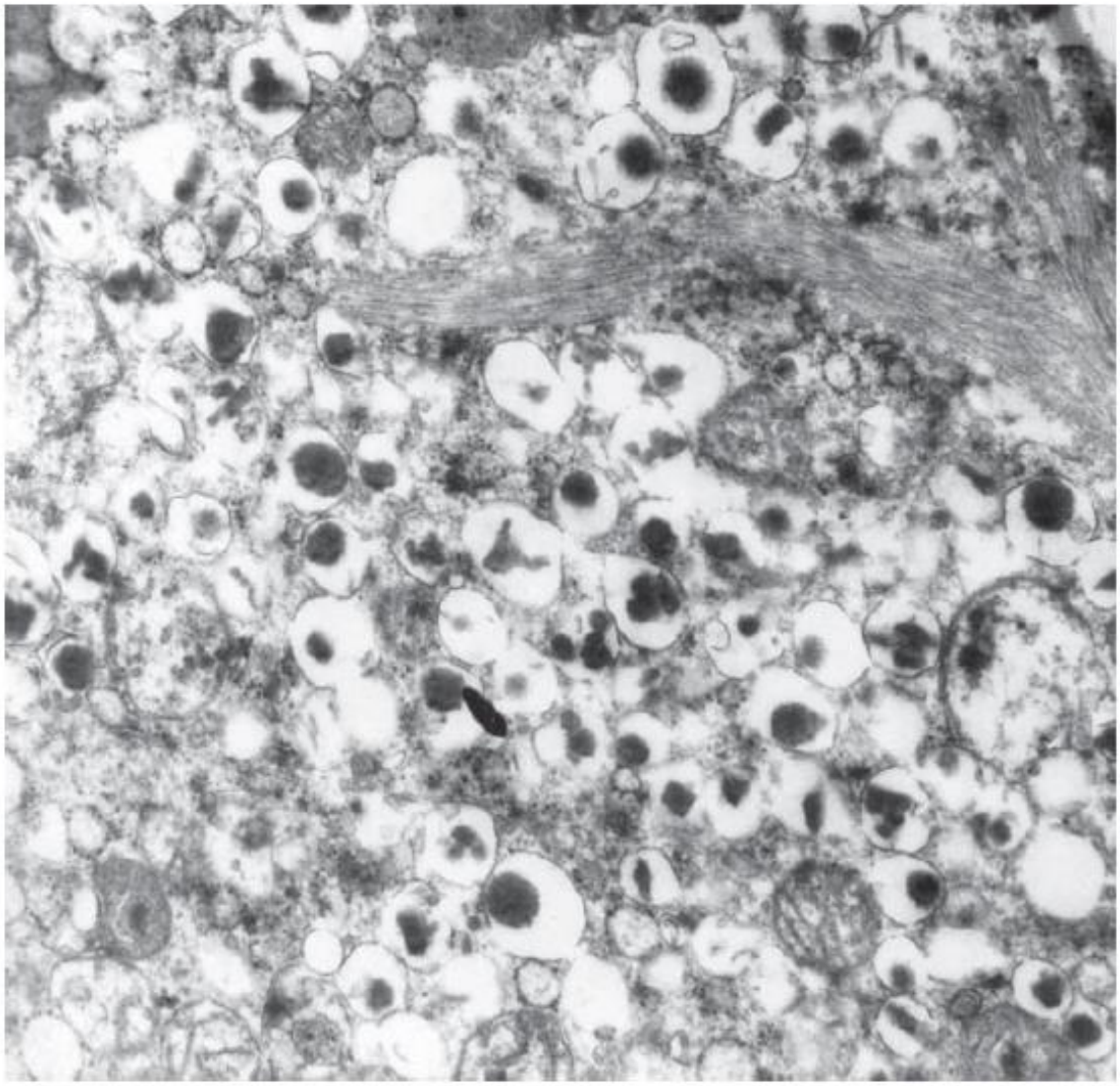

Figure 1.1. IAPP fibrils in a pancreatic islet from a patient who had T2D. Electron micrograph of a field of secretory granules containing electro-dense material with a bundle of fibrils projecting into the field of view (image from Westermark (2011)).

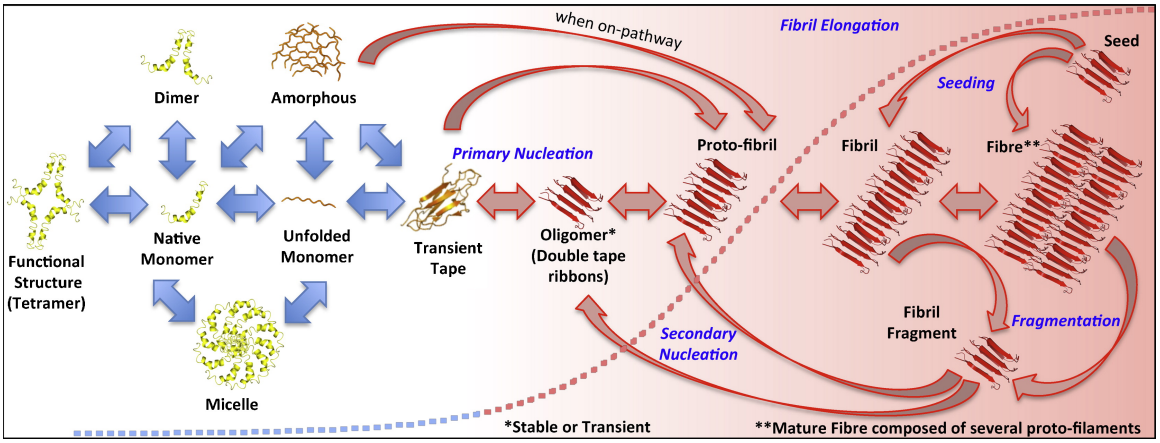

Figure 1.2. Misfolding pathway of amyloid proteins. General pathway for the interconversion of amyloid monomer to fibre (figure from Invernizzi et al. (2012).

1.1.3 IAPP fibrillization

1.1.3.1 Important regions for fibrillization

IAPP belongs to the calcitonin related peptide family which is comprised of adrenomedullin, α-and β-calcitonin gene-related peptide (CGRP), intermedin, and calcitonin (Muff et al., 1995). IAPP is most similar to CRGP, sharing reasonable sequence homology, however they diverge the most within the peptide segment 20-29. hIAPP is very amyloidogenic whereas CRGP is not, prompting the initial hypothesis that the region 20-29 dictates amyloid formation of IAPP. Comparison of the amino acid sequences of IAPP among different animal species, combined with in vitro experimentation with synthetic IAPP has led to the identification of an "amyloidgenic" region essential for formation of fibrils (Betsholtz et al., 1989; Ashburn and Lansbury, 1993; Westermark et al., 1990). In addition single proline substitutions within the 2029 segment have been shown to significantly reduce the amyloidogenicity of hIAPP (Green et al., 2003). Notably mice and rats to not develop diabetes or plaques naturally and human and rat IAPP differ by only six amino acids, five of which occur in the 20-29 region (fig. 1.3). Interestingly, although IAPP from dogs can form amyloid, it is not associated with T2D but the presence of insulonmas, indicating that at least in this case increased expression of IAPP is important to form amyloid (Johnson et al., 1991).

Other fragments have also been shown to form amyloid: 3037, 820, and 1019 (Nilsson and Raleigh, 1999; Scrocchi et al., 2003; Gilead and Gazit, 2008). In particular the maximal binding of full length hIAPP was found to be to a 11-20 region of hIAAPP (with the sequence RLANFLVHSS) which led to the suggestion that contacts within this region were important for initial hIAPP-hIAPP contacts during fibrillization (Mazor et al., 2002). In support of this, the use of an IAPP-MBP construct revealed pairs of hIAPP peptides made contact in this region (Wiltzius et al., 2009). The 20-29 region is not the only determinant of whether hIAPP fibrillizes. Amyloid formation is abolished by multiple proline substitutions outside of this region (Abedini and

Raleigh, 2006) as well as by replacement of Asn-14 and Asn-21 (Koo et al., 2008). Clearly the potential to form amyloid is not just due to the 20-29 region.

	1 11 21 31	Forms Amyloid
Human	KCNTATCATQ RLANFLVHSS NNFGAILSST NVGSNT	Yes
Rat	·····R·· ··L·PV·PP· ·····	No
Mouse	·····R·· ··L·PV·PP· ·····	No
Cat	·····IR· ··L····P· ·····	Yes
Monkey	·····R·· ····T···· ·····	Yes
Dog	·····RT· ··L····P· ·····	Yes*

Figure 1.3. Capacity of IAPP from different species to form amyloid. The red dashed rectangle represents the region that is believed to be important for amyloid formation. Red letters represent amino acids that form part of amyloid forming IAPP. The asterix for dog IAPP is due to its ability to form IAPP but its lack of association with T2D (adapted from Jeong and An (2015)).

1.1.3.2 Structure of fibrils and on-pathway intermediates

Since IAPP readily forms amyloid fibrils it is not possible for it to be crystallized. Thus it has not been possible to gain high resolution X-ray crystallographic data of IAPP in its native mature form. Use of IAPP-MBP constructs revealed that hIAPP could adopt α-helical structure at residues 8-18 and 22-27 and that IAPP could dimerize (Wiltzius et al., 2009). In addition several other in vitro studies have provided evidence for the population of α helical intermediates during the formation of amyloid in solution (Williamson and Miranker, 2007)(Williamson et al., 2009)(Abedini and Raleigh, 2009)(Wiltzius et al., 2009).

However information for models of IAPP fibril structure has come from solid state nuclear magnetic resonance (NMR) spectroscopy of hIAPP as well X-ray diffraction experiments using microcrystals formed of small peptide fragments of hIAPP. In general, the resulting models describe a fibril composed of two related columns of IAPP monomers (Wiltzius et al., 2008; Luca et al., 2007) with each column containing two in register parallel β-sheets. The N-terminal strand encompasses residues 8 to 17 and the C-terminal strand residues 28 to 37 (Luca et al., 2007). Two structures have been proposed from the NMR data which differ in terms of the register of the side chains. In one structure Arg-11, Ala-13, and Phe-15 are all solvent exposed but in the other they are buried in the core of the fibril. Burial of an Arg-11 is energetically

unfavourable making a fibril structure with it exposed the more likely case (Akter et al., 2016). Interestingly most of the 20-29 segment is not part of the ordered β-sheet structure in the NMR structural models but instead forms a loop linking the two β-strands (Akter et al., 2016) initially making it unclear why mutations in this area would have a dramatic impact on amyloid formation. However, a transient "non-native" intermediate was found that has parallel β-sheet structure localized in residues 2327 (Buchanan et al., 2013) which must be disrupted in order for the loop in region 20-29 to be formed supporting the NMR based model. However, head-to-tail dimerization of hIAPP has been proposed as another on pathway conformation where His18 makes critical contact with Tyr37 (Tu et al., 2014; Vaiana et al., 2009).

The only known natural mutation found in mature human IAPP is a S20G mis-sense mutation, found with a small frequency in Chinese and Japanese populations (Lee et al., 2001; Sakagashira, S. Sanke, T. Hanabusa, T. Shimomura, 2013). The mutation appears to be associated with increased risk of early onset type 2 diabetes (Morita et al., 2011). Early experiments showed IAPP(S20G) to undergo faster fibrillization and to be more toxic to cells (Sakagashira et al., 2000). Accelerated fibrillization of this mutant has also been shown more recently by Cao et al. (2012).

Artificial mutations have been used to explore how fibrillization is affected (fig. 1.4). F15L mutation generated from a single-point mutation, which altered the α-helix and β-sheet propensities of the protein, resulted in formation of amyloid that was almost twice as rapid for the F15L mutant as for the wild type. The rate of fibrillization of the Y37L and F23L mutants were almost 2-fold slower and almost 3-fold slower, respectively. (Tu and Raleigh, 2013). In support of this, in silico experiments showed that the Y37L mutant resulted in greater flexibility of the C-terminus, with loss of the steric zipper interactions, and that the F23L mutation showed slower amyloid formation (Bernhardt et al., 2013).

Although use of mutant IAPP has shed light on important regions for fibrillization, it has been noted that care must be taken when comparing different mutational studies as a range of conditions have been used and the rate of amyloid formation of IAPP

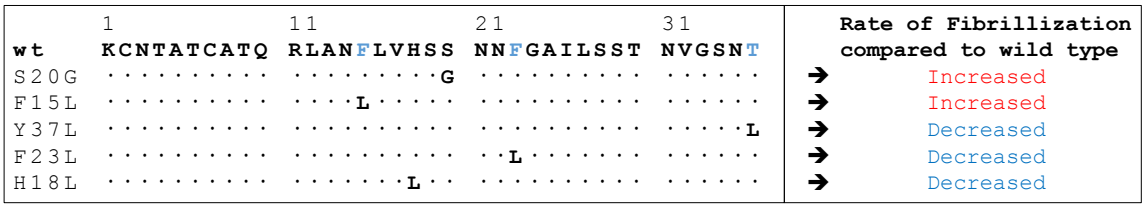

Figure 1.4. Effect of mutations on the rate of fibrillization of IAPP. Mutants of hIAPP and there propensity to form amyloid (adapted from Jeong and An (2015)).

is sensitive to slight changes in buffer composition, including salt, pH, as well as even the degree of agitation and volume of sample (Akter et al., 2016).

Before introducing specific aspects regarding hIAPP and its toxicity as an amyloid peptide, it is pertinent to talk about how it is processed and secreted for the following reasons. Firstly, intermediates along the synthesis pathway have been investigated for their ability to form amyloid and cause toxicity, and secondly, the environment in which IAPP processing takes place is highly regulated, making it a reasonable hypothesis that disruption to this environment where IAPP is processed and stored may contribute to formation of amyloid and cellular toxicity.

1.2 IAPP: synthesis and granule environment

1.2.1 Synthesis and processing

The details of the cellular processing of IAPP have been elucidated primarily by Marzban et al. (2005a). IAPP is synthesised as an 89 amino acid pre-prohormone and undergoes several cleavage events before being expressed in its mature form as a 37 amino acid peptide with an amidated C-terminal tyrosine residue. The N-terminal 22 amino acids constituent the signal peptide enabling the peptide to reach the Golgi apparatus, and once there it is subsequently cleaved leaving the 67 amino acid pro-IAPP. Between leaving the Golgi apparatus and entering the immature secretory granule three cleavage events take place. First, prohormone convertase 1/3 (PC1/3) produces an N-terminal proIAPP intermediate (Marzban et al., 2004). The second main cleavage event is by prohormone convertase 2 (PC2) and is believed to happen in the mature secretory granule (Wang et al., 2001).

Contemporaneously, Carboxypeptidase E (CPE) removes the C-terminal lysine and arginine amino acids (Marzban et al., 2005a) enabling peptidylglycine monooxygenase (PAM) to remove the remaining glycine and amidate the C-terminus, resulting in the mature peptide. In addition an intramolecular bridge is formed between cysteine 2 and 7. This process is summarised graphically in figure 1.5.

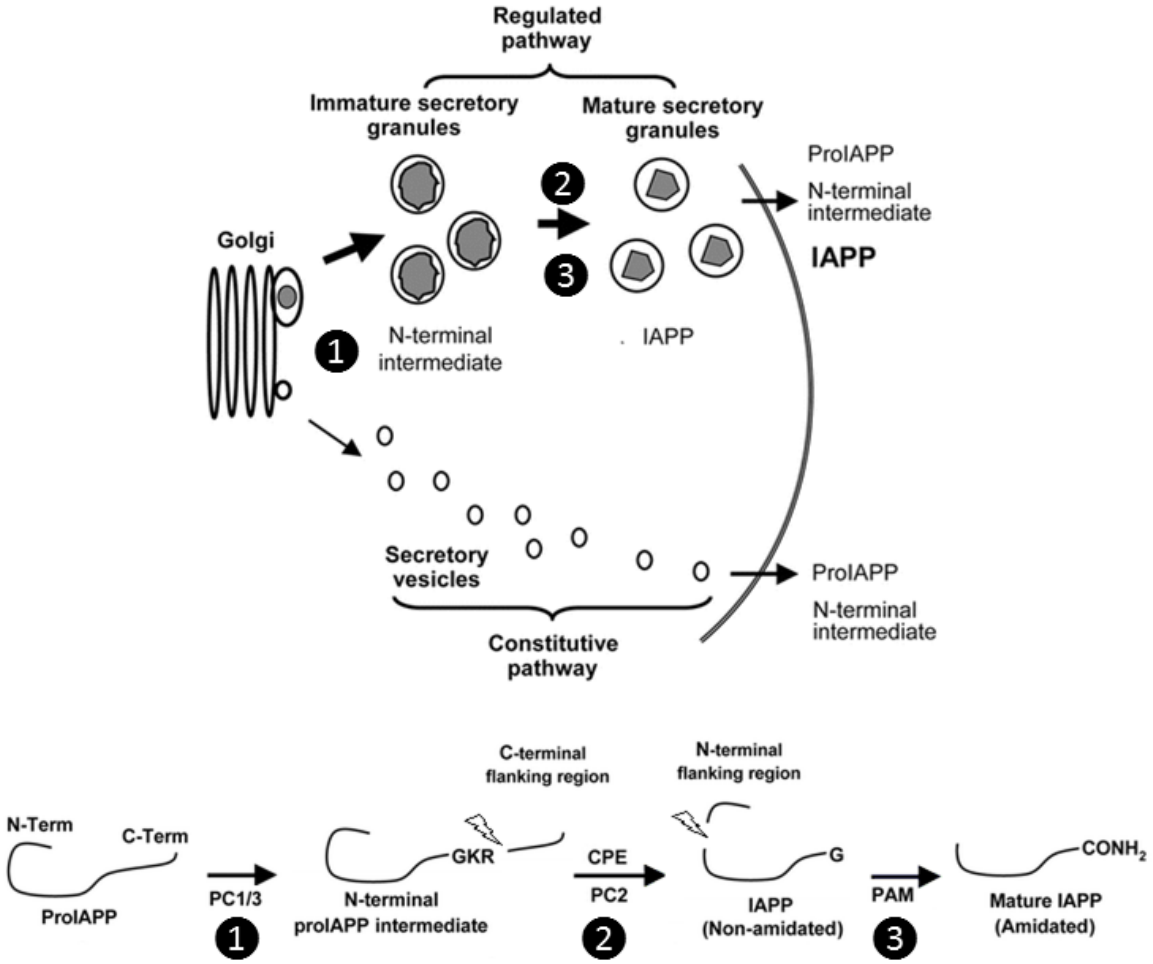

Figure 1.5. Enzymatic processing pathway of IAPP. The white embossed numbers relate to the locations of processing reactions. Lighting bolts indicate where cleavage has occurred (modified from Marzban et al. (2005a, 2004)).

Processing of IAPP in the secretory pathway takes place alongside insulin processing, with PC1/3 and PC2 responsible for cleavages that create mature insulin and C-peptide (Kaufmann et al., 1997; Fricker, 2004; Zhu et al., 2002; Furuta et al., 1997). In the regulated pathway, prohormone convertase 3 (PC3) is active at the B chain-C-peptide junction under conditions of neutral pH and low calcium concentration. This

is followed by PC2 activity at the C-peptide-A chain junction under conditions of more acidic pH and higher calcium concentration (Hutton, 1994). This is in line with PC1/3 preceding PC2 cleavage activity on IAPP in the maturing granule (Higham et al., 2000).

1.2.2 Granule environment and IAPP

The basis of cellular production provides clues to factors in the processing environment that might influence amyloid formation. The main role of the secretory granule is to secrete insulin in response to glucose levels. The defining structural feature of a mature secretory granule is the presence of a crystalline core, composed of insulin coordinated with zinc ions as a hexamer (Emdin et al., 1980; Li, 2014) with estimates of zinc concentrations in the low to high millimolar range (GRODSKY and SCHMID-FORMBY, 1985; Hutton, 1983; Foster et al., 1993). In addition to the role of crystallizing insulin, zinc has also been found to effect the in vitro misfolding of IAPP in a complex manner, with low concentrations thought to inhibit, and high concentrations accelerate, fibrillization (Brender et al., 2010). Insulin has also been shown to interact with hIAPP affecting fibrillization (Brender et al., 2011; Larson and Miranker, 2004) and this interaction is dependent on the state of insulin (Nedumpully-Govindan and Ding, 2015). The area around the core, known as the 'halo' region, is thought to be surrounded by an acidic halo containing IAPP, C-peptide and soluble insulin (Michael et al., 1987). It has been found that solubility of insulin is affected by C-peptide (Landreh et al., 2012).

As the secretory granule matures it becomes more acidic, with the pH of the mature granule thought to be about 5.5 pH (Hutton, 1982). This is consistent with the knowledge that the low pH environment inside mature granule favours the binding of Zn^{2+} to insulin, whereas the higher pH of interstitial fluid and blood favours the dissociation of Zn^{2+} from insulin, making it soluble (Robertson, 2011). In addition it has been found that at low pH the fibrllization of IAPP is inhibited and that processing of pro-IAPP generates increasingly amyloidogenic peptides (Yonemoto

et al., 2008). Therefore, reduction in pH may serve to prevent misfolding of hIAPP in the granule.

There is also a high concentration of calcium and magnesium in the insulin secretory granule (Njus et al., 1986) with the concentration of calcium found to be particularly high (173mM). However due to the complexity of the mixture of granule components and their possible interactions, this may not imply high activity of the ion (Reiffen and Gratzl, 1986). Indeed the high concentration of calcium was found not to have a significant effect on fibrillization of hIAPP in solution (Chargé et al., 1995). However, more recently calcium was shown to have an affect on the way IAPP interacts with lipids in vitro (Sciacca et al., 2013).

1.3 The role of hIAPP in T2D

1.3.1 How does T2D manifest and develop

T2D has been characterised as a "heterogeneous, multifactorial, polygenic disease characterized by a defect in insulins secretion (the β-cell secretory defect) and action (insulin resistance)" (Hayden, 2002; Höppener et al., 2000). Risk factors for T2D include a positive family history, ageing, and obesity (Zimmet et al., 2001; Jack et al., 2004; Sladek et al., 2007; Zeggini et al., 2007). It has been shown that insulin resistance precedes the development of hyperglycaemia in subjects that eventually develop T2D subjects with the onset of β-cell dysfunction (Martin et al., 1992; Lillioja et al., 1988). However, it has also been realised that T2D develops in insulin- resistant subjects with the onset of β-cell dysfunction (Kahn, 2003; Porte, 2001; Leahy, 2005; Prentki et al., 2002; Poitout and Robertson, 2002).

The secretory defect is initially caused by dysfunction of the β cells and then reduction in β cell mass due to apoptosis. Initial post-mortem studies of T2D patients suggested β-cell mass was reduced by 25-50% (Clark et al., 1988; Klöppel et al., 1985). In addition, a more recent study matching diabetic patients and control subjects for body mass index (BMI) showed there was a significant reduction in β-cell mass and

a threefold increase in β-cell apoptosis (Butler et al., 2003a). This evidence suggests that the decrease in β-cell mass in T2D is secondary to increased rates of β-cell apoptosis. A model for β-cell failure has been posited such that when there is stress on the β-cells there is a compensatory response (Prentki and Nolan, 2006). For people with robust β-cells, a sustained adaptive response can take place consistent with normal glucose tolerance. However, if β-cells are susceptible, due to genetic and acquired defects, various metabolic stresses can lead to cellular dysfunction and impaired glucose tolerance, and eventually progression to overt T2D.

Several factors are considered to be responsible for loss of β-cell function and mass (Wajchenberg, 2007) including glucotoxicity, lipotoxicity, pro-inflammatory cytokines and leptins are reviewed in more detail by others (Wajchenberg, 2007; Cernea and Dobreanu, 2013) and the possible mechanism by which these factors result in toxicity have also been discussed previously (Popa and Mot, 2013). Since this thesis is concerned with the toxic effect of IAPP, we will focus on its association with T2D and β-cell dysfunction.

1.3.2 Role of IAPP in β-cell dysfunction

1.3.2.1 Loss or gain of function?

Aggregation of IAPP might preclude it from carrying out its function, thus contributing to T2D as a result of 'loss of function'. The physiological function of hIAPP and rIAPP are likely similar, and although experiments with IAPP knockout mice have demonstrated minor changes to physiology (Hay et al., 2015) and even demonstrated improved insulin secretion and glucose tolerance in one mouse model (Gebre-Medhin et al., 1998), generally loss of function is not hypothesized to be the major contributing factor to the pathology of T2D. Therefore, as with most diseases associated with an amyloid peptide, the pathological significance of hIAPP in relation to diabetes has been understood through a gain of function, as opposed to a loss of function, mechanism.

1.3.2.2 The role of IAPP processing intermediates

A variety of animal and cell studies have shown that expression of hIAPP has a substantial toxic effect. One avenue that has been explored is the failure of processing enzymes along the synthesis pathway resulting in higher levels of pro-IAPP and intermediates that may act to seed fibrillization of mature hIAPP and cause cell toxicity (Marzban et al., 2005b; Paulsson and Westermark, 2005; Westermark, 2011; Westermark et al., 2011). However, this type of seeding would have to be a rare event since if the majority of amyloid found in plaques is mature IAPP, the process that results in IAPP maturation would need to be largely intact. In addition, synthetic pro-IAPP was found to be less amyloidogenic in the presence of lipid membranes (Khemtémourian et al., 2009) in contrast to mature hIAPP for which fibrillization is accelerated by the presence of lipid membranes (Tomasello et al., 2015). It was suggested that amyloid deposited in β-cells, formed of IAPP processing intermediates (pro-IAPP and N-terminal IAPP), likely reflected a general defect in protein homoeostatic control known to occur in diabetes, rather than a specific feature of T2D pathology (Yonemoto et al., 2008). Therefore, in seeking a role for misfolded or misfolding hIAPP in cellular toxicity, it is appropriate to consider mature hIAPP as the main pathological agent.

1.3.2.3 Accumulation of IAPP is associated with loss of β cells

Support for a role of IAPP amyloid in the pathophysiology of T2D is evidenced by the spontaneous occurrence of T2D in monkeys and cats (Howard, 1986; O'Brien et al., 1986) which share a high degree of sequence homology in the 11-20 region of IAPP (see section 1.4). Transgenic mice expressing human islet amyloid polypeptide (hIAPP) in β-cells, when obese, spontaneously develop diabetes characterized by islet amyloid and decreased β-cell mass (Soeller et al., 1998). Prospective studies in these mice support the hypothesis that the mechanism of reduction β-cell mass is increased apoptosis (Butler et al., 2003b). In addition, IAPP induces apoptosis in cultured human pancreatic islets (Lin et al., 2005). Because islet amyloidosis in patients with

T2D is associated with a reduced mass of insulin-producing β-cells, it is most likely an important factor in the development of β-cell failure (Höppener et al., 2000). Patients who require insulin treatment have the greatest reduction in islet mass and the most prominent amyloid deposits, indicating that the degree of islet amyloidosis may be related to the severity of the disease (Westermark, 1994). This is supported by the decline in β-cell function that precedes loss of β-cell mass in the hIAPP transgenic rat models of T2D. Using a hIAPP transgenic rat model that develops islet pathology comparable to humans with T2D, it was found that β-cell apoptosis and impaired first-phase insulin secretion precedes the development of impaired fasting glucose (IFG), which coincides with a 50% decrease in β-cell mass and onset of hepatic insulin resistance (Matveyenko and Butler, 2006).

Effect of intra and extracellular IAPP

The toxicity of IAPP originating from both intracellular and extracellular sources has been explored. There are currently two main hypotheses, outlined as follows: 1) that hIAPP forms amyloid intra-cellularly, with the resultant toxicity eventually leading to cell apoptosis and cell death and replacement of β-cells by amyloid plaques; and 2) hIAPP reaches the extracellular space but a change in the extracellular environment results in misfolding of peptide with subsequent formation of amyloid plaques; this disturbs the architecture of the islets resulting in dysfunction and induction of the path to cell death. The validity of the positions outlined above are important in terms of employing a strategy to prevent cellular toxicity. Whether formation of the toxic species is intracellular or extracellular has implications for how formation of such a species might be blocked and toxicity alleviated.

Some early studies using isolated islets from mice expressing hIAPP showed that extracellular fibrils were clearly apparent but that intracellular fibrils made up a small proportion of total fibril mass (MacArthur et al., 1999) and the organelles which contained these fibrils were not easily identifiable. In addition, intracellular fibrils did not occur before extracellular fibrils. They posit that fibrils are formed at the site of β-cell granule release. However there are studies supporting a role for IAPP

conversion to amyloid intracellularly (Gurlo et al., 2010; Hiddinga and Eberhardt, 1999).

Oligomers or fibrils as the major toxic species

Previously there was a general acceptance that the fibrillar form of amylin is the toxic species (Mattson and Goodman, 1995; Mirzabekov et al., 1996; Tomiyama et al., 1997; Kapurniotu et al., 1998; Bai et al., 1999; Hiddinga and Eberhardt, 1999). However, the findings from the Mayo Clinic that only a minority (about 10%) of the cases with IFG had islet amyloid present, while already having a deficit in presumptive β-cell mass of approximately 40%, is consistent with the suggestion that small IAPP oligomers are the cause of β-cell loss, whereas the large extracellular amyloid deposits visible by light microscopy are inert (Butler et al., 2003a). The more recent consensus is that the soluble oligomeric structures exert the toxic effect (Janson et al., 1999; Anguiano et al., 2002; Kayed et al., 2004; Konarkowska et al., 2006; Meier et al., 2006; Ritzel et al., 2007; Aitken et al., 2010). Indeed, inhibition of human IAPP fibril formation does not prevent β-cell death (Meier et al., 2006).

1.3.3 Mechanism of IAPP toxicity

In early experiments it was shown that aurintricarboxylic acid, an endonuclease inhibitor that stops apoptosis, is able to reduce hIAPP-mediated toxicity of islet cells (Lorenzo et al., 1994). This was further supported by the finding that hIAPP increases the expression of c-Jun, a gene involved in the apoptotic pathway, in RINm5F and the human insulinoma cell lines (Zhang et al., 2002). One proposed mechanism of hIAPP mediated toxicity is through the generation of reactive oxygen species such as hydrogen peroxide (H_2O_2) that result in cell death and it has been shown that hIAPP increases the accumulation of H_2O_2 in β-cells (Schubert et al., 1995; Mattson and Goodman, 1995). It was later also shown that high expression of hIAPP could trigger endoplasmic reticulum stress-induced apoptosis as well as accumulation of polyubiquintated proteins (Huang et al., 2007b,a).

More recently, it was found that hIAPP oligomers induced elevated cytosolic levels of Ca^{2+} in the rat insulinoma cell line INS 832/13 that resulted in hyperactivation of the protease calpain-2, leading to apoptosis (Huang et al., 2010). Evidence of the formation of intracellular hIAPP oligomers in the secretory pathway causing toxicity (Gurlo et al., 2010) and hIAPP causing cellular toxicity via mitochondrial dysfunction (Lim et al., 2010) has been reported. hIAPP oligomers have also been found to inhibit cell coupling, induce apoptosis, and impair insulin secretion in isolated human islets (Ritzel et al., 2007). These recently identified mechanisms of toxicity have been postulated to involve a common element- disruption of the lipid membranes (Engel and Walter, 2008). Indeed, it has been demonstrated that misfolded hIAPP localises with a variety of intracellular organelles and hIAPP has been shown to co-localise with the membranes of Golgi apparatus and mitochondria (Gurlo et al., 2010), and ER (Hiddinga and Eberhardt, 1999), lysozymes (Bram et al., 2014) and plasma membranes (Magzoub and Miranker, 2012). Therefore membrane interaction of IAPP in various confirmations may be the interface between different downstream mechanisms of toxicity and in the next section we will consider how IAPP and lipid membrane might interact resulting in cell toxicity.

1.4 The interaction of IAPP with membrane plays a central role in toxicity

It was shown early on in the research that cell membrane was important for mediating the toxicity of hIAPP (Lorenzo et al., 1994). It was also shown that at cytotoxic concentrations, IAPP forms voltage-dependent, relatively non selective, ion-permeable channels in planar phospholipid bilayer membranes, with the presence of negatively charged lipids leading to the presence of a higher number of pores (Mirzabekov et al., 1996). Using synthetic vesicles it was found that formation of a hIAPP amyloid pore is temporally correlated to the formation of early IAPP oligomers, and its disappearance to the appearance of amyloid fibrils (Anguiano et al., 2002). Permeabilization of lipid bilayers is a common conformation-dependent

activity of soluble amyloid oligomers in protein misfolding diseases (Kayed et al. 2004).

From work mostly done using lipid mimetics, such as LUVs and GUVs, it is clear that the presence of negatively charged lipids accelerates fibrillization of hIAPP. One of the first studies showing the effect of phospholipid on IAPP structure was by Knight and Miranker, who showed that lipid membranes catalysed fibrillization of hIAPP and that it was dependent on the charge of lipid present (Knight and Miranker, 2004). They showed that membranes composed of only zwitterionic lipids did not accelerate fibrillization and that it was necessary to include negatively charged lipids. In addition they showed that hIAPP did not bind to membranes composed only of zwitterionic lipids. rIAPP also binds to negatively charged membrane, although more weakly than hIAPP, but without formation of fibrils.

Since these studies, many more have been undertaken to look at the effect of lipids on IAPP structure. hIAPP was shown to undergo membrane-associated, α-helical aggregation with associated leakage of liposome content (Knight et al., 2006). Transient helical states in hIAPP measured in solution were found, a property that appears to be conserved across species (Williamson and Miranker, 2007). A position for fibrillation proceeding through an α-helical intermediate was further consolidated upon by Williamson et al. (2009) whereby they support the idea that catalysis of IAPP fibrillization is due to stabilisation of nucleation competent α-helical oligomers that also exist in solution.

Small to moderate proportions of negatively charged lipids accelerate fibrillization, however large amounts of negatively charged lipids have been shown to over-stabilise hIAPP in α-helical structures ,effectively trapping it in that form. The conversion of monomers to fibrils is affected, for instance, by the use of a high percentage of negatively charged lipid PS at a low ionic strength to kinetically trap hIAPP in α-helical state (Apostolidou et al., 2008; Jayasinghe and Langen, 2005). This is not only demonstrated in the context of negatively charged lipids; it has also been demonstrated through the use of high concentration of HFIP (Higham et al., 2000).

Mutations affecting the ability of hIAPP to form helical intermediates eliminates the toxic effect in insulin secreting cell lines (Hebda and Miranker, 2009; Magzoub and Miranker, 2012). Although the variant lacks the ability to form α-helical structure, it is able to form β sheet strands and assemble into fibrils. This indicates that this variant assembles to fibrils via a different pathway.

Study of toxicity extracellular peptide suggests a few toxic mechanisms including pore formation and a cell crossing peptide (CCP) mechanism. Pore formation is normally considered from the perspective of calcium dysregulation leading to cell death. CCP toxicity is a mechanism usually thought about in the context of antimicrobial peptides (Last et al., 2013; Magzoub and Miranker, 2012). An alternative way in which IAPP may be toxic is from the active assembly of monomeric peptide into fibrils at lipid interfaces. It has been shown that growth of IAPP fibrils at lipid membranes can lead to significant disruption and incorporation of lipids into the growing fibril (Sparr et al., 2004; Engel et al., 2008).A detergent mechanism for IAPP induced membrane perturbation has been ruled out by Last et al. They showed that continued leakage of liposomes by rIAPP, and hIAPP, are inconsistent with a detergent or carpet model for leakage, and instead assign an all-or-none model where leakage is dependent on a conformational change and/or stabilisation of a surface tension induced defect, which is postulated to be some kind of pore, including toroidal, barrel or chaotic (Last et al., 2011).

1.5 Summary and aims

So far, the nature of IAPP and our understanding of it as an amyloid has been introduced and the most important elements of the peptide in relation to fibrillization have been discussed. The process of IAPP synthesis, and the consistency of the secretory granule, including important interrelated factors such as the presence of zinc and the role of insulin, C-peptide and pH, have been noted. The wider evidence of the role of hIAPP in toxicity has been discussed. Finally, the idea of reciprocal

influence of phospholipid membranes and hIAPP on each other, and the resultant toxicity, have been introduced.

This exposition has revealed a number of areas for further research. The use of membrane mimetics has often involved the use of only negatively charged lipids, or a high proportion of such, in order to increase the rate of formation of fibrils or to probe the membrane perturbing properties of variants of IAPP. Therefore the use of a composition of lipids that more closely matches the physiological composition of membrane lipids should yield a more insightful understanding of IAPP-membrane interactions. As of yet no thorough investigation of the influence of secretory granule factors on IAPP membrane interaction has been conducted. The aim is to characterise the effect of zinc on the ability of IAPP to interact and perturb lipid membranes. In addition, together with the classical mechanisms postulated for IAPP membrane perturbation, I will be exploring the interaction of IAPP with separate lipid membranes, whether mixing between these separate membranes is possible and if this constitutes true fusion. Finally, the effect of IAPP on membrane order remains uninvestigated and changes in membrane order by peptides is thought to be an important mechanism for enabling fusion.

Consequently, my thesis addresses these areas in the following fashion. In chapter three, the roles of zinc and salt are investigated for their effect on the interaction of IAPP with membrane prior to fibrillization. In chapter four, for the first time, FRET is used to probe the ability of IAPP to induce lipid mixing between lipid membranes and investigate how this mixing is effected by zinc and salt. This is further expanded on in chapter five with the use of Nanoparticle Tracking Analysis (NTA) to examine the fusion of liposomes. Finally in chapter six, the effect of IAPP on the lipid order of membranes consisting of neutral and negatively charged lipids is explored using the the environmentally sensitive fluorescent dye laurdan.

Chapter 2

Methods

2.1 General

2.1.1 Peptide preparation

IAPP variants were obtained from several sources. hIAPP(wt), rIAPP(wt) and hIAPP(W38) were all synthesized by Generon; hIAPP(Y37W) was synthesised by Synpeptide. Mastoparan was from Sigma. All peptides had a purity of more than 95% (determined by high pressure liquid chromatography (HPLC) by the suppliers of the peptides).

All peptides were received lyophilized. Stocks of IAPP peptides for use in lipid mixing, fusion and leakage assays, were prepared as follows. IAPP peptides were dissolved in dimethyl sulfoxide (DMSO) at a concentration of 2 mg/ml in 1.5 ml tubes they were subsequently bath-sonicated for four rounds of 16 seconds at room temperature. The peptide solution was then added to polypropylene ultracentrifuge tubes (Beckman Coulter) and centrifuged on a TLA-100 for 1 hour at 75,000 revolutions per minute (rpm), 4°C. After centrifugation the peptides were aliquoted in volumes of 5-10 μL and kept at -80°C until use. Mastoparan was dissolved in distilled water (dH_2O) at a concentration 1 mg/ml without any further processing and stored at 4°C until use. For circular dichroism (CD) experiments, batches of lyophilized IAPP were dissolved in Hexafluoro-2-propanol (HFIP) at a concentration 2 mg/ml for 1 hour at room temperature and subsequently aliquoted and stored at -80°C.

2.1.2 Buffer preparation

Buffers were prepared using standard laboratory reagents. All buffers and solutions were filtered either through a 0.22 μM vacuum filter (Corning) or 0.22 μM Millex-GP syringe filter (Merck Millipore) and stored at RT.

2.1.3 Liposome preparation

2-Oleoyl-1-palmitoyl-sn-glycero-3-phosphocholine (PC) (Sigma, 42773) and 1-palmitoyl-2-oleoyl-sn-glycero-3-phospho-L-serine (PS) (Avanti Polar Lipids, 840034) were received lyophilized and dissolved in chloroform. They were then aliquoted and subsequently stored at -20°C until further use.

2.1.3.1 LUVs

Desired proportions of lipids were added to 1.5 ml siliconized tubes (Fisherbrand). A vortexer, on a low revolution setting, was used to create a centripetal force that coated the tube with the lipid solution whilst a stream of N_2 gas was passed over to evaporate the chloroform. The tube was then filled with a total volume of 1 ml of the desired buffer and heated for 15 minuites at 60°C. This solution was then vortexed for 30s and subsequently used to prepare liposomes. Preparation of liposomes (also known asLUV) was undertaken using the extrusion method (MacDonald et al., 1991) with a commercially available mini-extruder (Avanti Polar Lipids) by following a generalised procedure commonly used to prepare liposomes. The apparatus consists of two 1 ml gastight syringes, which fit into either side of a chamber holding a nitrocellulose membrane with pores of a defined size. Disposable membrane supports are inserted on either side of the membrane to avoid rupture of the membrane due to high pressures generated during extrusion. The lipid solution was passed 21 times through a 400 μM nitrocellulose membrane (Whatman) producing liposomes that were subsequently stored at 4°C and used within one week.

2.1.3.2 GUVs

Giant unilamellar vesicles GUVs were prepared using the technique of electroformation with a custom manufactured teflon chamber with a screwable lid with two platinum wires inserted (gift from Erdinc Sezgin, Eggeling group, WIMM, University of Oxford). The chambers were washed with chloroform then ethanol and finally dried with N_2 before each use. The required mixture of lipids was prepared in chloroform and added, drop wise, to the two platinum wires and dried using a stream of N_2.

Following a published protocol (Leite et al., 2015) the GUVs were made as follows. The teflon chamber was filled with 300μL of 300mM of sucrose and the lid screwed on, with the platinum wires now inserted into the solution. The chamber was subsequently inserted into a modified gene pulse holder (Bio-Rad) and connected to a k8016 function generator (Velleman Instruments) forming a circuit. The generator was controlled by PC lab 2000 software (Velleman Instruments) to apply 4.5 V peak to peak voltage at the following frequencies and timings: 10 Hz for 1800s, 3 Hz for 900s, 1Hz for 420s and 0.5 Hertz (Hz) for 420s. The electroformation was performed at room temperature.

2.1.4 Cell Culture

INS-1e cells were routinely cultured in RPMI 1640 medium supplemented with the following: 10% FBS, 2 mmol/L L-glutamine, 5 μmol/L βmercaptoethanol, 200 μg/ml G 418 disulfate salt solution (Sigma). HeLa cells were routinely cultured in Dulbecco's Modified Eagle's Medium (DMEM) supplemented with: 10% FBS, NEAA and Penicillin/Streptomycin. All cells were incubated at 37°C in 5% CO_2.

2.1.5 Plasmid DNA preparation and transfection

The DNA plasmid was purified using a QIAprep spin mini prep kit (Qiagen) according to the manufacturer's protocol. Plasmids were introduced to cells using Lipofectamine

2000 (Thermo Fisher Scientific). Optimal Lipofectamine:DNA ratios for transfection were determined empirically in accordance with the manufacturer's protocol and cells were transfected for 48 hours prior to imaging.

2.2 ThT assay

A stock concentration of Thioflavin T (ThT) was prepared in dH_2O at 1.79 mM and stored at 4°C protected from light. The assay was performed using a concentration of 32 μM ThT in a 96 well μ-clear plate (Greiner Bio-one) at 37°C without shaking. Fluorescence was measured using a Fluostar Optima plate reader (BMG Labtech) operated in kinetic mode with excitation at 450 nm and emission recorded at 490 nm.

2.3 $TbCl_3$-DPA leakage assay

The assay used is based on a concept of an assay originally intended for the investigation of liposome fusion (Fraley et al., 1980). Instead of putting TbCl3 and diplonic acid (DPA) in separate liposome populations and then purifying each through a column, lipsomes containing TbCl3 were prepared and put through a column and DPA was added to the outside, explained in further detail below.

Liposomes were prepared in buffer consisting of 20 mM (4-(2-hydroxyethyl)-1-piperazineethanesulfonic acid (HEPES), 5 μM $TbCl_3$ and 50 μM Sodium Citrate. Additionally, the liposomes were eluted through a PD-10 G-25 Minitrap column (GE) according to the to manufacturer's protocol. The elution buffer was 20 mM HEPES, pH 7.4. The entire eluent volume, after the void, was collected.

Fluorescence emission was measured with a Fluorolog FL3-22 spectrofluorometer controlled by FluorEssence software v3.5 (HORIBA Jobin Yvon). Quartz cuvettes (10 mm 108.002F-QS, Hellma) were used for the assay. The following collection parameters were used: Excitation 272 nm (2 nm bandpass), emission 488 nm (5 nm bandpass), and integration time 0.1s. For time courses a baseline was established for

243 seconds before addition of peptide and measurements were taken every 81 seconds and stopped after the required time. For single end point measurements parameters were the same.

2.4 Tryptophan burial

LUVs were prepared as described with appropriate buffers and peptides were added to liposomes (50 μM) at a L:P ratio of 12:1 in a quartz cuvette incubated at 37°C for 10 minutes before tryptophan fluorescence was measured. The collection parameters were: Excitation 270 nm (5 nm bandpass), Emission 300 nm (5 nm bandpass), Increment 1 nm, Integration Time 0.1 seconds. Emission spectra were corrected for wavelength response of the monochromators and normalised to the resistance of the lamp in order to account for variations in lamp intensity.

2.5 Circular dichroism

A Jasco J-815 Spectropolarimeter was used to measure mDeg using a cuvette of path length 10 mm. The following parameters were used: Scanning speed of 50 nm/min for the wavelength range 190-250 nm, Bandwidth of 1 nm, data integration time (D.I.T) of 1 second, Data pitch of 0.5 nm. Data accumulation was set to four and all spectra were corrected for background using a blank sample calculated by the instrument associated software.

2.6 DiO-DiI lipid mixing assay

The rational of the assay is explained in detail in the results (Chapter Four) but the general procedure is detailed here. The assay consists of preparing three separate populations of liposomes with the fluorophores combinations: 3,3'-Dioctadecyloxacarbocyanine perchlorate (DiO) only, 1,1-dioctadecyl-3,3,3,3-tetramethylindocarbocyanine (DiI) only and both DiO and DiI. A fourth pollution of liposomes was prepared without any fluorophore. The

Fluorophore:Lipid (F:L) ratio was 1:20. For liposomes containing both DiO and DiI, lipid concentration was doubled to simulate the result of full mixing of separate populations of liposomes. Measurements were carried out in 96 well μ-clear plates (Greiner Bio-One) at 37°C. Fluorescence was measured using a Fluostar optima platereader (BMG Labtech) operated in kinetic plate mode with measurement taken every 243 seconds. Sample excitation and reading of emission were from the bottom of the plate.

For each well three measurements were taken of the emission from direct excitation of DiO (filter pair 480/520 nm) and direct excitation of DiI (filter pair 550/580 nm), and FRET between DiO and DiI (480/580 nm). Fluorescence quenching of the donor, DiO, was used to follow Förster resonance energy transfer (FRET) by measuring the emission after direct excitation. This was normalised to a percentage scale using DiO emission intensity from direct excitation of a control sample of a mixture of DiO and DiI populations (max fluorescence) and a DiO/DiI population (min fluorescence) using the following equation:

$$quenching = \frac{maxfluorescence - samplefluoresence}{maxfluorescence - minfluorescence} \times 100 \tag{2.1}$$

2.7 Liposome gold content fusion assay

A method for the preparation of gold encapsulated liposomes was modified from (Paasonen et al., 2007) using 5 and 20 nm colloidal gold particles (BBI International). Volumes of 5 nm and 20 nm gold particles were added to each liposome population so that the concentration (particles/ml) were approximately equal. The liposomes were than spun for 1 hour at 4°C on a benchtop centrifuge at maximum rpm.

TEM samples were prepared by Errin Johnson (Sir William Dunn School of Pathology) outlined as follows. 10 μL of a 50 μM liposome reaction volume was

applied to freshly glow discharged carbon formvar 200 mesh copper grids for 2 mins, blotted with filter paper and stained with 2% uranyl acetate for 10 s, then further blotted and air dried. Grids were imaged in a FEI Tecnai 12 TEM at 120 kV using a Gatan OneView CMOS camera.

2.8 Nanosight Tracking Analysis

Particle diameter measurements were carried out on a NanoSight LM10 with a high sensitivity sCMOS camera (Malvern). Capture and analysis of videos was performed using NanoSight NTA 3.1 software. The instrument was modified by the addition of a 10 capacity filter wheel controlled using a Lambda 10-3 unit (Sutter Instrument). The filter wheel modification was undertaken by K. Tec microscopes.

The temperature of the sample chamber was recorded after the acquisition of a single video using a digital thermometer (804U, Omega) and input manually when requested by the NanoSight software. For videos acquired as a time series, the temperature input was automated using point and click software (PTFB pro). The filters used in experiments were: 508 ALP (for DiI and Fluoresbrite) and 575 ALP (for octadecyl rhodamine B chloride (r18)) (Omega filters). The 488 nm laser unit was used for all measurements. Further data manipulation was undertaken in Matlab (Mathworks) and Origin (OrginLab).

2.8.1 Fluorescent beads

Fluoresbrite size range kit (0.1 nm, 0.2 nm, 0.5 nm, 0.75 nm, 1.0 nm diameter beads (Polysciences)) was used to demonstrate the resolving power of NTA. Acquisition parameters were adjusted because of fluorescence intensity difference due to increasing intensity at lower sizes of beads.

2.8.2 Liposome fusion by DiI fluorescence

Liposomes were prepared with DiI (F:L ratio of 1:20). Peptide was added 50 μM lipid and the reaction was incubated at 37°C and removed at desired time points. The sample was then diluted ten times yielding a final volume of 1 ml and transferred to a 1 ml plastic syringe. A syringe pump (Harvard Apparatus) connected to the sample chamber was set to a flow rate of 60 units and solution was flowed through the chamber and recorded for a 260 seconds. Parameters for recording movies were as follows: camera shutter 350, camera gain 350, histogram 0 - 16380. The following settings for Analysis were used: Detect Threshold 5, Blur Size and Max Jump Distance set to auto. In the case of time course measurements of hIAPP(wt) with liposomes, the concentration of L:P ratio was 6:1.

2.8.3 R18 liposome fusion by quenching

r18 (Sigma) was dissolved to make a chloroform stock. LUVs were prepared with a F:L ratio of 1:20. Sample was flowed through the chamber at a pump speed of 50. The following camera setting were used for acquisition of movies: Shutter 100, Gain 200, histogram 0-16380. The following settings for Analysis were used: Detection Threshold 5, Blur Size and Max Jump Distance set to auto. Further details are explained in chapter 6.

2.9 Membrane order

2.9.1 Laurdan measurements

A stock of 6-Dodecanoyl-N,N-dimethyl-2-naphthylamine (laurdan) stock was prepared in chloroform and stored at -20°C. Liposomes were created containing laurdan at a F:L ratio of 1:400. Fluorescence of samples were measured on a Fluorolog FL3-22 spectrofluorometer (HORIBA Jobin Yvon) in quartz cuvettes at room temperature. At each excitation wavelength (from 340 nm to 410 nm at 10 nm intervals) an emission spectrum was recorded (from 440 nm to 490 nm at 10 nm

intervals). This manifests as an excitation-emission matrix or a 3D scan. GPex and GPem curves were generated (as outline in chapter six).The collection parameters were as follows: Excitation (5 nm bandpass), Emission (5 nm bandpass), Increment 1 nm, Integration time 0.1 seconds. Background signal from a 3D scan of liposomes without fluorophore was subtracted from each 3D scan. Data processing was done using custom scripts in OriginLab.

2.9.2 DPH and TMA-DPH measurements

1,6-Diphenyl-1,3,5-hexatriene (DPH) and N,N,N-Trimethyl-4-(6-phenyl-1,3,5-hexatrien-1-yl)phenylammonium p-toluenesulfonate (TMA-DPH) stock solutions were made in chloroform and stored at -20°C. Liposomes were prepared with a F:L ratio of 1:400. Anisotropy measurements were made on the Fluorolog FL3-22 using the following parameters: Excitation 355 nm (5 nm bandpass), Emission 440 (5 nm bandpass), Increment 1 nm, Integration time 0.1 seconds, G Factor=1.

2.10 Viscosity measurements

2.10.1 Synthesis of Bodipy-C12 and Bodipy-SNAP

The Bodipy-C12 and Bodipy-SNAP were synthesised by Niall Moon (Prof. Tim Donohoe, Chemistry). Bodipy-C12 synthesis was based on the procedure of Levitt et al. (2009). Details pertaining to the synthesis and structure of Bodipy-C12 and Bodipy-SNAP were produced by Niall Moon in the format of a Final Honours Thesis.

2.10.2 Steady state intensity measurements

Emission spectra of 5 μM Bodipy-SNAP, BODIPY-C12 and selected intermediates in Methanol:Glycerol mixtures measured in 10 mm quartz cuvettes (Hellma). The following collection parameters were used: Excitation 480 nm (3 nm bandpass),

Emission 500-600 nm (3 nm bandpass), Increment 1 nm, Integration time 0.1 seconds.

2.10.3 Microscopy and fluorescence lifetime measurements

Imaging was carried out on a Olympus FV 1000 with a SPC-150 Time-correlated single-photon counting (TCSPC) card (Becker & Hickl) for lifetime measurements. A 488 nm laser pulsed at 80 MHz was used for acquiring lifetime measurements. The data were processed using the SPCImage v 4.9.7 (Becker & Hickl).

2.10.3.1 Viscosity calibration

Solutions of Methanol:Glycerol of various ratios were prepared. Solutions were well mixed at room temperature using a shaker overnight. The lifetimes of 15 μM Bodipy-C12 in these solutions were measured in 96 Well μ-Plate (Ibidi) with a 60X objective, in 'single' mode with data acquired for one minute.

2.10.3.2 GUV measurements

GUVs were generated according to method described in section 2.1.3.2. GUVs were prepared with a Bodipy-C12:lipid ratio of 1:20 from a stock of Bodipy-C12 in chloroform. Imaging was done using 60X magnification in first in first out (FIFO) mode and photons were recorded for five minutes.

2.10.3.3 Cell measurements

All cells were plated in a 96 Well μ-Plate (Ibidi). INS-1e cells were incubated in 15μM of Bodipy-C12 from a DMSO stock for 30 minutes at 37°C, 5% CO_2. Cells were then washed for a total of three times with RMPI-media, before replacing with fresh media and incubation for 30 minutes. A final wash was performed before imaging at room temperature. Imaging was done using 60X magnification in FIFO mode and photons were recorded for five minutes. The photon count histograms were fitted using an exponential decay model with two components with the following parameters: pixel

binning 10 and intensity threshold 5. The instrument response function (IRF) was automatically generated by the software, and is calculated using the highest intensity pixel.

HeLa cells were incubated in 15 μM of Bodipy-SNAP for 30 minutes at 37°C. Following a single wash, they were incubated in 0.1% delipidated BSA for 2.5 hours. Cells were washed once more before imaging. Imaging was performed using 100X using FIFO mode and photon counts were recorded for 5 minutes. The photon count histograms were fitted using an double exponential decay model with the following parameters: pixel binning 10 and intensity threshold 5. The IRF was automatically generated by the software, and is calculated using the highest intensity pixel.

Chapter 3

IAPP-membrane interaction

3.1 Introduction

The interaction of IAPP with lipid bilayers has been elucidated in a variety of contexts. The use of membrane mimetics, such as liposomes, in pull down and leakage assays, and planar lipid bilayers, in cross membrane voltage measurements, have established IAPP association with lipid membranes. Additionally in cellular studies fluorophore-labelled IAPP has been found associated with both extra and intra cellular membranes. Some of the factors that are believed to be important determinants of the interaction of IAPP with lipid membranes have been discussed previously (Chapter 1: introduction).

Although some of the basic requirements for interaction of IAPP with lipid membranes have been described (chapter 1 introduction), the connection between peptide structure and the subsequent effect on bilayers has not been fully evaluated. The consequence of various physiologically relevant factors, particularly in relation to the secretory granule, have mostly been investigated with regard to IAPP misfolding and fibrillization in solution. However, the role that these factors play in membrane interaction, and subsequent peptide and membrane structural change, has not received as much attention.

There are several aims of this chapter. The first is to describe IAPP variants in terms of their fibrillization potential and ability to induce leakage from liposomes of defined lipid compositions. The second is to investigate the position of a particular IAPP

variant at the membrane, hIAPP(Y37W) which has a C-terminal tryptophan (Trp) substitution and behaves like wild type. The final aim is to explore the effect of ionic strength and zinc on the interaction of IAPP with lipid membranes.

3.2 Choice of IAPP variants

The interaction of amyloid peptides with lipid membranes is often verified by liposome leakage assays, such as dequenching, or through visualisation of fluorophore labelled IAPP at lipid membranes. The use of labelled peptides is widespread, however in the case of IAPP, the possible effects this practice has on IAPP misfolding, assembly into higher order structures and interaction with membranes should not be ignored. IAPP, like Aβ, is amongst the shortest of the amyloid forming peptides and the effect of even modest modifications should be considered. Indeed, comparison between the kinetics of non-amidated and amidated hIAPP showed that the non-amidated form had a longer lag time before fibirillization (Yonemoto et al., 2008). It is therefore not unreasonable to think that other modifications used in order to follow peptide association with lipid membranes might result in significant differences in fibrillization dynamics and kinetics. With this in mind, before assessing the effects of IAPP variants on membranes, I first determined whether hIAPP, modified by either a C-terminal addition (W38) or substitution (Y37W), had any effect on its the ability to fibrillize.

The choice of including tryptophan by addition is due to tyrptophan making up one of the top three residues in terms of aggregation potential (the other two being phenylalanine and tyrosine) as determined by predictive amyloid propensity tools (Pawar et al., 2005; Tartaglia et al., 2005) and so it was thought that this might increase fibrillization potential. Although no examples of the use of IAPP variants with aromatic additions or substitutions were initially found, a subsequent literature search revealed that C-terminal amidated hIAPP, with a tyrosine substituted for a tryptophan (hIAPP(Y37W)), had been created for use in triplet quenching experiments (Vaiana et al., 2009). The aim of the work by Vaiana et al was to

examine the contact dynamics of interaction between the C-terminal tryptophan and N-terminal disulphide bond, in order to reveal information about the structure of IAPP. Although in their study the formation of amyloid fibrils by hIAPP(Y37W) was demonstrated by transmission electron microscopy (TEM) and showed no observable differences compared to hIAPP(wt), no information on the kinetics of assembly using an amyloid sensitive dye, such as ThT, was undertaken. Therefore we decided to synthesise hIAPP(Y37W), in addition to hIAPP(W38), for use in tryptophan membrane burial experiments.

3.3 Kinetics of IAPP fibril formation

Formation of amyloid by the various peptides was assessed using the commonly employed ThT assay. The assay involves following an increase in fluorescence emitted from ThT thought to be due to binding of the fluorescence molecule to grooves created by β sheet formation. Therefore, fluorescence of ThT incubated with amyloid peptide allows one to follow the kinetics of monomer assembly to amyloid fibrils. The kinetics of this assembly is described by a sigmoidal curve (fig. 3.1) demonstrating three key aspects of the kinetics of amyloid formation: 1) a lag phase where monomers are coming together to form oligomeric species, acting as nuclei for assembly, and culminating in the initiation of fibrillization; 2) a rapid growth phase whereby such oligomers or nuclei undergo conversion to fibrils by continued addition of monomers to the nuclei; and 3) steady state or saturation, in which the on and off rates of monomer binding and fibrils breaking are now equal and is exemplified by a plateau in the fluorescence emission which correlates with the presence of peptide that is in a mature amyloid state. These various components are often used to compare kinetics of assembly between different conditions.

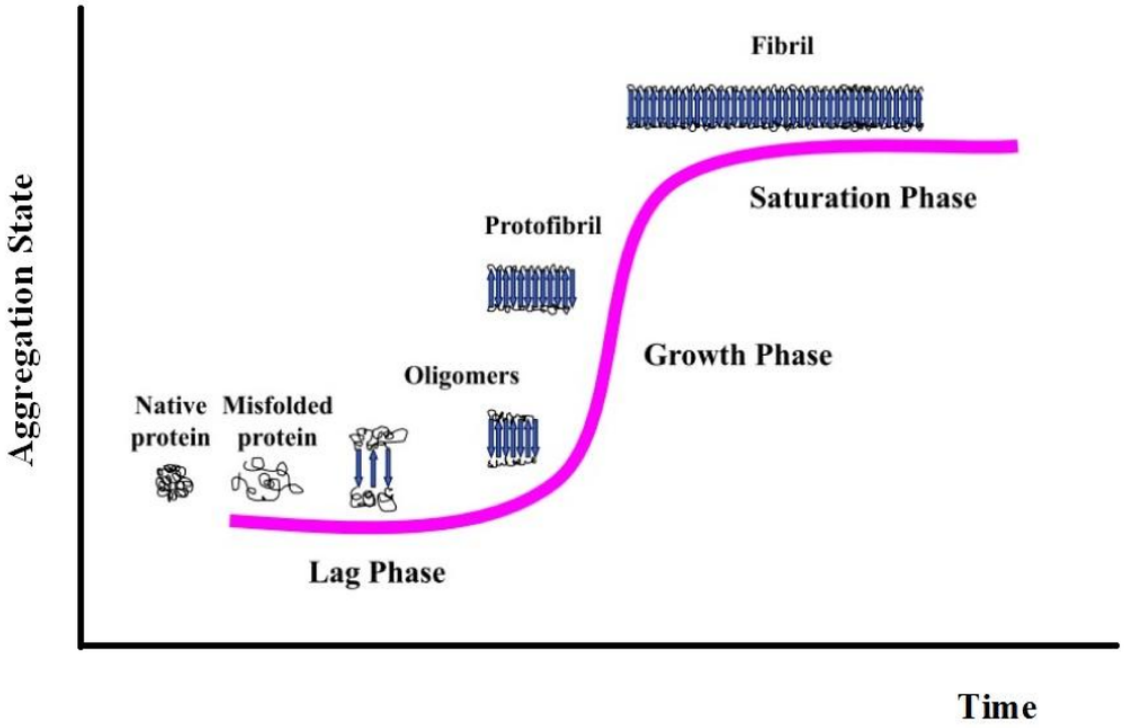

Figure 3.1. Typical amyloid growth curve. Natively folded peptide undergoes structural changes on the pathway to becoming part of an amyloid fibril. The end point is signified by the presence of supramolecular polymers characterised by a regular repeating arrangement of subunita (Figure from Iannuzzi et al. (2013)).

3.4 Results

3.4.1 Examining kinetics of fibril assembly of IAPP variants

Four variants of the peptide were tested for their ability to form amyloid: Wild type hIAPP(wt), hIAPP(W38), hIAPP(Y37W) and rIAPP (fig 3.2). rIAPP is known not to form amyloid, and so is used as a negative control. A completely unrelated peptide, mastoparan, was used as another negative control, for the ThT assay, as well a positive control in leakage assays that have been used to assess the perturbation of the membrane by IAPP variants. Mastoparan is a peptide produced by wasps and is contained within their venom. It causes the release of histamine from mast cells causing the accompanying pain following a wasp sting. It has previously been characterised as a pore forming peptide (Arbuzova and Schwarz, 1999; Whiles et al., 2001; Hori et al., 2001).

As mentioned in the introduction, the presence of lipid accelerates hIAPP

```
hIAPP(wt)      KCNTATCATQ RLANFLVHSS NNFGAILSST NVGSNTY
rIAPP(wt)      KCNTATCATQ RLANFLVRSS NNLGPVLPPT NVGSNTY
hIAPP(_W38)    KCNTATCATQ RLANFLVHSS NNFGAILSST NVGSNTYW
hIAPP(Y37W)    KCNTATCATQ RLANFLVHSS NNFGAILSST NVGSNTW
```

Figure 3.2. Sequences of IAPP variants used. From top to bottom: Human wild type, Rat wild type, hIAPP with tryptophan addition (W38), and hIAPP with trytophan substition (Y37W). Differences in sequence between wild type rat and human IAPP are highlighted in red and, where present, tryptophan(W) is highlighted in green.

fibrillization. We can see that compared to buffer alone, presence of PCPS liposomes leads to a much shorter lag time before initiation of hIAPP(wt) fibrillization (fig. 3.3). Indeed, hIAPP(wt) incubated in the absence of PCPS liposomes does not even reach the rapid growth phase at 2000 minutes (∼33hrs), clearly showing the accelerating effect of this lipid composition on fibrillization of hIAPP(wt). As expected, rIAPP produces no change in ThT emission representing a lack of fibrillization. DMSO was included to check for any interference with the ThT assay; indeed, there is no change in ThT emission during the measurement time period with incubation of DMSO and ThT alone.

Comparison between wild type and modified peptides revealed interesting results. hIAPP(Y37W) resulted in an increase in ThT signal described kinetically by a sigmoidal curve, similar to that of hIAPP(wt), with a similar plateau being reached as well as a similar rate of growth; however the lag time is shorter, possibly indicating faster formation of a nucleus (fig. 3.4). The ThT data is consistent with the EM data from Vaiana et al. which showed hIAPP(Y37W) forms amyloid. The ThT data further shows that this variant shares similar kinetics of fibrillization with hIAPP(wt). hIAPP(W38) also has the capacity to form amyloid, but the kinetics are clearly different from both the wild type and hIAPP(Y37W). First, the lag time before initiation of the growth phase is 100 minutes, at least five times longer than the wild type. Additionally, the plateau height is reduced, indicating the creation of fewer fibrils. It is clear that while hIAPP(W38) forms fibrils it does so with a reduced capacity.

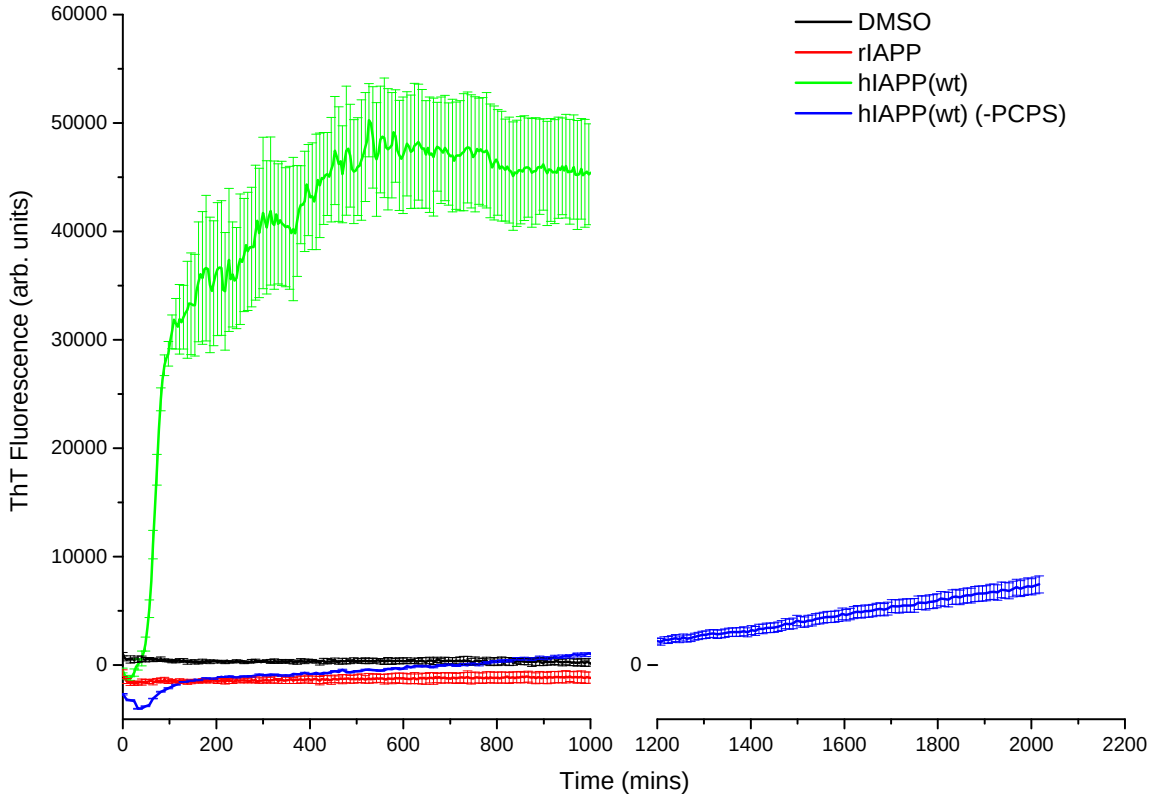

Figure 3.3. Addition of negatively charged lipids accelerates fibrillization. ThT emission of DMSO, rIAPP(wt) (4.2 μM) and hIAPP(wt) (4.2 μM) in the presence of PCPS liposomes (50 μM) was recorded for 1000 minutes; hIAPP(wt) without lipid (-PCPS) was recorded for a further 1000 minutes (total time of $\sim$33hrs). All reactions were carried out in a 100 μL volume of 20 mM Hepes, 7.4 pH and incubated at 37°C.

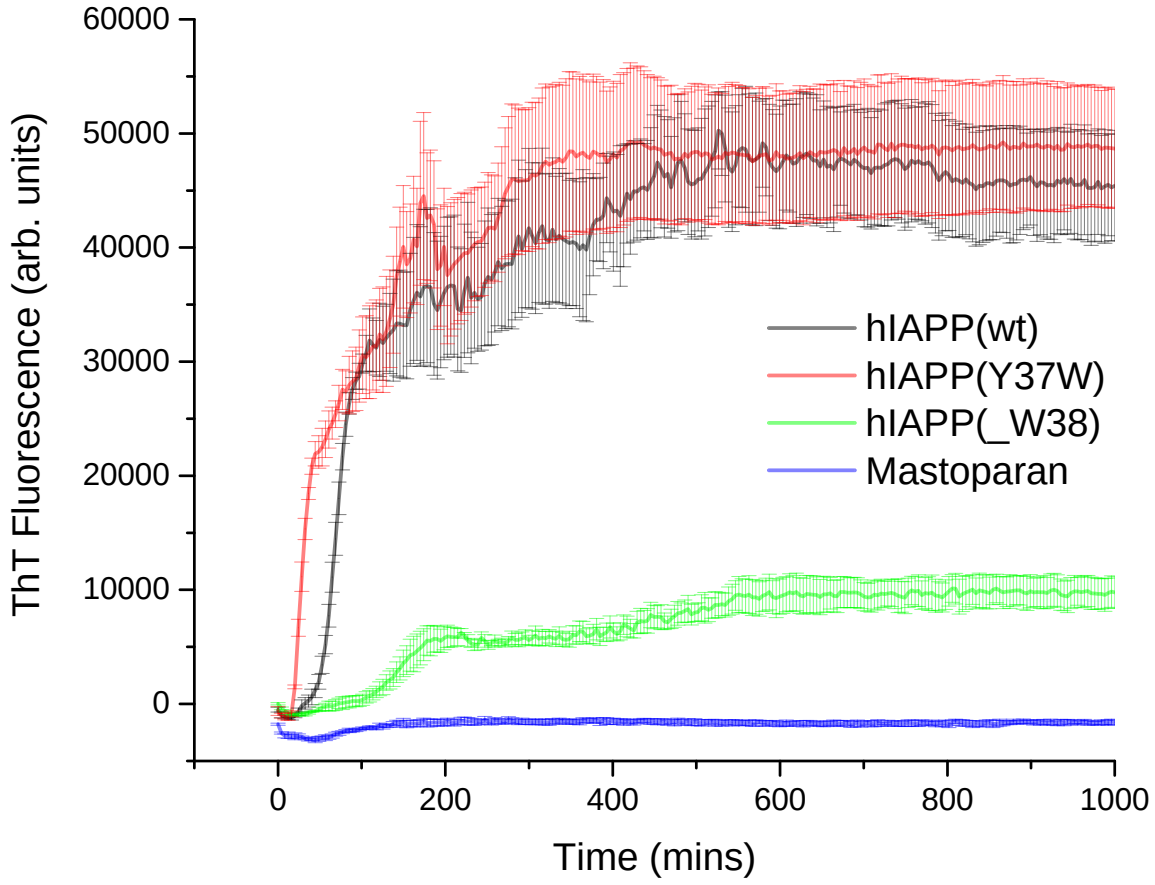

Figure 3.4. Comparison of different peptides for amyloid forming potential. 4.2 μM of each of the three IAPP variants and 25 μM of mastoparan were incubated with PCPS liposomes (50 μM) at 37°C. For each curve error bar indicate SEM for n=3.

These experiments were done in the presence of lipid and which accelerates formation of fibrils by many orders of magnitude. The effect on lipid membrane during the acceleration of fibril formation may or may not cause damage to membrane depending on the lipid composition and ionic environment. In addition to investigating the effect of negatively charged liposomes (PCPS) on the kinetics of amyloid formation, I also investigated the effect of neutral liposomes, composed only of the zwitterionic lipid POPC. Unexpectedly, I found that the addition of salt resulted in accelerated fibrillization compared to POPC alone (fig. 3.6). The four conditions in which hIAPP was incubated, as shown in figure 3.6, are buffer only, buffer + NaCl, PC, and PC + NaCl. The presence of NaCl leads to a decrease in lag time compared to buffer alone; however, the addition of PC and NaCl shifts the curve even more, suggesting a cooperative effect that requires both components, leading to an accelerated fibrillization at the surface.

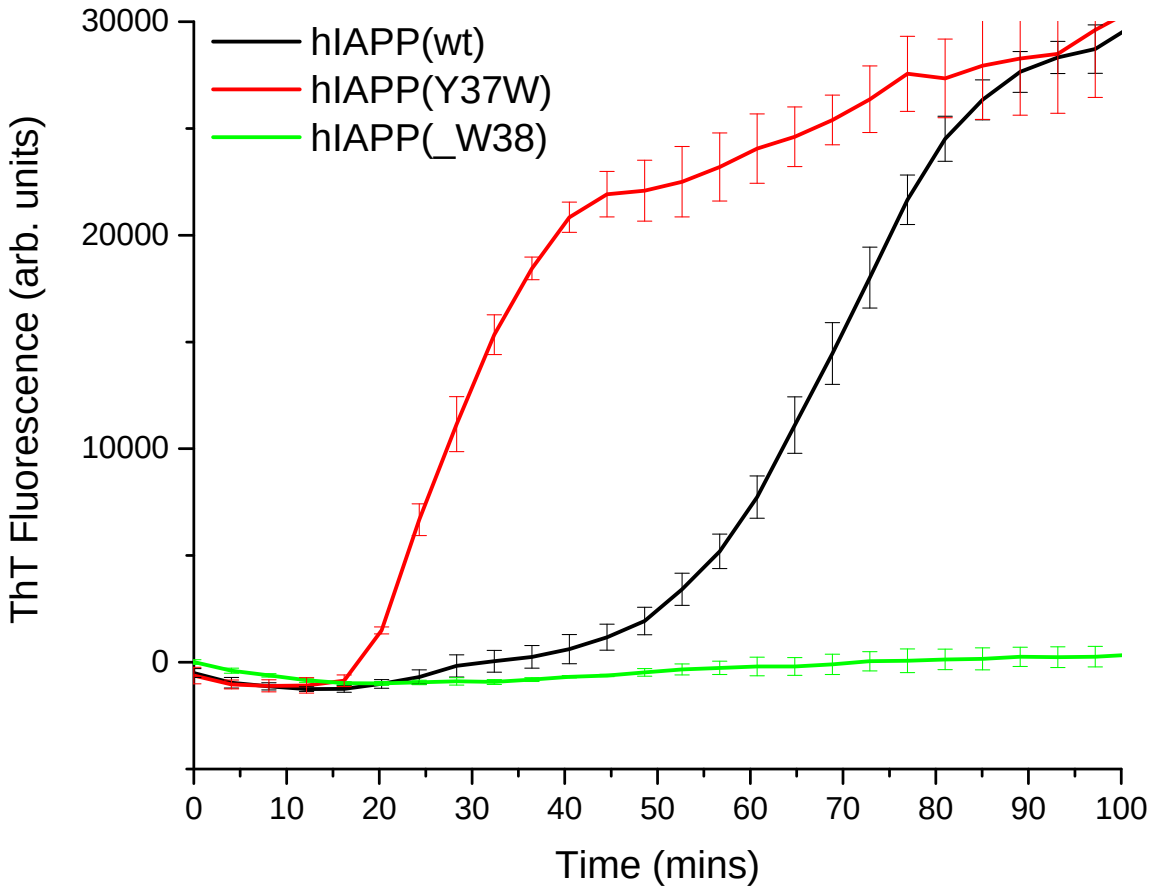

Figure 3.5. Difference in lag time of IAPP variants. IAPP peptides (4.2 μM) were added to 50 μM of PCPS liposomes and incubated at 37°C. For each curve error bar indicate SEM for n=3.

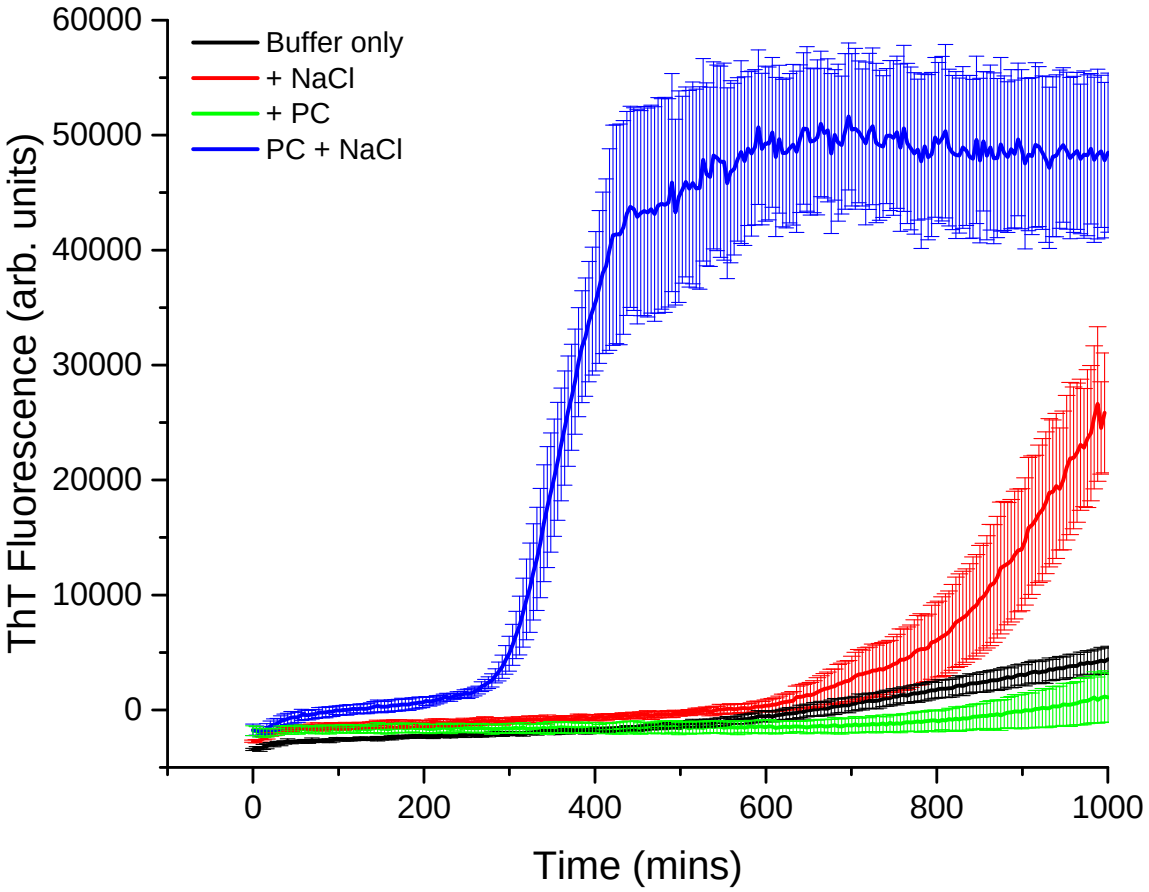

Figure 3.6. Combined effect of PC and high ionic strength on hIAPP fibrillisation. IAPP was added at ac concentration of 4.2 μM to solutions at pH 7.4 of either Buffer (Hepes 20 mM) Buffer+NaCl (Hepes 20mM, NaCl 100 mM, Buffer+PC (Hepes 20 mM, PC 50 μM), or (PC 50 μM, NaCl 100 mM). For each curve error bars indicate SEM (n=3).

Although the ThT assay elucidates whether modified hIAPP is comparable in terms of fibrillization behaviour to wild type, it does not provide information about the subsequent effect on membrane structure. Although the kinetic behavior of hIAPP(W38) fibrillization was very different from wild-type, on both short and long time scales, I decided to test the ability of hIAPP(W38) to cause leakage of membranes. This was because of evidence relating to α-helical conformations being responsible for membrane damage. Since there is no significant fibrillization of hIAPP(W38), compared to hIAPP(wt) and hIAPP(Y37W), up until 100 minutes, I wanted to see if there would be a difference in ability to cause leakage. Lipid membranes have a differential ability to accelerate formation of amyloid, which is dependent on lipid composition as well as the ionic strength and composition of the solution surrounding the membrane. In the next section we explore the influences of these factors on the ability of IAPP to cause membrane perturbation.

3.4.2 Membrane interaction: leakage from perturbation

A number of putative mechanisms have been put forward in order to explain amyloid peptide induced membrane perturbation. Pore formation and detergent action (Hebda and Miranker, 2009), fibril elongation (Engel et al., 2008) and cell crossing (Magzoub and Miranker, 2012) have all been implicated as mechanisms. From the kinetic data on amyloid assembly, one can see that the lag time before initiation of the growth phase is around 10 minutes for hIAPP(Y37W), 20 minutes for hIAPP(wt) and 100 minutes for hIAPP(38W) (this may be considered a lower limit as there is a delay between adding peptide to all wells and initiating recording of the fluorescence emission). Using a spectrofluorometer based liposome leakage assay, I examined the ability of the various peptides to cause membrane perturbation. Use of such assays are common for examining the extent to which peptides perturb lipid membranes.

Typically liposome leakage has been assessed by leakage of the fluorophore calcein. This entails producing liposomes that have a very high concentration (in excess of 50

mM) of fluorophore within liposomes. At such high concentrations calcein is quenched within the luminal volume of the liposome meaning that the fluorescence intensity is very low upon excitation. Release of calcein into the extra luminal space results in a decrease in its concentration due to dilution into the bulk volume, resulting in dequenching, and a concomitant increase in the intensity of the fluorescence emission. However, in order to observe this dequenching, the extra liposomal calcein must be removed before initiation of leakage so there is a minimal background fluorescence above which an increase in fluorescence can be readily seen. This is normally achieved by utilising column chromatography, commonly in the form of commercially available pre-packed columns.

However, the calcein assay was not the preferred assay for the following reasons. A practical issue is that in order to get a low enough background often only the first part of the eluent is usable, which has two key implications. Firstly, in order to get an appreciable number of liposomes that have quenched dye in the internal volume, a considerable number of liposomes must be put through the column as a large amount of liposomes will be lost in the initial eluent in order to avoid too much extra-luminal calcein. Secondly, the use of millimolar concentrations of fluorophore requires the elution buffer, as well as any buffer used for subsequent dilution, to be isotonic in order to avoid osmotic stress, and potential loss of integrity, of the liposomes.

Instead another form of leakage assay was used based on the interaction of the metal ion terbium (Tb) and DPA (Wilschut et al., 1980). Terbium is weakly fluorescent in solution but chelation by DPA results in a 20,000 fold increase in fluorescence. An advantage of this is that the concentration of both terbium and DPA can be kept low, micromolar range. The version of the assay I adopted was that of TbCl3 in the luminal volume with DPA subsequently added to the extra-luminal volume; this was done to reduce interaction of Tb with peptide added to the system. Perturbation of liposome membranes, such that there is interaction between the intra and extra-luminal volumes results in an increase in fluorescence. A version of this assay was first tried that relied on an increase over the background fluorescence of interaction extra-luminal Tb and DPA. This provided a reasonable signal-to-noise ratio, potentially

obviating the need for the use of chromatography. However, the dynamic range was further improved by use of a column which, importantly, enabled the use of the whole eluent. To check for any considerable changes in lipid concentration, I compared the kinetics of fibrillization of hIAPP(wt) between three different preparations of liposomes: 1) liposomes without TbCl3; 2) eluent from a column that had received preparation 1; and 3) eluent from a column that received liposomes prepared with TbCl3 (fig.3.7). The kinetics of amyloid formation, as judged by ThT, did not change considerably (fig. 3.7) validating comparison of the fibrillization kinetics of IAPP incubated with lipsomes prepared using these three different procedures. It was of further use to compare the kinetics of assembly of IAPP with and without terbium in order to check if terbium had any influence on the kinetics of assembly, which it does not.

Using the Tb-DPA assay I was able to measure the amount of leakage induced by the IAPP variants, as well as by the control peptide mastoparan. When added to PCPS liposomes composed of 70% POPC and 30% POPS (fig. 3.8) all hIAPP peptides caused leakage. hIAPP(wt), hIAPP(Y37W) and hIAPP(W38) all resulted in statistically significant leakage described by mono-exponential kinetics. Such leakage kinetics are commonly described for antimicrobial peptides (Gregory et al., 2008) and Mastoparan (Yandek et al., 2009). Interestingly, the amount of leakage resulting from hIAPP(38W) relative to hIAPP(wt) was lower, mirroring the results of the ThT assay, where hIAPP(38W) reached a lower plateau height compared to hIAPP(wt).

It is of interest to speculate on the nature of the species responsible for leakage. Such species are unlikely to be fibrillar or proto-fibrillar in nature as approximately half of the total leakage for hIAPP(wt) and hIAPP(Y38W)took place within 4.05 minutes. The speed of leakage resulting from all three peptides is consistent with leakage competent conformations that are either adopted in solution or are rapidly converted to such conformations at the membrane. Given that lag times are related to the ability of nuclei to form before initiation of fibrillization, it is possible that the reduced capacity of hIAPP(38W) to induce leakage is due to a reduced ability to form

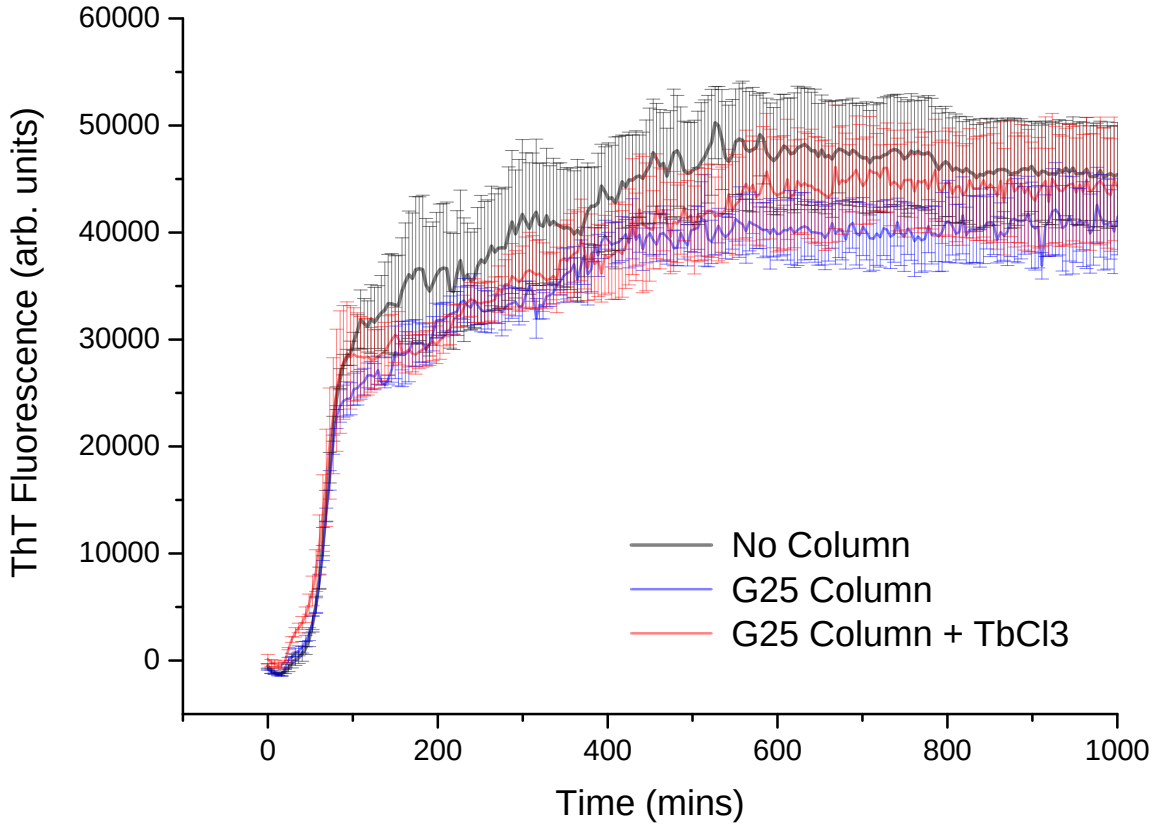

Figure 3.7. Effect of chromatography and TbCl3 on fibrillization kinetics. 50 μM of PCPS liposomes was the starting material. No Column curve represents no additional processing after production of liposomes. G25 Column curve represents the eluent of the starting PCPS liposome solution. The volume used for the assay was scaled to correct for the dilution from eluting through the column. G25 Column+$TbCl_3$ curve represents liposomes that were made with $TbCl_3$ and then put through the column; again volume used was scaled due to dilution of eluent. All samples had 4.2 μM of IAPP added. For each curve error bars reprsent SEM for n=3.

oligomers that are able to pertub lipid membranes. Such on pathway oligomers have been proposed to be composed of α-helical (Williamson and Miranker, 2007) and β-sheet (Buchanan et al., 2013; Jiang et al., 2011) structure. However, the fact that all three hIAPP variants reach plateau before or during the growth phase of fibrillization does not support a role for fibril growth of such oligomers at the membrane as a cause of leakage.

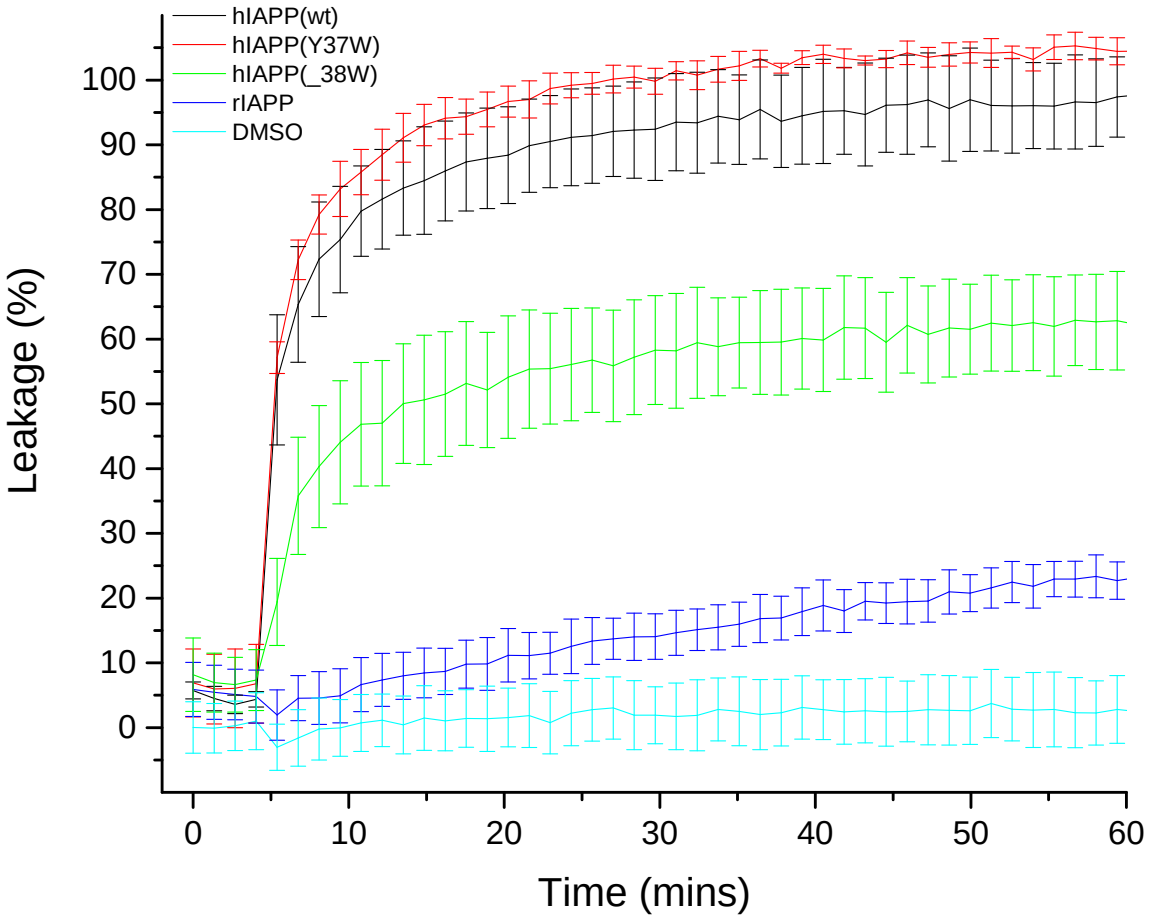

Figure 3.8. Leakage from PCPS lipsosomes is induced by all hIAPP variants. 4.2 μM of peptide was added to a concentration of $\sim$50 μM liposomes (the volume of liposome solution was adjusted for dilution due to elution through a column). The percentage leakage is calculated relative to total release from control lipsomes ruptured with 10% cholate. For each curve error bars represent SEM for n=3.

In comparison to PCPS, it was expected that liposomes composed only of PC would not undergo significant leakage as this had not been previously reported. However, in light of the finding of the combined kinetic effect of NaCl and neutral 2-Oleoyl-1-palmitoyl-sn-glycero-3-phosphocholine (PC) on fibrillization, it was reasonable to check for perturbation and leakage of PC lipid bilayers. Rather than

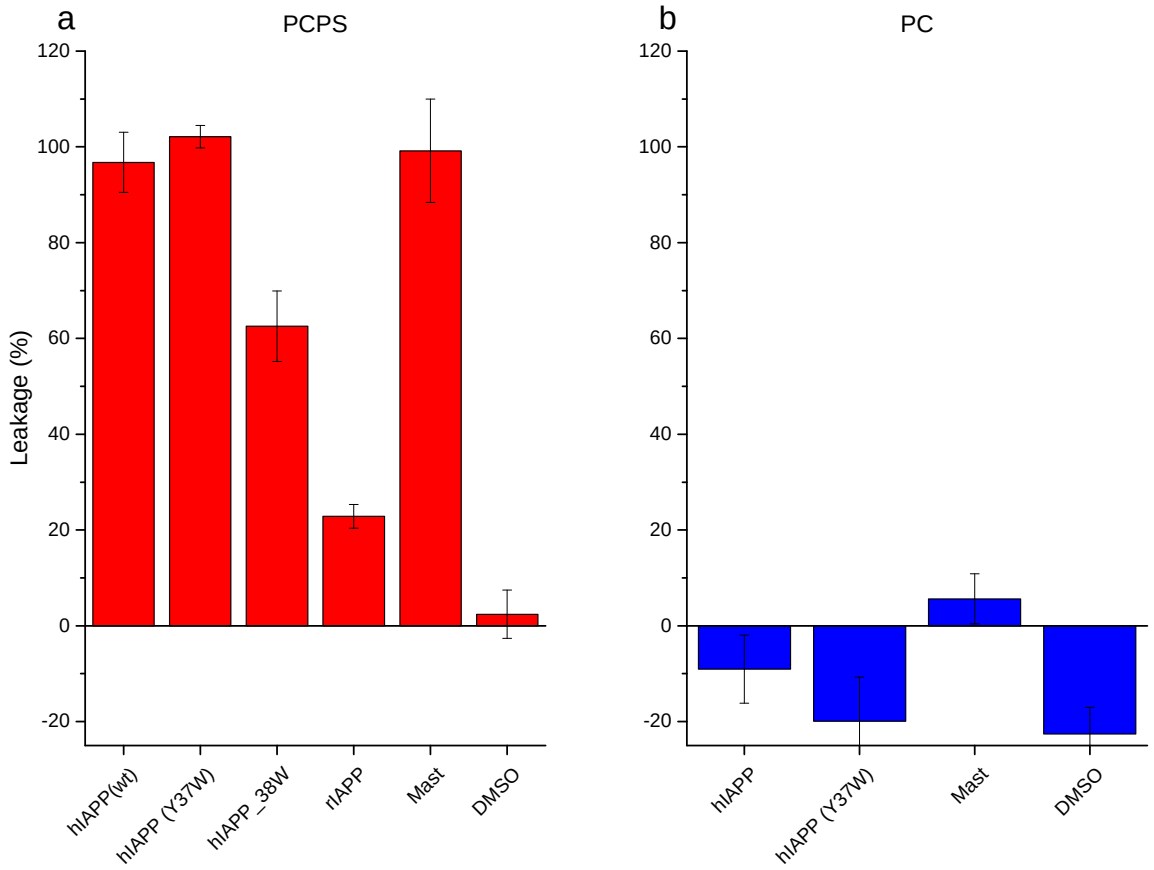

Figure 3.9. Peptide induced leakage of PCPS and PC liposomes after 1 hour. 4.2 μ of IAPP variants and 25 μM of mastoparan was added to liposomes and leakage at 1 hour recorded. Percentage leakage is calculated relative to the total release resulting from addition of 10% cholate. Error bars represent SEM for n=3. Significance between DMSO and peptides determined using a one way ANOVA with Tukey's posthoc test.

collect a timecourse to gain kinetic information, a single time point was taken at 1 hour as the expected result was that PC liposomes remained intact. Indeed, at this time point there was no significant leakage consistent with the membrane being intact (fig. 3.4.2). However, results from the ThT assay showing acceleration of fibrillization of hIAPP(wt) by PC, in the presence of a high concentration of NaCl, are clearly consistent with interaction of hIAPP(wt) with the this membrane. It was therefore reasonable to look for evidence of membrane interaction using the tryptophan variant hIAPP(Y37W) (see 3.4.3).

Investigation of the effect of zinc using the Tb-DPA assay proved challenging. Although use of chromatography removes a large proportion of extra-luminal terbium, enough remains that addition of DPA produces a background signal.

When trying to evaluate the impact of zinc on the kinetics of leakage, it was found that inclusion of zinc led to a decrease in the background signal of fluorescence, consistent with DPA chelating zinc. The concentration of zinc that I was using was 500 μM, about 20 times the concentration of terbium used when preparing the assay, effectively out-competing Tb in binding to DPA. Therefore the effect of zinc on leakage kinetics could not be investigated with this method.

Accordingly, I turned to the prototypical calcein leakage assay to try and asses the effect of zinc. Using commercial columns, I took the first part of the eluent containing liposomes with luminal self-quenched calcein. However, again the use of zinc resulted in unwanted effects. Addition of hIAPP(wt) resulted in an increase of fluorescence as compared to DMSO. However, addition of zinc alone to liposomes resulted in a similar increase in fluorescence, rendering it unsuitable for assessing the impact of zinc. This highlights an issue of investigating the role of such metals for their effect on membrane integrity through such fluorescence assays. Cobalt is well known to quench calcein and is the basis of many assays. There are fewer expositions on the effect of zinc on calcein fluorescence, however a fluorescence-enhancing effect has been noted (Markuszewski, 1976). It is difficult to draw conclusions on these issues given the paucity of literature on the topic but it appears there are general difficulties in assessing effects of metals on peptide induced leakage.

In the next part of this chapter we consider the position of the peptide in the bilayer by the use of the intrinsic fluorescence properties of tryptophan.

3.4.3 C-terminal membrane interaction: Trp burial

Intrinsic fluorescence of amino acids is often used to follow folding dynamics (Moens et al., 2004) and interaction (Loura, 2003; Wimley and White, 2000) of proteins and peptides with membranes. There are three amino acids with high enough quantum yields that can been used, all containing aromatic rings: phenylalanine, tyrosine and tryptophan. Both rIAPP(wt) and hIAPP(wt) have a C-terminal tyrosine as well as one and two phenylalanines, respectively. Initially I attempted to use the intrinsic

fluorescence of tyrosine which has been utilised previously (Padrick and Miranker, 2001). However, at the concentration of peptide I was using, the quantum yield was too low to provide an adequate signal to noise ratio acceptable for following small changes in fluorescence. Additionally, during preliminary experiments, the recording of tyrosine emission from hIAPP(wt) was affected by substantial scattering producing artefacts that made it difficult to measure the true fluorescence emission. Therefore any subsequent shift in wavelength due to burial in a hydrophobic environment (blue shift when interacting with membrane) could not be accurately measured. Accordingly, the use of hIAPP(Y37W) was appropriate due to the higher quantum yield of tryptophan and the similarity of kinetics of fibrillization to that of hIAPP(wt); thus hIAPP(Y37W) was used as an analogue for the investigation of the interaction of the hIAPP C-terminus with lipid membrane.

Using liposomes with compositions of PC and PCPS I investigated the effect zinc and NaCl had on the ability of the C-terminal part of hIAPP to interact with and bury into lipid bilayers. It is clear from the normalised spectra of PCPS, PC and Buffer (fig. 3.10a) that there is a difference in peak wavelength of peptide interacting with PCPS (∼347 nm) compared to PC or Buffer (∼342 nm). Interestingly, for PCPS, this blue shift is prevented in the presence of zinc or sodium chloride (fig. 3.10b. For PC liposomes, no significant shift is apparent regardless of the presence of zinc or NaCl (fig. 3.10c).

The normalised spectra serve to make the changes in peak wavelength more obvious. However, as well as changes to tryptophan emission wavelength, an increase in the quantum yield of tryptophan in a less polar environment results in a concomitant increase in the intensity of fluorescence emission. The changes in peak wavelength and intensity between the different conditions, as well as the errors of the mean, are illustrated using a scatter plot (fig. 3.11).

When interpreting the degree of Trp burial using the wavelength parameter, it is clear that the presence of negatively charged lipid in the form of PCPS results in the largest significant blue shift compared to peptide in buffer alone. The presence of

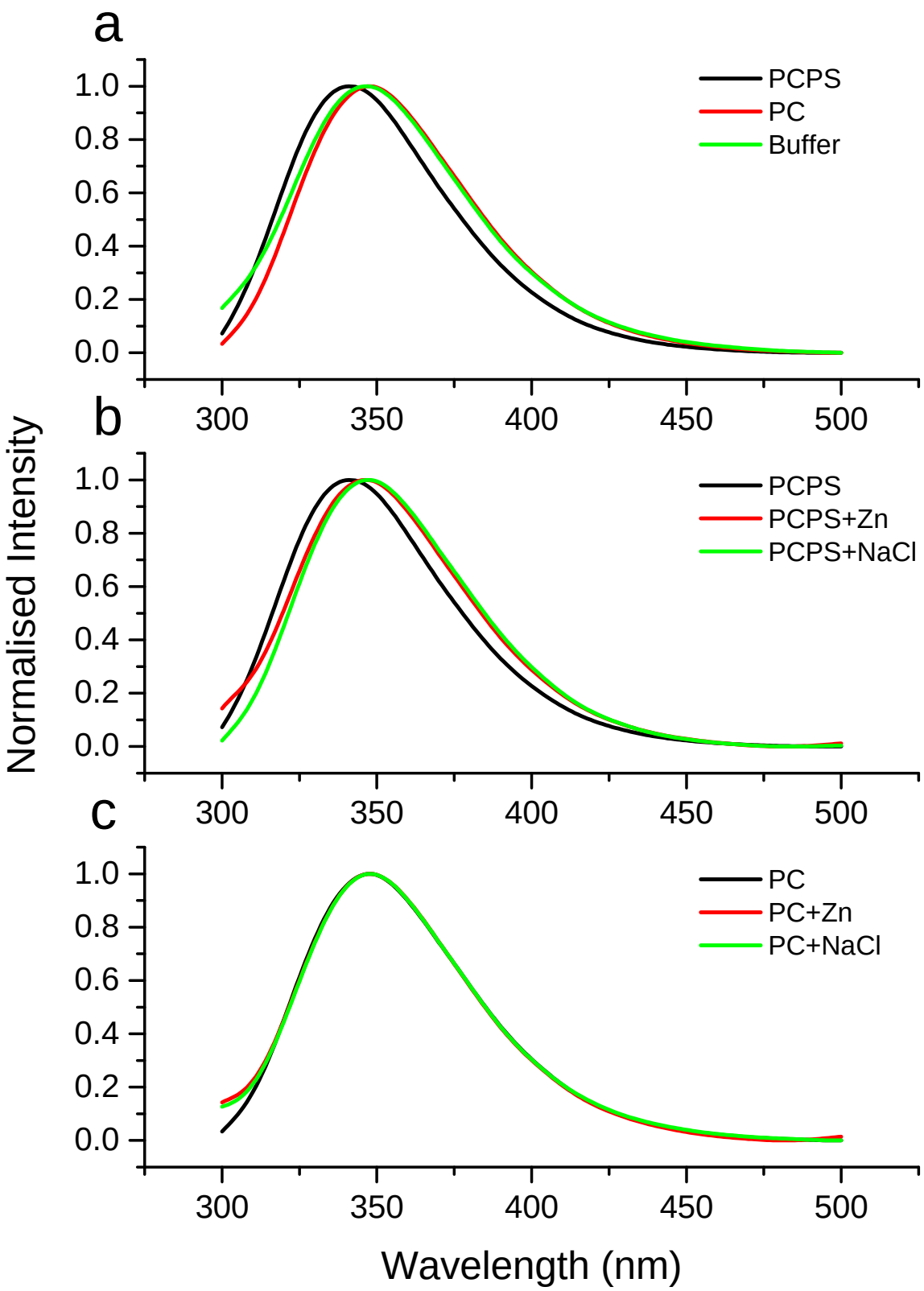

Figure 3.10. Effect of lipid compositions and ionic environment on C-terminal burial. Normalised emission spectra of C-terminal tryptophan from 4.2μM hIAPP(Y37W). (a) Comparison of peak wavelength of IAPP in buffer or negatively charged (PCPS) and neutral (PC) lipid; (b) Effect of zinc and NaCl on C-terminal burial in negatively charged lipsomes (PCPS) (c) Effect of zinc and NaCl on C-terminal on C-terminal burial in neutral liposomes (PC). Curves were smoothed and averaged (n=3).

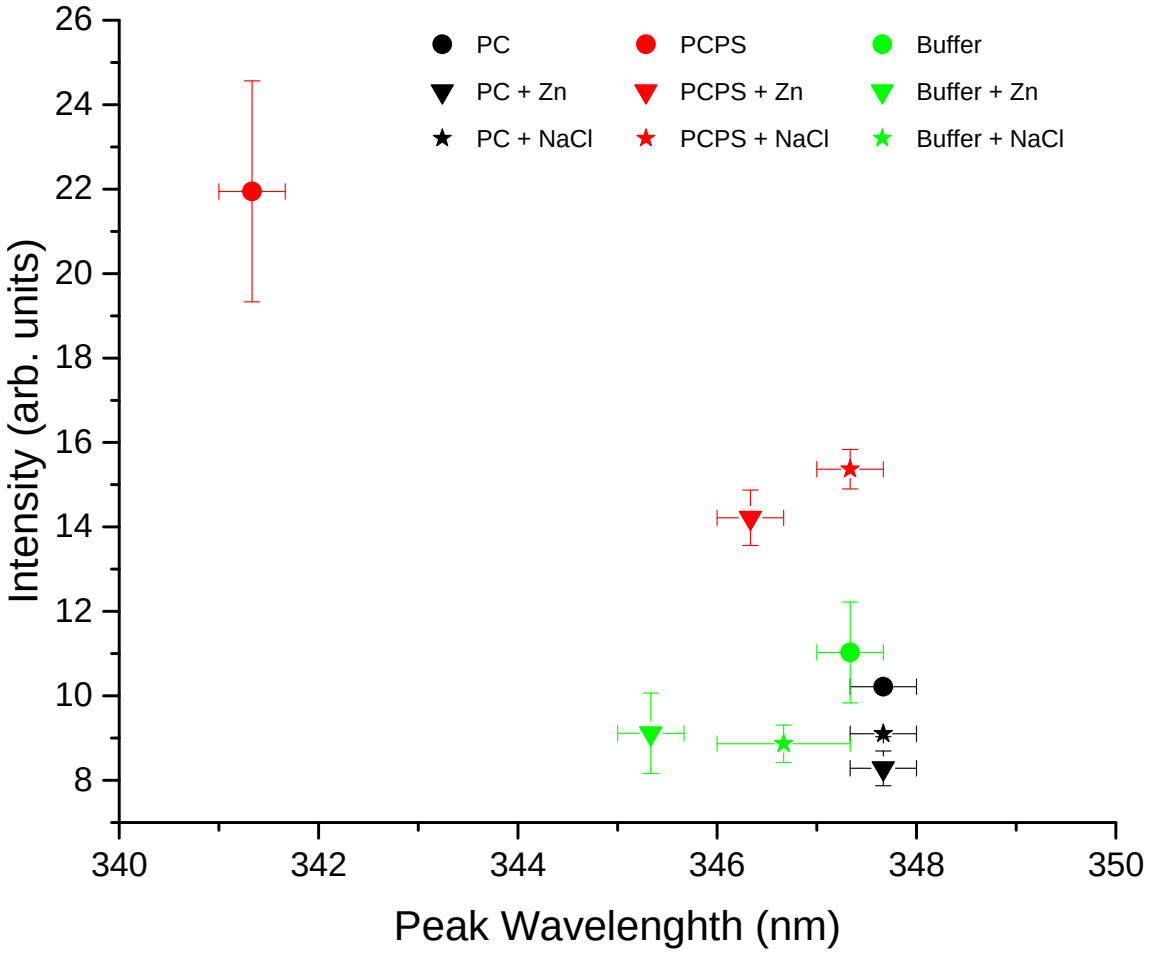

Figure 3.11. Peak wavelength vs intensity scatter plot. The peak value is created from averaging the peak values of 3 replicates. The significance between buffer alone and with varying lipids and conditions was tested using one-way ANOVA with Tukeys mean comparison. For each point error bar indicates SEM for n=3.

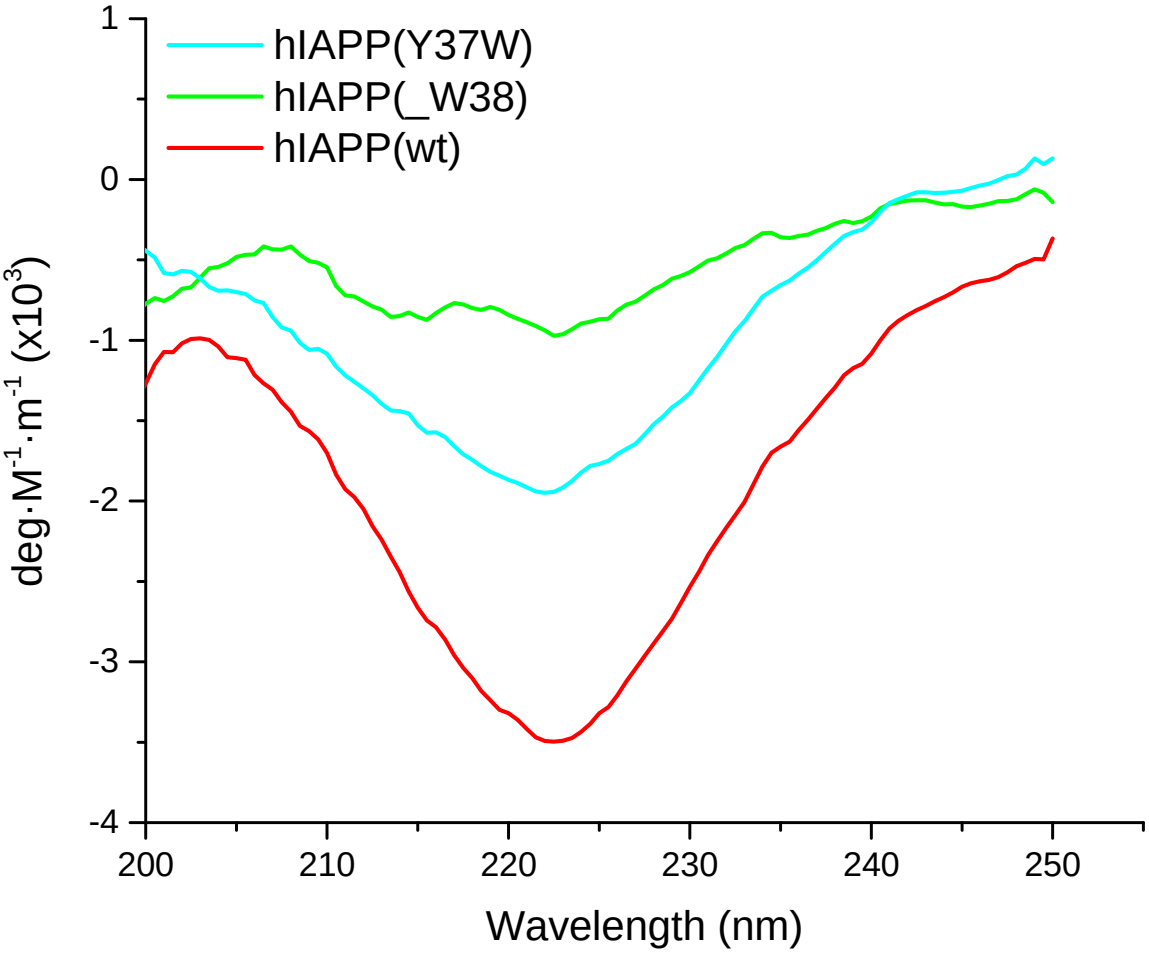

Figure 3.12. Confirmation of β sheet structure for hIAPP variants by CD. 4.2 μM hIAPP(Y37W), hIAPP(W38), hIAPP(wt), from a TFA prepared stock (2 mg/ml), were seperately added to phosphate buffer (20 mM, 7.4 pH) and incubated at ambient temperature for 1 hour. CD spectra were subsequently measured.

sodium chloride (NaCl) and zinc both abrogate this blue shift leading to no significant difference to buffer alone. However, there is a significant difference in intensity of hIAPP(Y37W) incubated with PCPS in the presence of NaCl and zinc compared to buffer alone. According to peak wavelength, there is no burial of Trp at the experimental time point of 10 minutes for liposomes composed of PC under any conditions.

3.5 Discussion

The effect that changing the aromatic residues of IAPP has on its folding in solution has been explored by others but has not generally been considered in the context of lipid membranes. The substitution of one aromatic for another (Y37W) has the

effect of reducing the lag time before the onset of rapid assembly (fig. 3.5). Previous work has been undertaken exploring the effect of substitution of aromatic residues on the kinetics of hIAPP fibrillization. Tu and Raleigh (2013) compared fibrillization kinetics of hIAPP variants with each of the three naturally occurring aromatic amino acids substituted, in turn, with leucine: IAPP(F15L), IAPP(F23L) and IAPP(Y37L). In comparison with hIAPP(wt), F15L resulted in a decrease, F23L caused an increase and Y37L resulted in an even greater increase in lag time. Therefore a tyrosine to tryptophan substitution (hIAPP(Y37W)), which constitutes a change to a more aggregation prone amino acid, might be expected to accelerate fibrillization. Indeed this is borne out in the date where hIAPP(Y37W) fibrillizes more quickly then the hIAPP(wt) (fig. 3.5). Although substitution of hIAPP(Y37W) results in a shorter lag time before the onset of the growth phase, the same plateau is reached indicating that the same amount of fibrillar material is produced. On the other hand, addition of tryptophan to hIAPP (hIAPP(W38)) affects amyloid formation resulting in a considerably longer lag time. In the absence of an explanation for this finding from existing literature, it could be suggested that an additional hydrophobic aromatic residue might interfere with Histandine(18)-Tyrosine(37) interactions. However, previous studies by Tu et al. (2014) using C-terminus amidated IAPP variants that contain the fluorescent TyrPhe analogue, 4-cyanophenylalanine, argue that the aromatic side chains remain solvated during the lag phase and suggest that aromatic-aromatic interactions involving Tyr-37 or interactions of Tyr-37 with a neutral His do not develop during the lag phase (Marek et al., 2008). Again, use of p-cyano substitutes for time resolved fluorescence assays and SternVolmer quenching indicated that significant sequestering of aromatic side chains does not occur until β sheet structure has developed, sufficient to bind ThT (Marek et al., 2010).

I do not have data regarding the absolute position of the C-terminal within the membrane, so it is difficult to draw conclusions about the role of the C-terminal. However, addition of tryptophan in the form of hIAPP(W38) results in a longer lag time as well as a lower signal at plateau. The reason for this is not completely

clear. The presence of the C-terminal tryptophan might make it more difficult for C-terminus to interact with other hIAPP peptides to form oligomers cable of membrane leakage. Clearly the structure of lag phase intermediates is important. The role of aromatics in peptide fragments have also been explored, however their relevance to full length peptide is not so clear. (Milardi et al., 2011) use a 12-18 fragment of IAPP to investigate the role of neutral lipid (DMPC) on fibrillization. hIAPP(wt) fibrillization was accelerated by DMPC without salt.

So far we have considered the effect of negatively charged lipid membranes, that is binary compositions of zwitterionic POPC and negatively charged POPS. In my experiments concerning hIAPP incubated in buffer only, the addition of NaCl resulted in a reduction in the lag time. Inclusion of liposomes composed only of PC, together with the addition of NaCl, resulted in an even greater acceleration in the kinetics of hIAPP fibrillization, consistent with an additive effect. The presence of PC liposomes alone did not have the same accelerating effect. Thus this data indicates that the presence of NaCl makes interaction of peptide with neutral membrane more favourable. A couple of groups have provided evidence for C-terminal interaction with lipid membranes through molecular dynamics. Qian et al. (2016) show that the adsorption process of monomeric hIAPP to bilayers composed of either zwitterionic (POPC) or anionic lipids (POPG) is different. They found that biding of hIAPP to POPC with 0.1 M salt resulted in IAPP that had a more restricted C-terminus, with burial into the membrane; use of negatively charged POPG resulted in C-terminus that was more free. Through molecular modelling it was also shown that under low pH condition, His-18 acts as an anchor, limiting the flexibility of the amyloidgenic region of the C-terminus. At neutral pH, His-18 is not protonated and it is thought that this allows the C-terminal region to be more flexible and therefore might contribute to the acceleration of fibrillization (Skeby et al., 2016). The result of the tryptophan burial data of hIAPP(Y37W) are not in line with this. The only condition that results in burial of the C-terminus is PCPS lipid in 20 mM HEPES. In the other conditions this suggest that the C-terminus is more free.

The results from my experiments also contrast with those from other studies, Caillon et al. evaluated lipids of various charges and chain lengths, and in various membrane geometries, for their effects on the fibrillization and secondary structure of hIAPP and their results differed from mine. They found using a ThT assay that compared with a lipid free system, addition of POPC liposomes resulted in an increase in lag time (Caillon et al., 2013). However, lag times calculated from changes in β-structure determined by CD, showed a reduction in lag time of hIAPP fibrillization incubated with POPC as compared to a lipid free environment. There is no explicit attempt to address this inconsistency but it is important to acknowledge that differences in experimental observations may be due, in part, to the use of peptide dissolved in different solvents; peptide prepared from a DMSO stock was used in the ThT assay and peptide from a HFIP sock was used in CD measurements. There has been consideration of the effects of different solvents on membranes. Indeed, Miranker et al., when first investigating the role of lipids on IAPP assembly, adopted DMSO as the solvent of choice since HFIP was shown to accelerate both fibrillization of hIAPP as well as perturb lipid membranes at low V/V% (Knight and Miranker, 2004).

Interestingly it has been shown that leakage of DMPC LUVs is possible after incunation of hIAPP(wt) and that there is a lag phase before initiation of leakage which seems to correlate with ThT fibrils growth (Milardi et al., 2011). Aβ has also been found to perturb PC membranes (de Planque et al., 2007). Kinnunen et al. (2015) show, like many others, that PC only liposomes, specifically SOPC slows down fibrillization in comparison to bulk. Addition of NaCl in the absence of lipid results in a decrease in lag time for fibrillization (Marek et al., 2012).

In conclusion, we find that changes to the peptide that might be considered to be minor can profoundly effect the fibrillization and membrane perturbation potential of hIAPP. In the next chapter we report a novel type of membrane perturbation not currently attributed to hIAPP, that of lipid mixing and membrane fusion.

Chapter 4

Lipid Mixing

4.1 Introduction

The preceding chapter concerned itself with establishing the interaction of IAPP variants with lipid membranes and resultant leakage. In this chapter I describe the ability of hIAPP to cause lipid mixing between liposomes, an effect not previously ascribed to hIAPP. A correlation between lipid mixing and fibrillization is also discussed. Additionally, I show that the process of lipid mixing can be modulated through the use of the zinc.

A recent publication points to hIAPP being capable of inducing curvature in lipid membranes (Kegulian et al., 2015) and hIAPP was found to have a preference for membranes with high negative curvature (Smith et al., 2009); such behaviour is consistent with an ability to induce lipid mixing between membranes, and indeed fusion of liposomes. Induction of fusion between membranes has been described for fragments of amyloid proteins including C-terminus of Aβ (Vestergaard et al., 2013), prion (Pillot et al., 1997; Dupiereux et al., 2005) and α-synuclein (Fantini et al., 2011). Full length α-synuclein has been shown to induce curvature of membranes (Braun et al., 2012; Varkey et al., 2010; Westphal and Chandra, 2013). However, there is no report of liposome fusion in vitro induced by a physiological, full length, amyloid peptide. Unwanted fusion between membranes can be expected to have disastrous consequences for the cell and fusion between organelles, for

example the secretory granule and lysozyme, has been shown to be a contributor to the pathology of lyposomal storage disorders (Park et al., 2016).

4.2 Results

4.2.1 Basics of FRET and assay concept

In order to investigate IAPP induced fusion, a FRET based assay was employed. The concept and uses of FRET in the context of membrane fusion are well described (Loura and Prieto, 2011; Marsden et al., 2011; Yoon et al., 2006; Kyoung et al., 2013) but a brief explanation is pertinent. Implicit in the name, FRET involves the transfer of energy from a donor fluorophore to an acceptor fluorophore. The resonance term relates to how well the emission spectrum of the donor and the excitation spectrum of the acceptor overlap; the larger the overlap, the more efficient the transfer will be. For an idealised FRET pair, excitation of the donor would lead to almost complete transfer of energy to the acceptor, without any radiative emission from the donor.

With the appropriate model, Foïster distances can be calculated and appropriate distance constants can be obtained for a given interaction between donor and acceptor fluorophores. Measurement of FRET can be done either by measuring steady state intensities of acceptor and donor emission or measuring lifetime of the donor fluorescence. For my purposes, relative measurements of FRET were sufficient to follow the kinetics of lipid mixing and so an intensity based assay was used.

4.2.2 Ratifying the assay

There are a variety of lipid mixing assays employing FRET-based readouts that have been used, particularly in the study of snare mediated fusion of liposomes (Yoon et al., 2006; Zick and Wickner, 2014; Zucchi and Zick, 2011). Lipid mixing assays are often used to follow fusion between membranes and, for the purposes of investigating IAPP fusion, I chose to use a FRET lipid mixing assay with the lipophilic fluorophores DiO and DiI, as donor and acceptor, respectively. Although

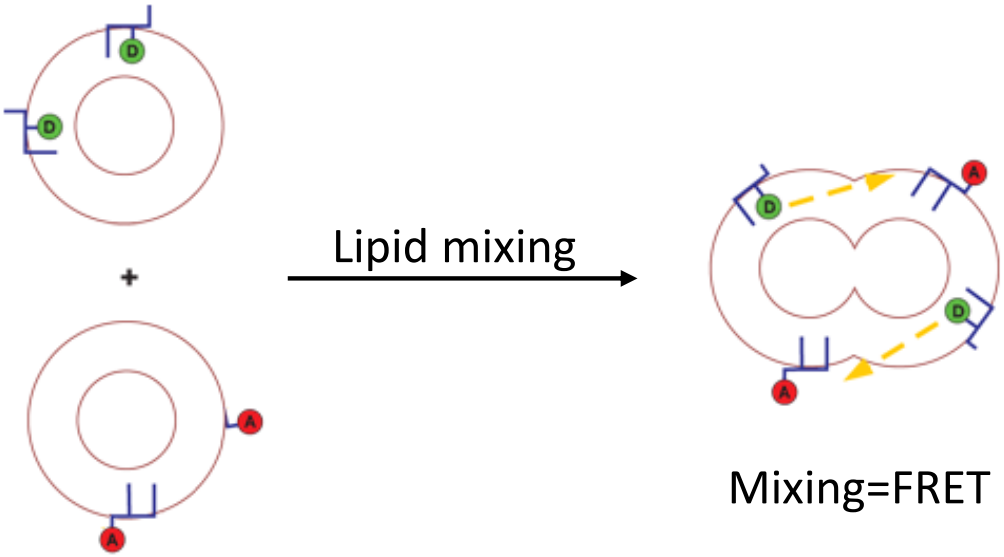

Figure 4.1. Cartoon of lipid mixing assay. Two populations of liposomes are mixed toegther. One population has donor fluorophores (D), shown in green circles, in the lipid membrane and the other liposome population has acceptor fluorophores (A), shown in red cricles. When D and A fluophores are brought close enough together, due to lipid mixing by fusogenic peptide, FRET between D and A is possible (shown by yellow arrow). Subsequently, direct excitation of D results in a simulatenous decrease of its own emission and an increase in emission from A.

FRET-based lipid mixing assays are relatively well established, there are a few caveats that need to be considered when designing an assay. In particular certain aspects relating to the mixing of fluorophores with lipids became apparent and warrant a brief explanation.

Initially the use of a dye to lipid ratio of 1:1000 was used, resulting in relatively poor signal to noise (S/N) ratios. In order to keep consistency between methods in terms of lipid concentrations but to increase the signal to noise ratio, this was eventually increased to 1:20. Secondly, there was a concentration dependent effect in the ability of the dye to incorporate into lipid, since preparation of lipid films with identical proportions of dye, but dried from differing amounts of added solvent, resulted in liposomes preps with significantly different fluorescence intensities. This was taken into account when producing liposome with varying amounts of lipid.

Such high ratios of dye to lipid are not uncommon, especially in dequenching approaches, but in order to rule out changes in fluorescence other than lipid mixing,

a few control experiments were undertaken. To exclude the possibility of micellised donor and acceptor dyes interacting due to amyloid formation, donor and acceptor populations of dyes were prepared without lipid and incubated with the relevant peptide. A low fluorescence emission from dye without lipid is expected since the fluorescence emission of carbocyanine dyes are known to increase many-fold when incorporated into lipid. In this case the acceptor and donor signals, before addition of peptide, were negligible compared to lipid preparations containing dye. Importantly, there was no significant change in the donor signal, demonstrating no mixing of fluorophores took place.

As mentioned, intensity based measurement of FRET can be done using either a decrease in donor fluorescence emission or an increase in acceptor emission. Increase in acceptor emission under 'FRET excitation' conditions is often used to follow FRET. It was found that donor emission would increase when incubated with non-fluorophore liposomes. Because the precise density of fluorophores in liposome membranes was unknown and the uncertainty of how lipid mixing would change fuophore density, I decided to use a decrease in donor emission as a measure of FRET and, by extension, a measure of heterotypic mixing of lipid vesicles. An idealised population of liposomes, composed of DiO and DiI was used to represent the maximum amount of lipid mixing; in this case the individual F:L ratios would change from 1:20 before lipid mixing fusion to to 1:40 after lipid mixing.

The non-amyloid peptide mastoparan which was previously shown to cause leakage of PCPS liposomes, was demonstrated to cause lipid mixing of liposomes of the same composition (fig. 4.2, upper panel). Mastoparan has previously been shown to cause fusion of liposomes (Yandek et al., 2009) and so it is used here as a positive control. Concurrently, a separate population of liposomes was incubated with mastoparan and the intensity of ThT was measured without an increase indicating a lack of fibrillization as expected (fig. 4.2, lower panel). The quenching was very rapid and already reaches 60% during the dead time of the measurement. These experiments confirmed mastoparan caused lipid mixing without formation of amyloid.

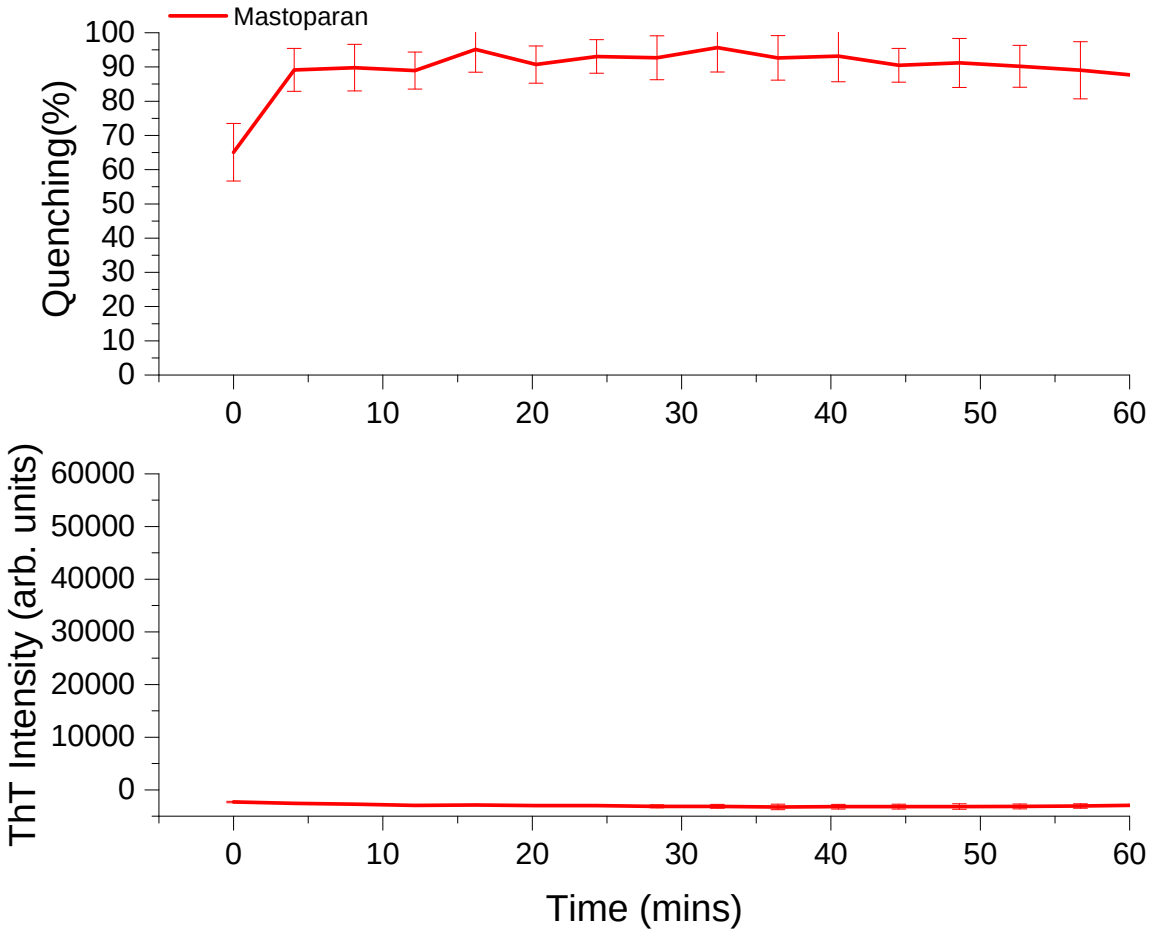

Figure 4.2. Mastoparan causes fusion of negatively charged liposomes. Kinetics of lipid mixing (upper panel) and fibrillization (lower panel) over 1hr as result of the addition of 25 μM mastoparan to 50 μM liposomes. For each curve error bars represent SEM (n=3).

4.2.3 Examining fusion of negatively charged liposomes

Next we wanted to establish whether hIAPP and rIAPP could cause lipid mixing of negatively charged liposomes. hIAPP(wt) is capable of causing lipid mixing of PCPS (fig. 4.3, upper panel), displaying a kinetic profile that mirrors fibrillization, indicating in this case that formation of fibrils is needed for lipid mixing. rIAPP does not cause fusion and, as expected, does not produce fibrils (fig. 4.3, lower panel). The use of DMSO at 0.81% v/v does not cause any lipid mixing. Even though DMSO is not known to cause membrane perturbation to same degree as commonly used solvent HFIP (Knight and Miranker, 2004; Wang et al., 2014) it was important to establish that DMSO at this concentration did not cause lipid mixing. It is clear that at this concentration DMSO does not affect the membrane in a way that favours lipid mixing; in addition, it has no effect on the fluorescence emission of ThT.

Next we looked at the influence of high ionic strength in the form of 100 mM NaCl. As rIAPP did not exhibit a lipid mixing ability, we continued only with hIAPP variants when investigating the influence of various ionic factors. It is clear that NaCl has the effect of retarding the emergence of lipid mixing. Again this kinetic profile is mirrored in fibrillization, with an increase in the lag phase. The presence of NaCl alone has little effect on lipid mixing. Interestingly, the presence of NaCl has the effect of lowering the ThT intensity at which the growth curves plateau, suggesting a lower amount of fibril mass at steady-state.

Addition of zinc has a modulatory effect on lipid mixing. The presence of 500 μM of zinc results in a dramatic change in the lipid mixing kinetics of negatively charged PCPS liposomes induced by hIAPP(wt), with a clear transformation from a sigmoidal profile with a lag phase to one of mono-exponential growth. There is also a profound effect on fibrillization, with a complete absence of any fibrillization as measured by ThT fluorescence.

One concern was that the presence of zinc interferes with the ThT assay. From the groups that have used zinc in ThT assays Brender et al. (2010) visualised the effect of high concentration of zinc on hIAPP using EM. They found that there was a

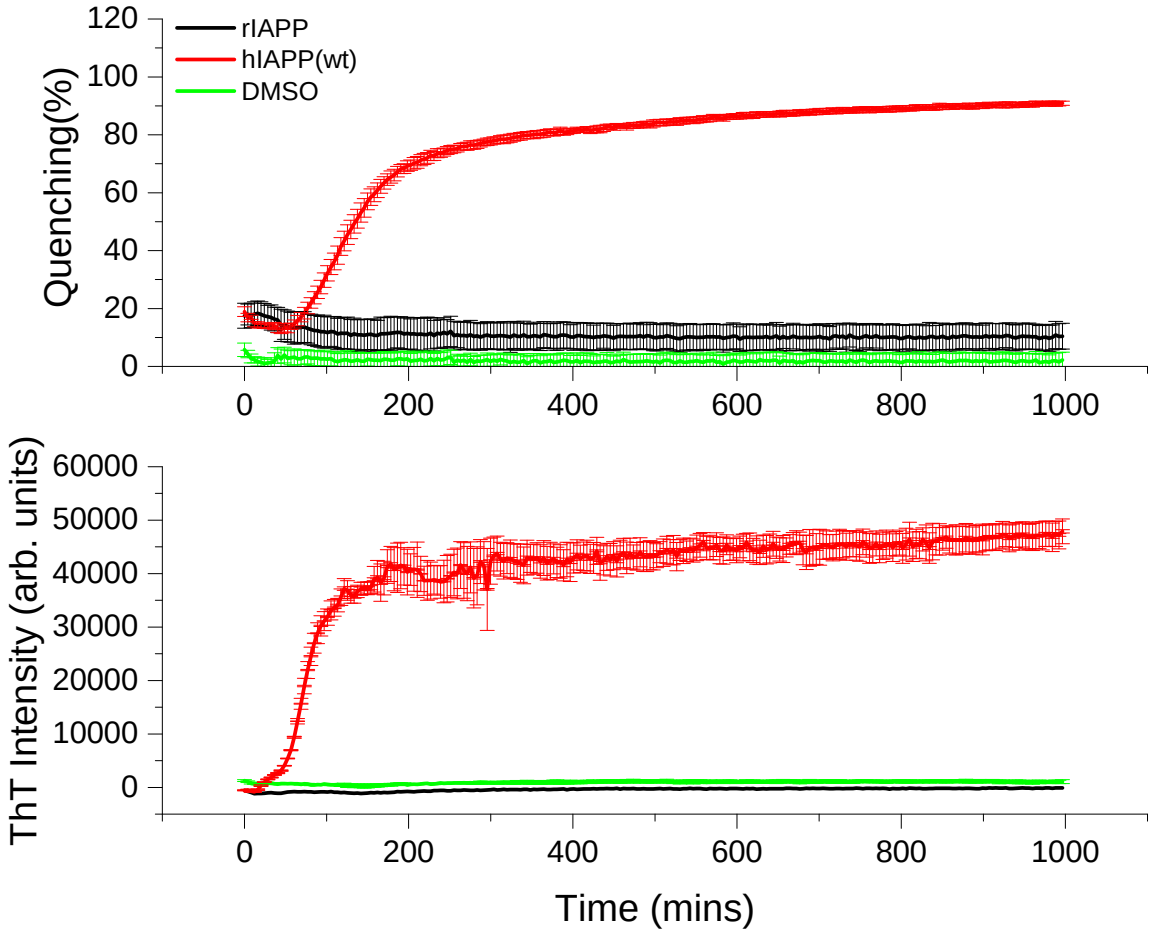

Figure 4.3. Ability of hIAPP and rIAPP to cause lipid mixing of negatively charged liposomes. Kinetic traces of lipid mixing (upper graph) and fibrillization (lower graph) of rIAPP and hIAPP (4.2 μm) incubated with negatively charged populations of DiO and DiI liposomes (total lipid concentration 50 μM. Each curve represent n=3 and error bars are the SEM).

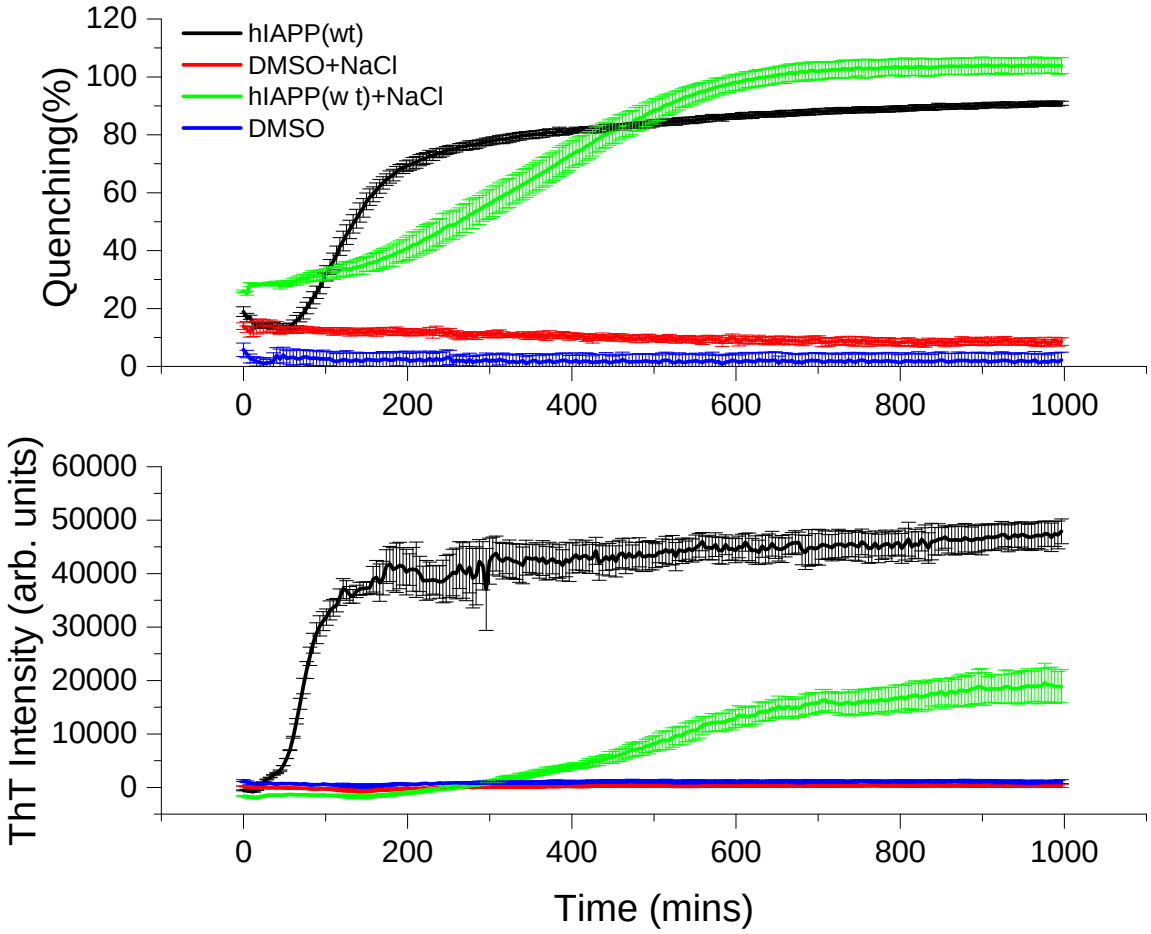

Figure 4.4. Effect of high ionic strength on fibrillization of hIAPP(wt) and lipid mixing of negatively charged liposomes. hIAPP(wt) (4.2 μm) incubated with DiO and DiI liposome populations (total lipid concentration of 50 μm), with and without 100 mM of NaCl. Kinetic trace of lipid mixing (upper panel) and fibrillization (lower panel). Each curve represent n=3 and error bars are the SEM.

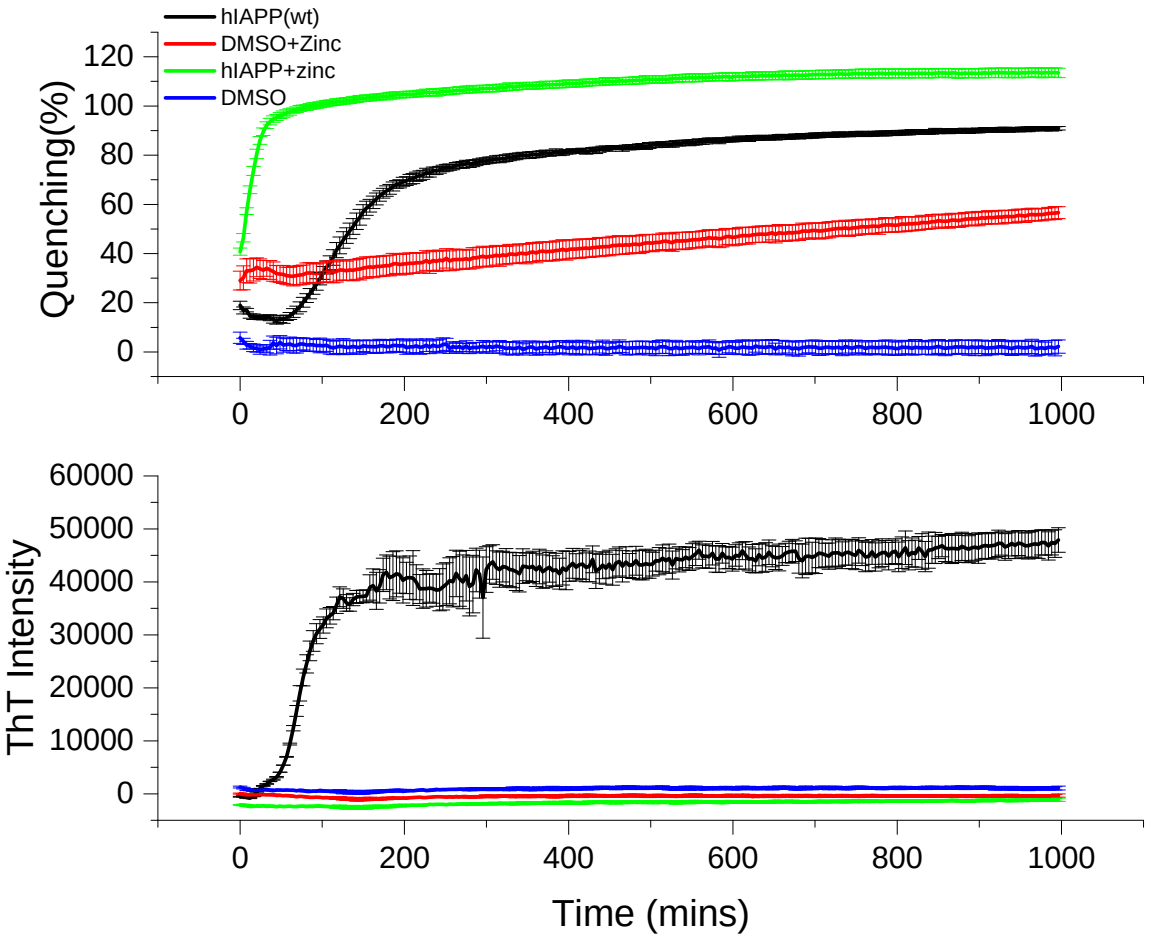

Figure 4.5. Zinc accelerates lipid mixing of negatively charge PCPS liposomes whilst blocking fibril formation. hIAPP(wt) (4.2 μM) incubated with DiO and DiI liposome populations (total lipid concentration of 50 μM), with and without 500 μM of $ZnCl_2$. Kinetic traces of lipid mixing (upper panel) and fibrillization (lower panel). Error bars for each curve represent SEM (n=3).

substantial reduction in fibrils in the presence of zinc consistent with the results using zinc in ThT assays. I additionally confirmed that there was no effect of zinc on the ThT assay by producing IAPP fibrils and subsequently adding ThT in the presence and absence of zinc. In both cases there was an increase in emission, consistent with zinc not interfering with ThT binding to fibrils.

Several different concentrations were used to further examine the effect of zinc on lipid mixing. Concentrations of 0, 50 and 200 μM zinc resulted in the same change in kinetics. Control reactions with zinc show a gradual increase from baseline, but the summation of the percentage change from hIAPP and zinc separately is less than when combined. This indicates that it is the combined effect of hIAPP and zinc that is responsible for acceleration of fusion. However it is only possible to draw a conclusion regarding the effect of zinc up to a concentration of 500 μM. At higher concentrations, the contribution of zinc to lipid mixing was at a level that the sum of percentages of lipid mixing from peptide and zinc alone was equal to peptide and zinc together. Therefore, it is not possible to draw conclusions about how zinc modulates lipid mixing at concentrations higher than 500 μm. However, at the lower concentrations it is clear that zinc has a major effect in shifting the kinetic profile of lipid mixing.

I also wanted to check that hIAPP(Y37W) was able to cause lipid mixing and was also amenable to modulation by zinc (fig. 4.7,top panel)). Indeed, hIAPP(Y37W) does cause lipid mixing and correlates with the kinetics of fibrillization. Similar to hIAPP(wt), the addition of zinc to hIAPP(Y37W) has a major accelerating effect, resulting in transformation to mono-exponential kinetics. The presence of zinc also abolishes fibrillization of the hIAPP(Y37W).

Since hIAPP(W38) did not mirror the fibrillization and leakage kinetics of hIAPP(wt) (Chapter 3), its relevance to pathological or physiological fusion was not a primary interest. However, it was of interest to see if the addition of tryptophan resulted in a change in fusogenic potential in line with its effect on leakage kinetics the ability of hIAPP(W38) to induce lipid mixing is substantially reduced compared to both

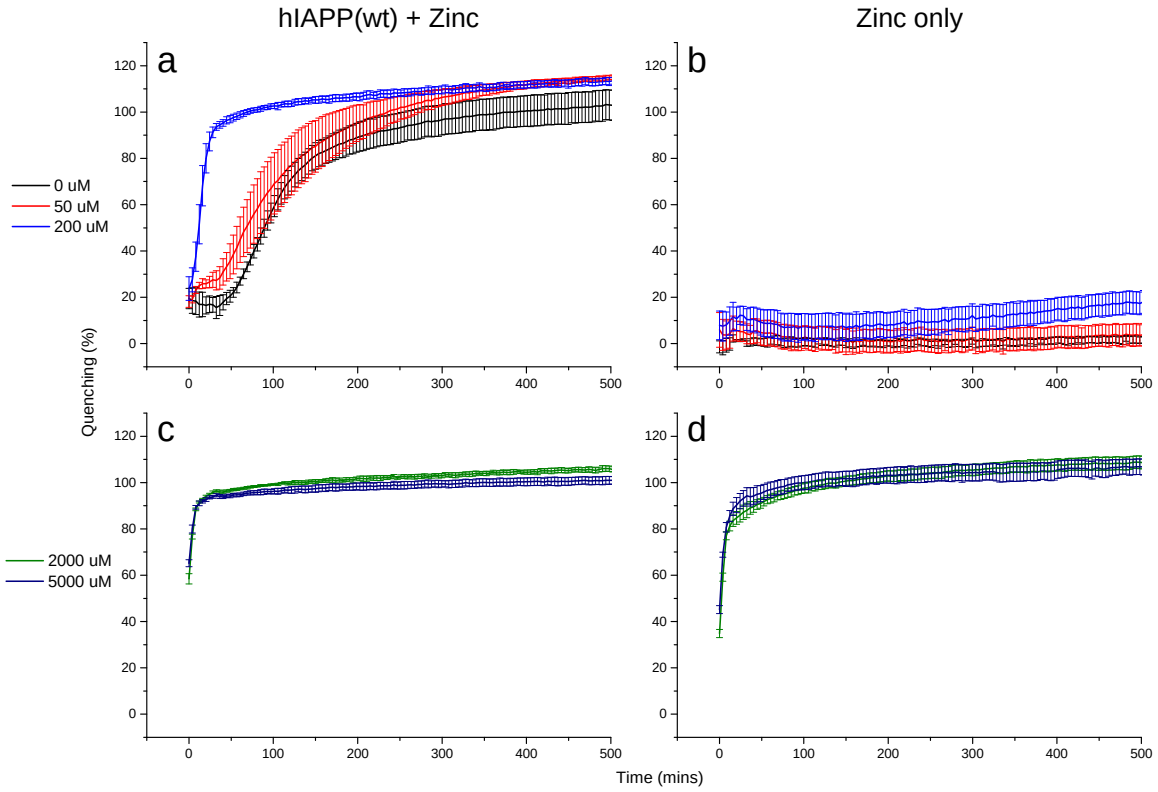

Figure 4.6. Effect of different concentrations of zinc on hIAPP(wt) induced fusion. Two populations of PCPS liposomes (DiO and DiI) were incubated with various concentrations of $ZnCl_2$ with hIAPP(wt) (a and b) and without hIAPP(wt) (c and b). Error bars for each curve represent SEM (n=3).

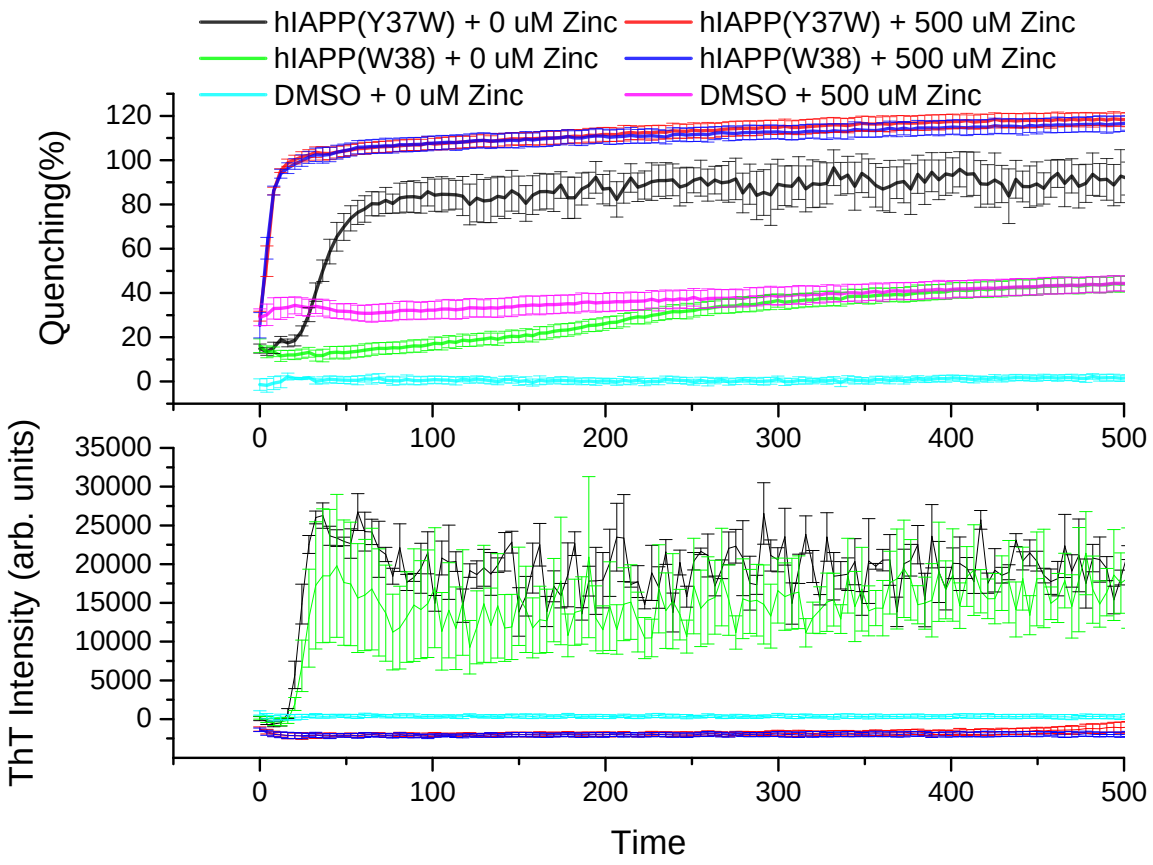

Figure 4.7. Tryptophan variants also cause lipid mixing of negatively charged lipids. Donor(DiO) and acceptor(DiI) populations of PCPS liposomes incubated with 4.2 μM of hIAPP(Y37W) or hIAPP(W38), in the presence or absence of $ZnCl_2$. Lipid mixing (upper panel) and fibrillization (lower panel). Error bars for each curve represent SEM (n=3).

hIAPP(wt) and hIAPP(Y37W) (fig. 4.7, top panel). The reduced capacity for lipid mixing is in line with a reduced capacity to induce leakage, as well as a reduced potential for fibrillization. As is apparent, the ThT emission is a more noisy than in previous kinetics traces for fibrillization. The issues in reproducibility of ThT assays and the stochastic effects on kinetics have been discussed in the literature (Hudson et al., 2009; Giehm and Otzen, 2010; Eisert et al., 2006) attention. In the case of hIAPP(W38) and hIAPP(Y37W), there appears to be slightly more variability in the fibrillization profiles than with hIAPP(wt).

4.2.4 Neutral liposomes

In the previous chapter we see that the presence of neutral liposomes in the presence of high ionic strength results in an acceleration of fibrillization. For completeness, I investigated whether the presence of high ionic strength and zinc resulted in induction of lipid mixing of neutral liposomes by IAPP.

As expected, there was no increase in quenching, suggesting that there is no lipid mixing. Instead there is a decrease in the quenching, resulting in negative percentage values. There are a few possible reasons for this. One explanation is that DiO in PC only liposomes is arranged in the membrane in such a way that its fluorescence is quenched. Upon addition of DMSO, for example, there is a rearrangement such that DiO molecules are not quenched, raising the intensity of DiO, resulting in negative percentage value for quenching. Negative values for the percentage of quenching are seen again with the addition DMSO and NaCl together. Interestingly, addition of hIAPP(wt) removes the effect of NaCl. The acceleration in hIAPP(wt) fibrillization with the addition of NaCl shown previously in Chapter 3 is reproduced here together with the trace for lipid mixing. Despite an increase in ThT emission consistent with fibrillization, there is no lipid mixing, evidenced by no increase in quenching. The effect of zinc on lipid mixing of PC vesicle is shown in figure 4.10. In this case there is no fibrillization or lipid mixing. Although there is still an effect in the form of a negative value for quenching from the addition of zinc alone (fig. 4.10), it is not as

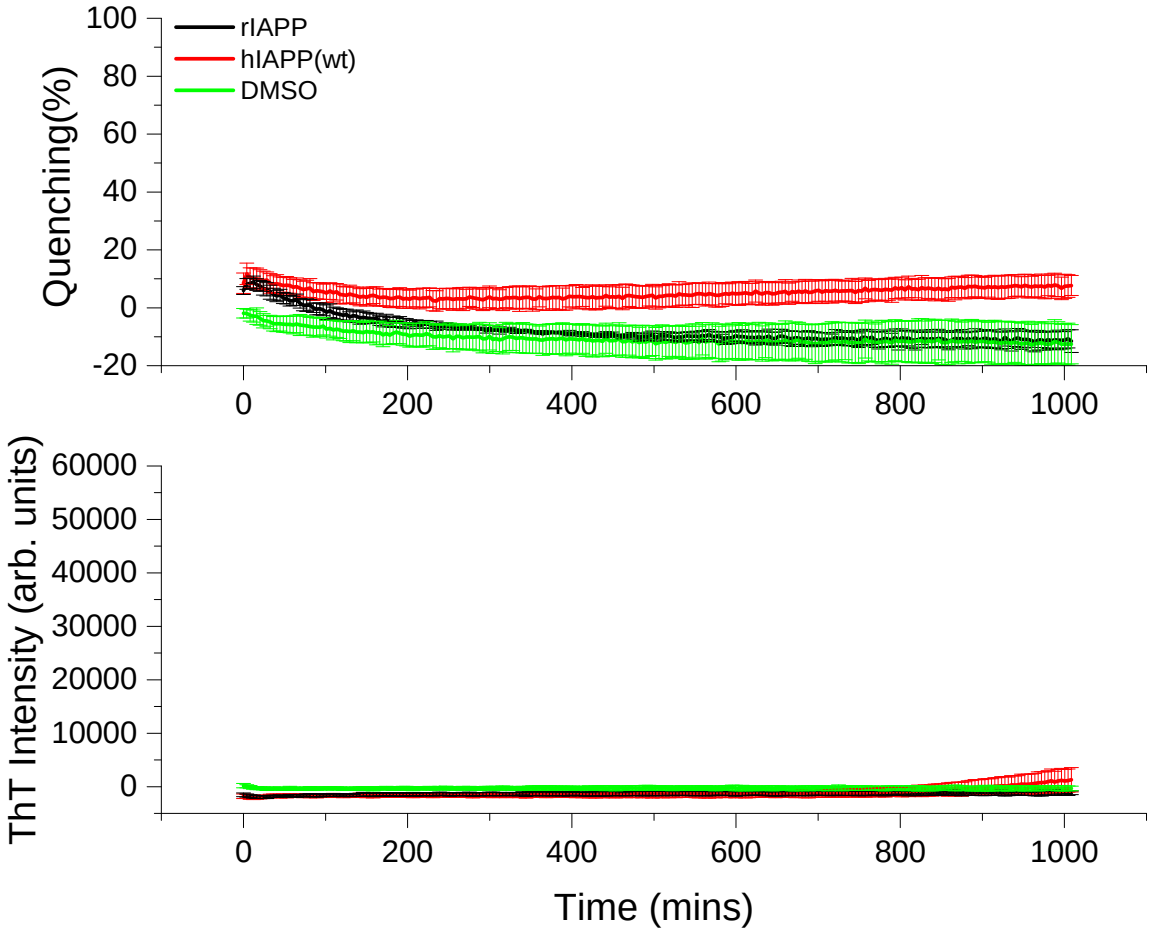

Figure 4.8. hIAPP and rIAPP are not able to cause lipid mixing of neutral membranes. Donor(DiO) and acceptor(DiI) populations of PC liposomes (50 μM) were incubated with 4.2 μM of hIAPP(wt) or rIAPP(wt); lipid mixing (upper panel) and fibrillization (lower panel). Error bars for each curve represent SEM (n=3).

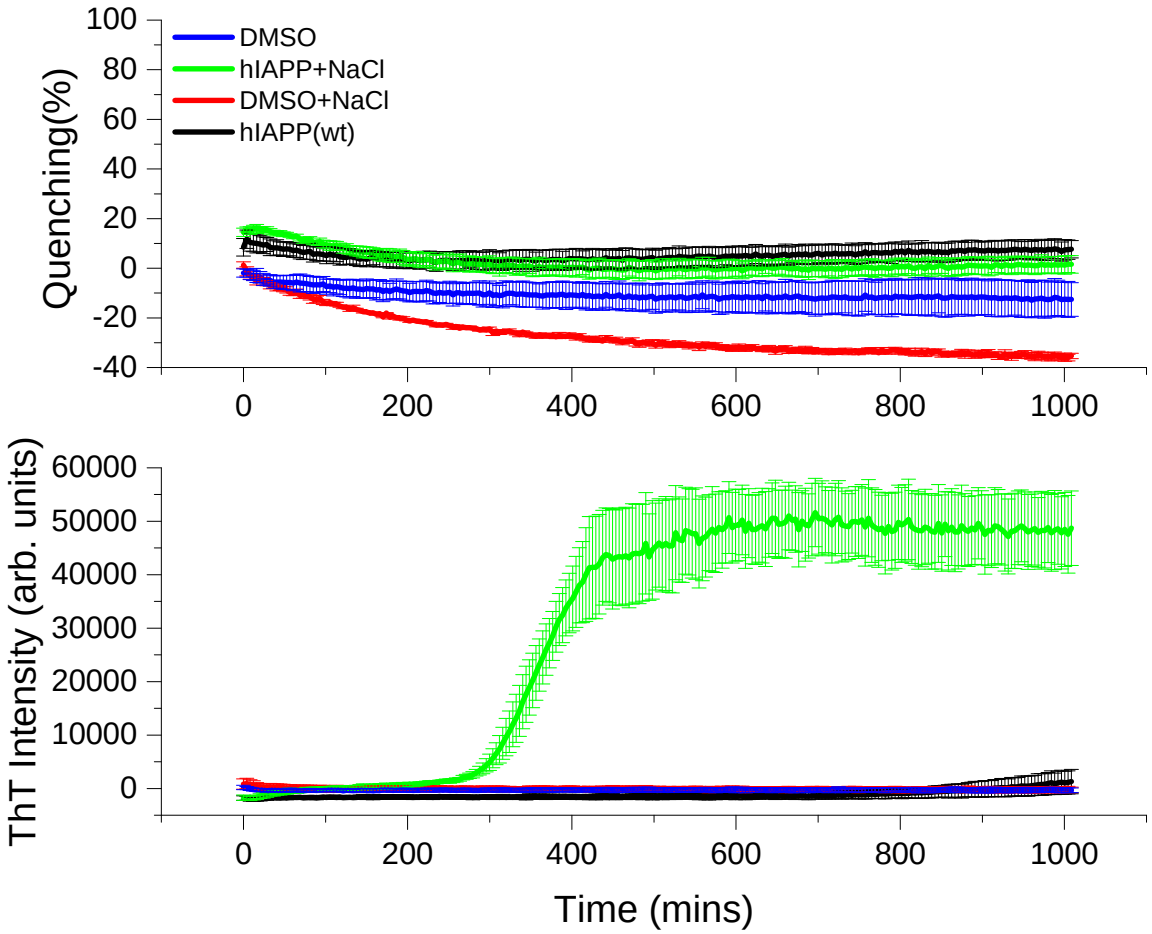

Figure 4.9. Addition of NaCl does not enable lipid mixing of PC liposomes by hIAPP(wt). Donor(DiO) and acceptor(DiI) populations of PCPS liposomes (50 μM) incubated with 4.2 μM of hIAPP(wt), in the presence or absence of 100mM NaCl; lipid mixing (upper panel) and fibrillization (lower panel). Error bars for each curve represent SEM (n=3).

profound as that with NaCl (fig. 4.9). It is unclear why there is negative quenching but one possibility is that the DiO and DiI partition differently in different order domains (Baumgart et al., 2007).

4.2.5 Evidence of content mixing

Having established lipid mixing, it was of interest to see if content mixing was taking place. Throughout this chapter I have referred to lipid mixing and not explicitly to fusion. This is because although lipid mixing is consistent with fusion taking place, transfer of lipid form one bilayer to another can take place through the hemi-fusion. Although it is common to use evidence of lipid mixing as the sole identifier of fusion, we decided to investigate whether there was content mixing

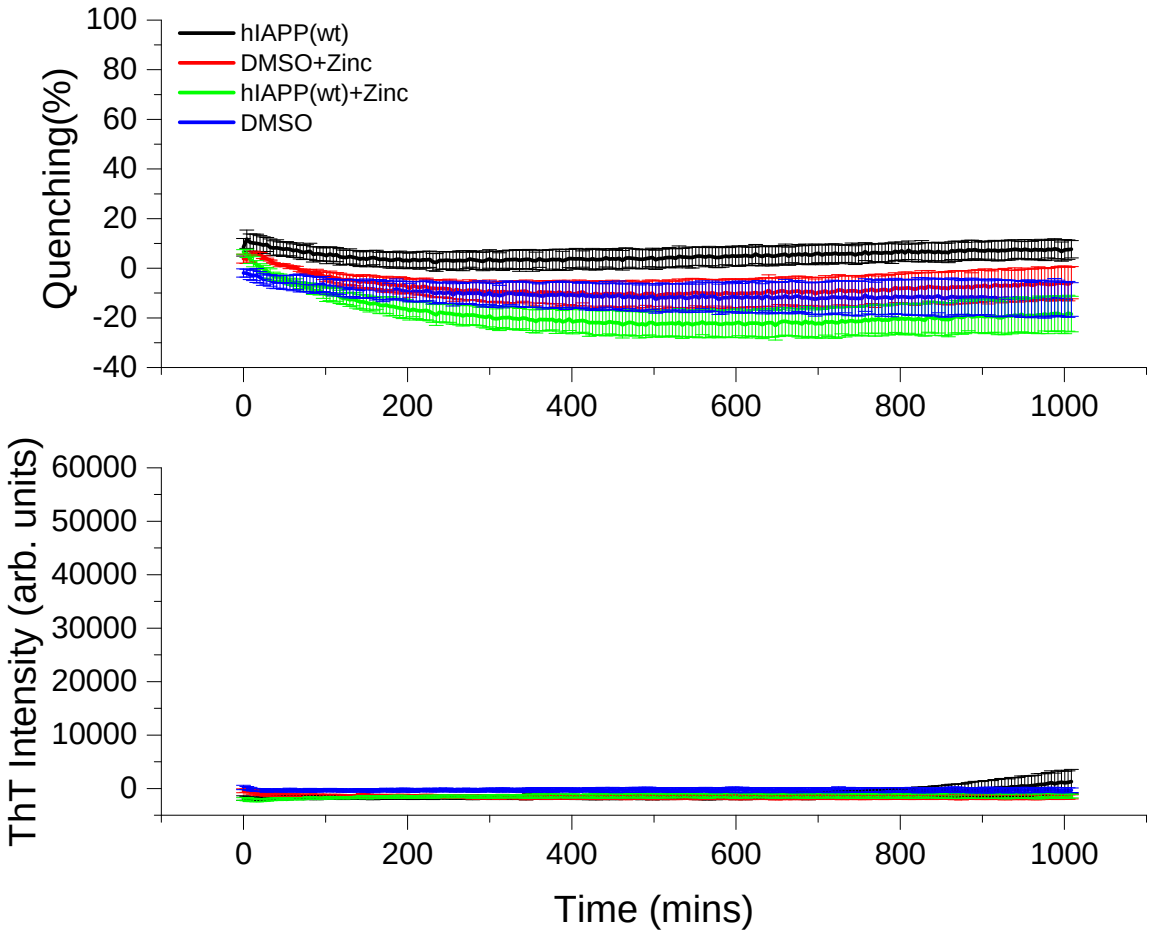

Figure 4.10. Addition of zinc does not enable lipid mixing of PC liposomes by hIAPP(wt). Donor(DiO) and acceptor(DiI) populations of PCPS liposomes (50 μM) incubated with 4.2 μM of hIAPP(wt), in the presence or absence of 100 mM NaCl; lipid mixing (upper panel) and fibrillization (lower panel). Curve represent n=3 and error bars are the SEM.

In order to find evidence for content mixing and also gain information about the structure of the membrane, we decided to use electron microscopy to image liposome populations with different sizes of gold. Fusion resulting from the addition of peptide is visible as the presence of both sizes of gold in a membrane bound structure. Standard negative stain EM was performed.

PCPS liposomes were incubated with mastoparan and it is clear that both sizes of gold are present in the same membrane structure (fig. 4.11). The same PCPS liposome mixture was incubated with hIAPP(wt) (fig. 4.12). The number of gold particles present, of both sizes, is not as high. However, it is evident from both micrographs that the presence of either size of gold particle is associated with liposome membrane. This indicates that different size gold particles are only able to come into apposition

if associated with membranes. This is mostly likely due to induction by the fusogenic peptide but it is also possible that the process of negative staining can cause the appearance of fusion.

To my knowledge this is the first documentation of lipid mixing by hIAPP and as such the dynamics of such a process are unknown. Unlike mastoparan, hIAPP exists in different structural states, evolving from monomer to oligomeric assembles and fibrils. How this affects dynamics of fusion, such as the number of rounds of fusion a particular IAPP assembly can participate in, is unknown. The abundance of gold particles in liposomes incubated with mastoparan may be the result of many rounds of fusion compared to that of hIAPP(wt), where gold particles are not as numerous.

The previous discussion brings me to the more general issue of quantifying a process such as fusion. EM is an extraordinarily good technique for visualising the component dynamics of processes such as fusion on individual particles and at high resolution. Much information about fibrils assembly has been gained from EM. However, it is a necessarily destructive technique with the potential for unexpected artefacts due to the preparation process, particularly for negative stain EM and in relation to structures such as liposomes. Cryo-EM is a modality which offers more protection against such artefacts. However, the use of EM as a tool for following fusion is limited by the number of events that can be viewed. Coupled with the desire to follow kinetics of a process such as fusion, EM does not lend itself to being the first choice modality.

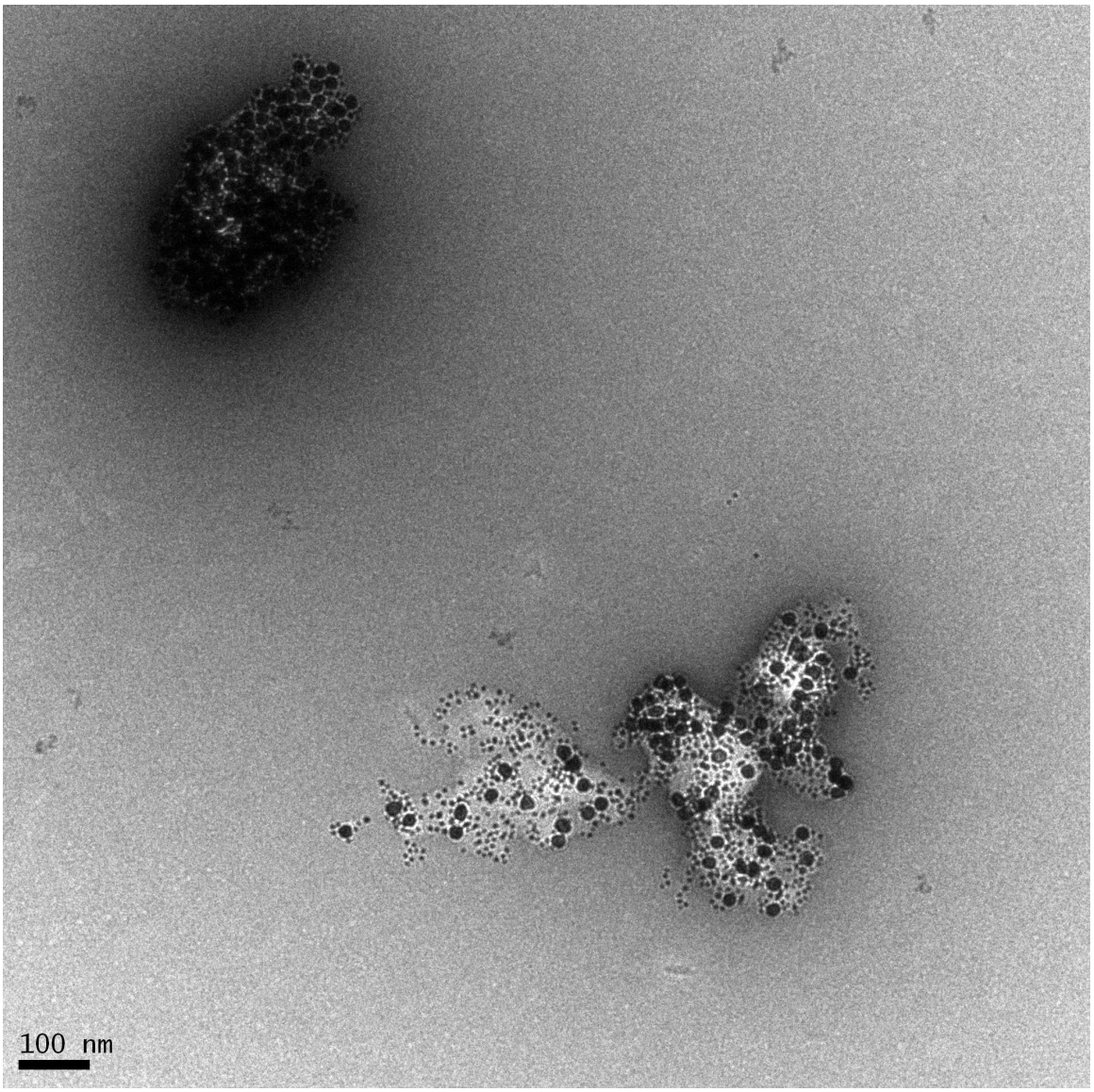

Figure 4.11. TEM micrograph of fused PCPS liposomes after incubation with mastoparan. Liposomes from two different populations, containing 5 nm and 20 nm gold particles, incubated with 25 μM mastoparan. Mastoparan, was incubated with a mixture of liposomes made up from the two populations. In the EM micrograph, two sizes of gold particles can clearly be seen distributed amongst the liposomes.

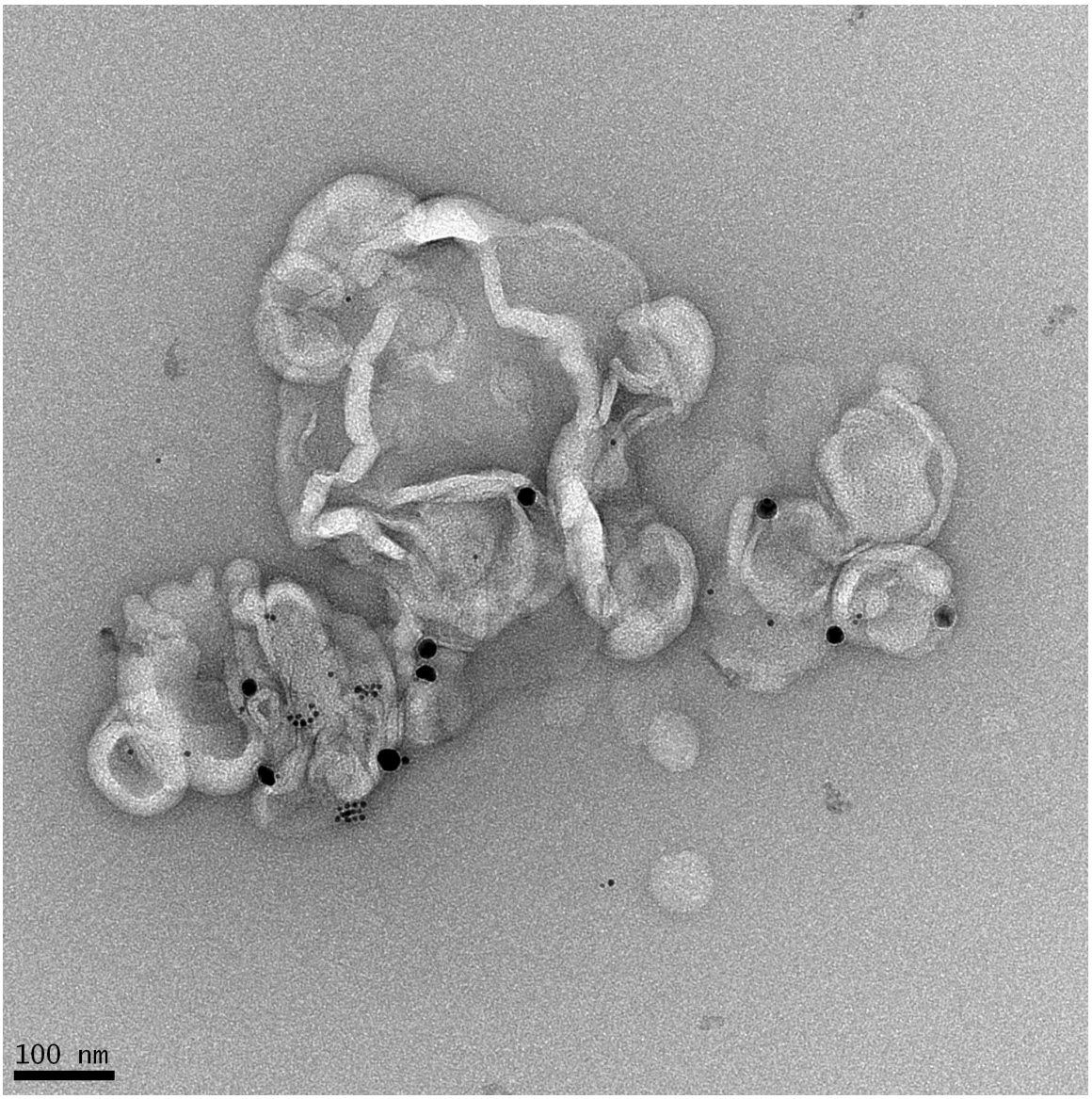

Figure 4.12. TEM micrograph of fused PCPS liposomes after incubation with hIAPP(wt). Two different populations of liposomes containing 5 and 20 nm gold particles were incubated with 4.2 μM hIAPP(wt); evidence of fusion from the presence of both 5 nm and 20 nm in close apposition.

4.3 Discussion

The ability of hIAPP to induce fusion is firstly dependent on the presence of sufficient negative charge in the membrane and secondly, at most a six amino acid difference from rIAPP. This sequence difference involves a difference in structure. From the data, the kinetic correlation between lipid mixing and increase in ThT emission implies that it is due to a change from a structure that is mostly α-helical to one that contains β sheet.

However, there is the possibility of threshold effect. Since the binding of ThT to amyloid causes a change in the spectral properties such that there is a change in fluorescence emission. hIAPP fibrillization is accelerated due to peptide interacting with lipid membrane, therefore it is difficult to separate fusion from fibrillization. Threshold effects of the assay could mean that fusion is actually happening before any fibrillization has taken place but that it is not measurable. Therefore, it is more appropriate to be appropriate to compare Time till half maximal intensity ($t_{\frac{1}{2}}$) rather than lag times. The estimated $t_{\frac{1}{2}}$ value is 130 minutes for lipid mixing of PCPS by hIAPP(wt) and 20 minutes for ThT emission. This implicates formation of assemblies with β sheet structure are important inducing fusion. At this point, one cannot say in what form hIAPP(wt) is fusogenic. Use of hIAPP tryptophan variants provided interesting results with hIAPP(Y37W) and hIAPP(W38) having strikingly different abilities to induce fusion. Both peptides have a sigmoidal kinetic profile but incubation of hIAPP(W38) results in substantially less lipid mixing. We have previously seen that hIAPP(W38) has a reduced ability to form ThT positive material.

As zinc appears at relatively high concentration in the secretory granule (Li, 2014), it was pertinent to explore its effect on lipid mixing. hIAPP with 500 μM clearly results in an acceleration of quenching over hIAPP alone. However, it is clear that zinc alone also hase the ability to facilitate liposome fusion as shown by the slow rise in amount of quenching. Strikingly, acceleration of lipid mixing is not accompanied by any increase in ThT intensity consistent with a lack of hIAPP adopting a β

sheet structure. Interestingly, inclusion of zinc results in a switch in the kinetics of lipid mixing by hIAPP(Y38W) and hIAPP(W38), resulting in near identical profiles. This result suggests that whatever the structure of the assembly that causes lipid mixing, extension of the C-terminus affects its ability to do so. However, addition of zinc results in hIAPP(W38) having the same lipid mixing profile as hIAPP(Y37W), while simultaneously halting fibrillization of either peptide within the timescale of measurement. It seems that zinc interacts with part of the peptide in a way that increases the abundace of species capable of causing fusion, but prevents formation of conformations that bind ThT. Are these structures off-path conformations?.

In solution, it was found that hIAPP rapidly associate into transient low-order oligomers such as dimers and timers (Wei et al., 2011) and perhaps these conformations can be stabilised by zinc. The effect of zinc on hIAPP fibrillization has been examined in solution (Salamekh et al., 2011; Brender et al., 2010, 2013). Salamekh et al. (2011) investigated the effect of zinc on IAPP fibrillization and intermediate structures with the following results. Using an mass spectrometry (MS) approach there was a peak corresponding to the expcted molecular weight of dimeric hIAPP. However, inclusion of zinc inhibited formation of hIAPP dimer and mature fibres while promoting the formation of oligomers. This led them to suggest that zinc supressed natural self-association of the peptide. They state the crystal structure of dimeric hIAPP argues against incorporation of zinc into a helical dimer, since in this structure the His18 is rotated away from the dimer interface. Isothermal titration calorimetry experiments showed that zinc binds to hIAPP with low micro molar efficiency. Since a minimum of three histidines are required to achieve this low affinity and zinc prefers 4-6 ligands, the authors suggest a complex of approximately one zinc for every six hIAPP (Salamekh et al., 2011). A different action of zinc on assembly was found by Brender et al. (2013). Stabilisation of pre-fibrillar oligomers was also found in the presence of zinc, with an increase in density of aggregates. However, in the presence of zinc, typical fibrils are formed at a faster rate in the presence of micromolar zinc. However their substrate

for assembly was not lipid, but mica, and so it is difficult to draw comparisons with use of planar lipid or liposomes.

My data is consistent with results of Salamek et al. whereby zinc stabilises an oligomeric, off-pathway species that causes fusion; it is considered off pathway as there is no fibrillization. Although it can not be determined from my experiments whether such an oligomeric assembly is formed of α-helical or β sheet structures, the possibility of both is consistent with the data. Five stacked β sheets are thought to be necessary for binding of ThT (Biancalana and Koide, 2010). It is therefore possible that the fusogenic species formed in the presence of zinc are made up of stabilised oligomers that are less than this number and so unable to bind ThT. Interestingly, the N-terminal fragment of HIV gp41 adopts small, β-strand oligomers capable of causing fusion (Qiang et al., 2009; Gabrys et al., 2013). A fusogenic sequence from sea urchin fertilization protein Bindin, B18, has also been shown to be modulated by zinc (Ulrich et al., 1999). At low concentration and in the presence of Zn^2, B18 adopts a predominantly alpha-helical conformation in zwitterionic (neutral) and negatively charged membranes, which correlates with its fusogenic activity. Further work, using higher P:L ratios in the absence of zinc, showed the presence of only lamellar lipid morphologies, consistent with the absence of fusion (Grage et al., 2004). They conclude that the peptide conformation of the peptide at high P:L ratios is not fusogenic and that in this case the structure associated with the membrane is beta sheet (Grage et al., 2004). The results from the work on Bindin provide further evidence that an amyloid peptide is capable of true fusion, with an added caveat that hIAPP may also be able to cause fusion via β sheets assemblies.

Although I have demonstrated fusion of liposomes is dependent on lipid composition and presence of peptide, it is possible in cells that hIAPP acts in a different way to modulate fusion between membranes. Indeed, non-aggregated α-synuclein has been shown to inhibit SNARE dependent vesicle fusion at low concentrations (Lai et al., 2014) by binding acidic lipids, but not v-SNARE. At low concentrations α-synuclein oligomers have also been found to inhibit SNARE dependent vesicle fusion by a

mechanism that requires v-SNARE interaction (Choi et al., 2013). Such a mechanism is also plausible in the context of a pancreatic beta cell. SNARE mechanism is important for docking of granules to the plasma membrane and interaction of hIAPP with the SNARE components might result in inhibition of granule fusion.

One of the most common systems in which fusion has been studied is that of snare proteins. Proteoliposomes containing SNARE proteins have been used in liposome fusion assays in order to study which proteins are sufficient to enable fusion. SNARE proteins in this context can be seen as a model system for several reasons. One is that any fusion only happens between liposomes containing complementary parts of the SNARE complex proteins and as such only heterologous fusion is possible. Also, although vesicles have been reported to go through multiple snare mediated fusion events (Parlati et al., 1999; Cypionka et al., 2009), the system does not evolve in such a way that the constituent parts of the SNARE system are depleted.

In contrast to the previous example, fusion induced by amyloid peptides is complicated by the evolution of hIAPP into higher order oligomeric structures. hIAPP undergoes structural changes both on an individual peptide basis, from unstructured to α-helical to β sheet, as well as ensemble changes whereby the various individual structures can interact, eventually evolving to form highly ordered fibrillar structures. As mentioned previously, these structural changes of hIAPP are accelerated in the presence of lipid Therefore any fusion that takes place does so in the context of continuous structural changes to both peptide and lipid bilayer.

Although the sole use of lipid mixing assays to establish fusion is commonplace, the demonstration of true fusion is often supported by a content mixing assay. In the case of SNARE machinery, components reconstituted in an in vitro liposome system, such content mixing is relatively simple to demonstrate due to the nature of the membrane fusion that takes place: that of non-destructive peptide interaction. Content mixing assay can be divided into several types: broadly these are based on 1)chelation of a quencher; 2) chelation causing increase in fluorescence; 3) complementary binders

e.g. avidin/biotin, dextran/concanavalin A. Having established in the chapter 3 that the interaction of hIAPP permits considerable leakage of the molecules DPA and Tb, molecules of the order of 0.6 kda as soon as introduced to liposomes, it was not appropriate to use content mixing assay based on small molecule chelation. Large binding partners have been used, such as avidin-biotin or dextran-concanavalin A, associated with donor and acceptors for FRET, but practical limitations in terms of labelling density of proteins required large amounts of donor and acceptor in order to get high signal/noise. In addition, it is not possible to obtain information about the size of liposomes or their evolution over time since these are ensemble measurements. Therefore in the next chapter we look to a technique which enables non-destructive measurement of individual particles to shed light on fusion of the liposomes.

4.4 Conclusion

In this chapter I have demonstrated that via a lipid mixing assay that hIAPP(wt) is able to induce fusion of negatively charged (PCPS). This fusion is clearly modulated by zinc resulting in two different kinetic regimes. From the data, it is not possible to provide concrete information about the structure of the fusogenic conformations only that it is likely that there are two conformations, one of which is not a species on the path to fibrillization.

Although the amount of fusion induced by hIAPP(38W) is a lot lower than both hIAPP(wt) and hIAPP(Y37W), addition of zinc results in the same amount of fusion and kinetics. This is striking as it suggests that the mechanism by which zinc enhances fusion is not effected by the C-terminal tryptophan addition.

Chapter 5

Single Particle Analysis

5.1 Introduction

Having established that hIAPP can induce mixing of lipids between liposome membranes, we were interested in how this would manifest on a single particle level. As mentioned in the previous chapter EM is not an optimal technique for measuring sizes of a large number of particles. A common technique for measuring particle size is dynamic light scattering (DLS) which utilises the change in scattering intensity of particles over time to calculate size (Maas et al., 2015). However, this technique provides an ensemble measurement of particle size. Additionally, sizing is biased towards larger particles. Therefore a technique which allows many particles to be counted in solution without further manipulation or processing is desirable. A technique with such attributes can be found in the form of NTA. Relevant discussion pertaining to theoretical and practical aspects of NTA are included in the exposition of the results since they are relevant in understanding both the nature of the data and indeed what information may be derived from it.

The aims of this chapter are to establish working parameters for single particle analysis of liposome fusion reactions and to extend the use of the FRET assay to an NTA based context.

5.1.1 Theory of Nanoparticle Tracking Analysis

The sizing of particles by NTA is based on using Brownian motion to calculate the diffusion coefficient. This is achieved by shining a laser through a solution of particles which scatter the light. This scattered light is picked up by a camera enabling visualisation of the particles. A video recording of the scattered light is made. The centre of each particle is tracked, frame by frame, enabling the average distance moved by each particle to be determined. With the temperature and viscosity of the solvent known, the sphere-equivalent hydrodynamic diameter for each particle can then be calculated, thus producing a size distribution of particles. This data is then used to provide the concentration of parcels as well as the particle size distribution (PSD) for the given sample. Only particles that meet certain criteria are include in the distribution (this is in some way dependent on number of frames the particle has been tracked for, although the exact details of the selection criteria are proprietary and therefore unknown). The recording of particle motion and procedure for analysis is outlined in figure 5.1.

5.2 Results

5.2.1 Establishing parameters

5.2.1.1 Sizing and finite track length adjustment: mono and polydisperse distributions

The ability of NTA to separate particles by size can be demonstrated using fluorescent carboxylate beads. We separately sized five sizes of beads, at a range of nominal sizes (100, 200, 500, 750 and 1000 nm). For each of the sizes measured we obtained a distribution that was comparable to the nominal size (fig. 5.2). This demonstrates that NTA can accurately determine the size of particles from monodisperse populations, for a range of sizes. Additionally, sizes of these particles of a nominal size are represented by a normal distribution.

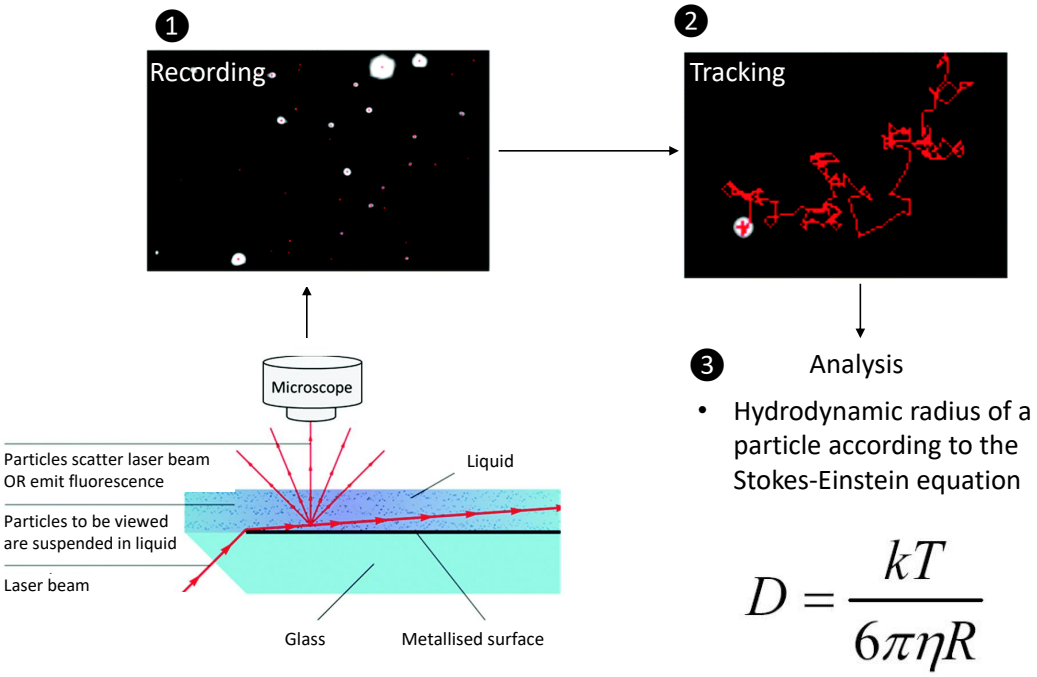

Figure 5.1. Principle of NTA. Overview of the required steps to acquire a PSD via NTA.

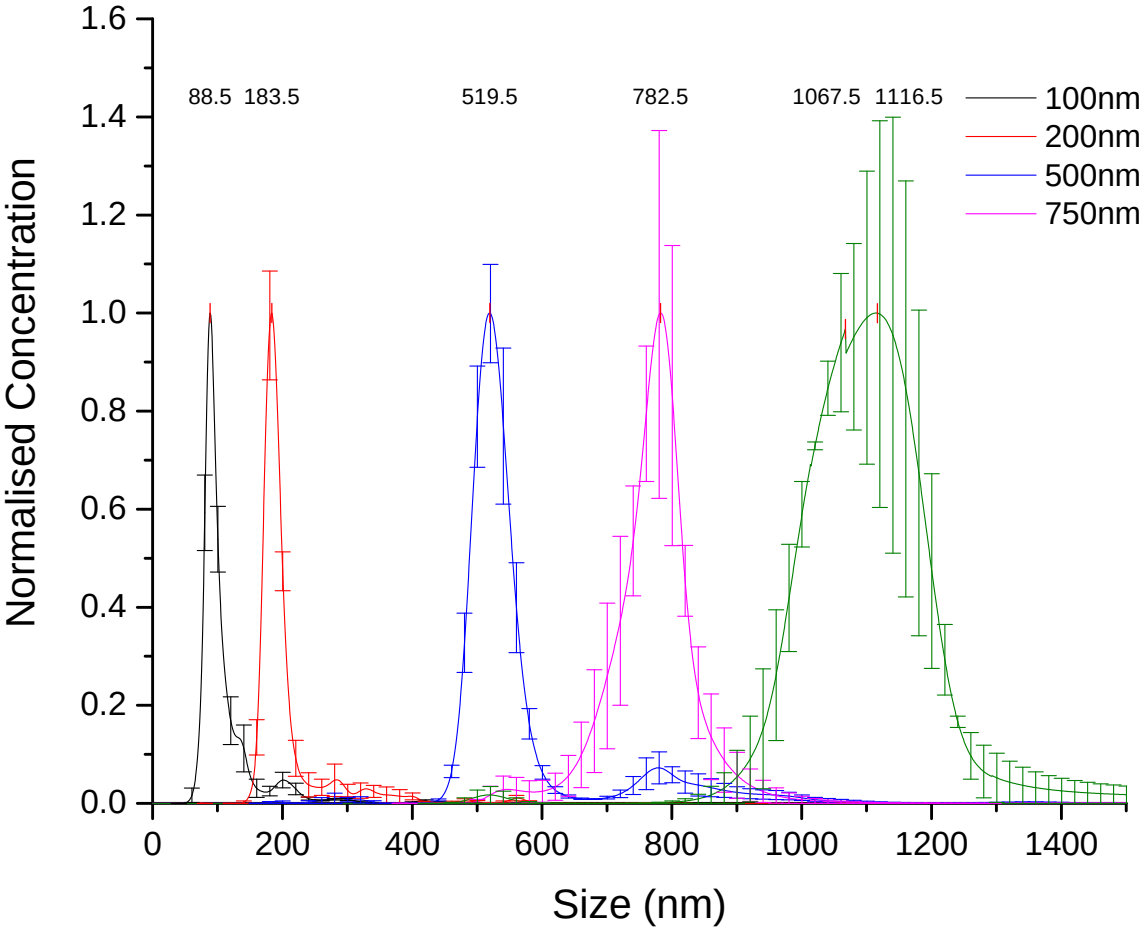

Figure 5.2. Diameters of beads of a nominal size analysed by NTA. The size distribution of beads of various sizes were independently determined by NTA. Various concentrations of beads were used and so the distrubutions have been normalised to show the peak sizes. Each curve represents 1 nm binned distributions made from three recordings of each sample. Error bars are the SEM (n=3).

The data presented in figure 5.2 was transformed from the raw data by a finite track length adjustment (FTLA) algorithm, implemented by the NTA software. In order to determine any given particle's size, the Brownian motion trajectory needs to be tracked for a sufficient number of steps so that an accurate average value of the step-length can be generated. Due to the very small depth of the scattering volume, particles can often be present for a very limited period of time. This manifests itself as a broadening of the measured distribution due to the reduction in accuracy associated with limited duration trajectories (Carr and Wright, 2013). This artefact can be compensated for by applying the FTLA, recovering the true distribution width of a population of particles (Saveyn et al., 2010).

Application of FTLA is recommended for monodisperse particles (Carr and Wright, 2013) although not explicitly ruled out for polydisperse samples. A comprehensive study by van der Pol et al. (2014), comparing various methods of measuring size distributions of exosomes and vesicles, considered the appropriateness of FTLA. They found that its application to raw PSDs of a reference mixture of polystyrene beads (sizes of five nominal diameters) resulted in a decreased accuracy of the determined mean diameters as well as an additional peak. Thus they conclude that use of FTLA was not appropriate for polydisperse samples (van der Pol et al., 2014).

Nonetheless, the PSD of a sample containing a mixture of two distinct sizes of particles, 200 and 750 nm, was determined with FTLA applied (fig. 5.4). This figure is typical of the representation of size distributions. Concentration per ml (y axis) is estimated using the the scattering volume based on the optical field of view and the depth of the scattering beam (Carr and Wright, 2013). The x axis represents bin centres with corresponding bin widths of 1 nm. The NTA software accurately reveals that there are two main populations of particles in the distribution, with peak heights of 206 nm and 711.5 nm, consistent with the nominal diameters of the added carboxylate beads.

Additional information can be found from size versus intensity scatter plots. As described, scattered or emitted light is the sole factor allowing visualisation of any

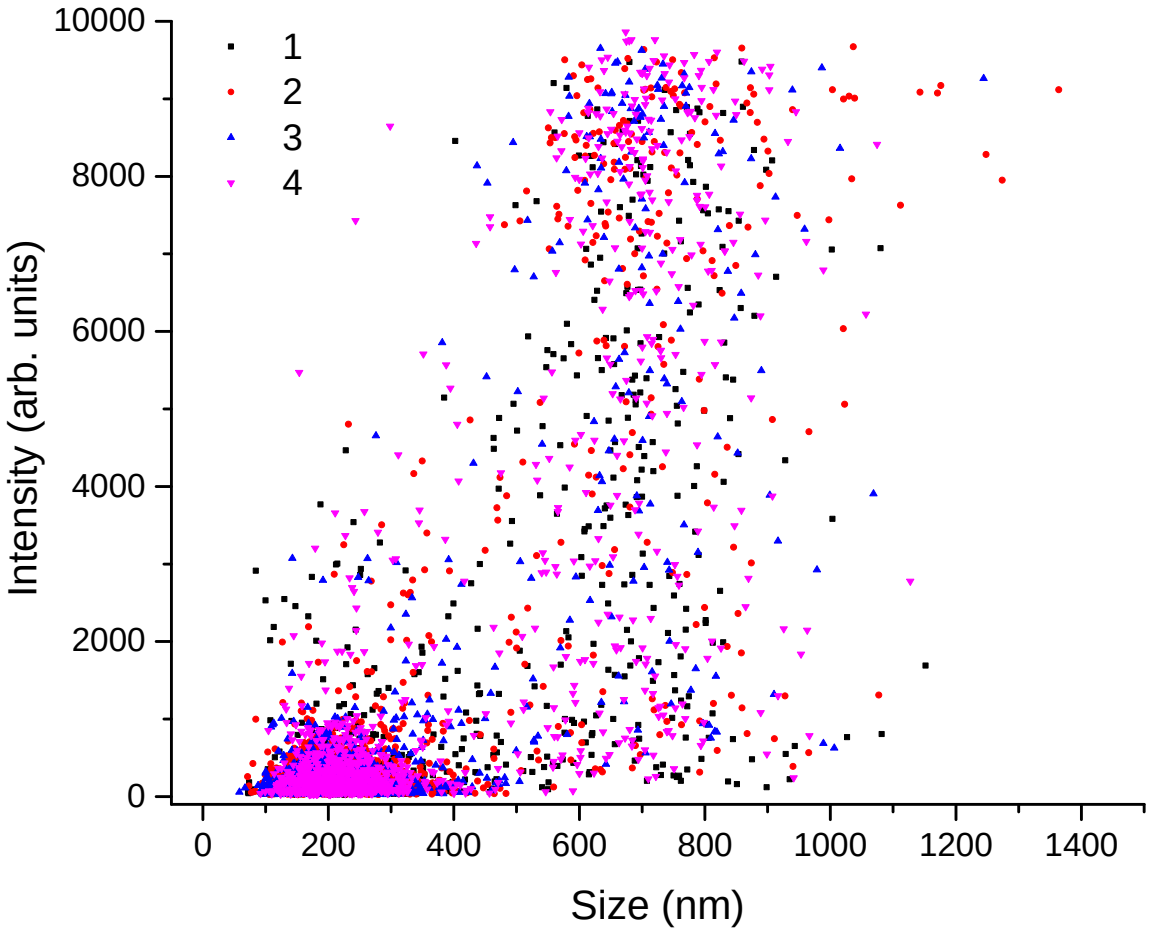

Figure 5.3. Scatter plot of sample containing two size distributions of 200 nm and 750 nm particles. A solution of 200 nm and 750 nm carboxylate beads was prepared with 10 fold higher volume of 750 nm carboxylate beads in order to have more equal numbers of each size. The carboxylayte samples were added to 20 mM HEPES buffer, pH 7.4. Four samples were prepared and a recording of 1 minute was made for each sample. The individual scatter plots of the raw data (1 to 4) are represented.

given particle. However, the intensity of scattered light can be used to resolve particles of different refractive indices. Additionally, differential labelling of particles with fluorophores and appropriate filters, can allow further separation of particles.

When we look at the raw scatter of size versus intensity of the two particle sample (fig. 5.3), we can see that the population of particles around 200 nm is quite well centred in terms of intensity, but particles around 700 nm have a range of intensities, with the concentration density of particles at a higher intensity, as would be expected for larger beads which should contain more fluorophore. The variation in intensity may be due to an inherent variation in fluorophore labelling or due to aggregation of 200 nm beads. Therefore, one can see that examination of both size and intensity can provide more information about the nature of the sample.

The use of NTA is not as widespread as other sizing modalities and this is reflected in the extent of the literature. When NTA is used to deterimine sizes of biologically relevant particles, such as EVs, the application of FTLA is often not explicitly referred to. In addition, information such as size of bins is often not reported, making it difficult to draw conclusions about the appropriateness of parameters for acquisition and subsequent analysis of data. Biological samples are often classed as polydisperse as technically there is more than one size of particle present. We expect that a polydisperse sample of particles such as beads prepared to be a certain size will easily be separated when such a procedure as the FTLA is applied to the raw data. However, the application of FTLA is not appropriate to resolve major populations of particles in a polydisperse sample. The situation appears to be more complicated when there is a change from a normal distribution. If the underlying distribution of a polydisperse population is made up of particles which are themselves represented by a normal distribution, then resolving the sizes in the population is simple enough. However when this underlying distribution changes in a way in which the specifics of the distribution are unknown, the underlying distribution of such a population can no longer assumed to be normal. Such a situation might be expected from fusion of liposomes by amyloid peptides due to the possibility of different fusogenic

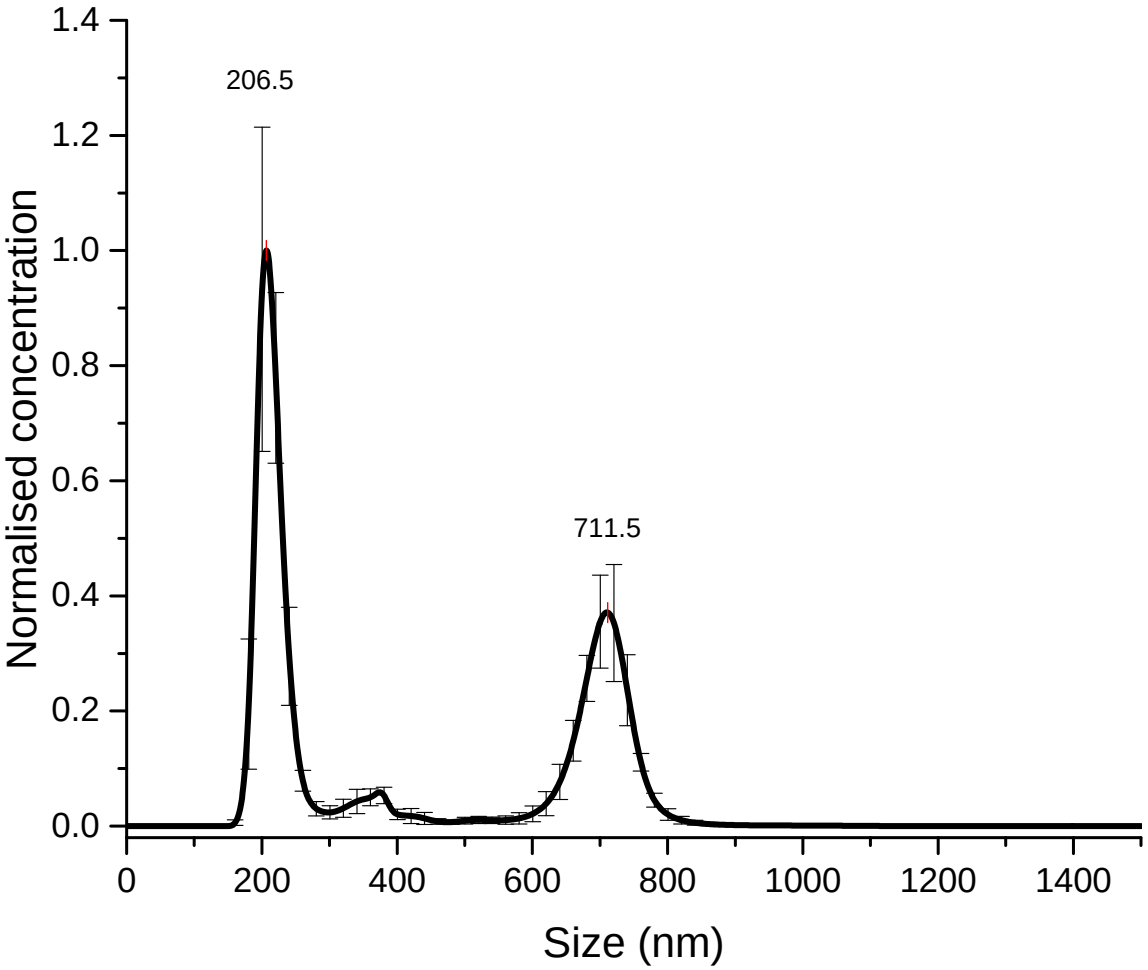

Figure 5.4. Sizes of two populations of beads resolved in a single sample. The data from fig. 5.3 represented as a histogram showing 200 and 750 nm beads separated by size. The FTLA has been applied in this case as the 2 populations are expected to be normal distributed. 1 nm binned distributions made from four recordings of each sample. Error bars represent SEM (n=4).

confirmations of hIAPP as well as the interconversion between these confirmation in time.

5.2.1.2 Creating PSDs from measurements in scatter and fluorescence mode

The videos used in processing are acquired on a standard camera. The scattered light recorder by the camera is determined by several parameters which may be set by the user: camera shutter, camera gain and camera histogram. A series of pre-set camera levels, with various settings of these parameters, are pre-loaded, however all settings are independently modifiable. Manipulation of these parameters are necessary for optimal sizing as subsequent analysis of the data is affected in various ways.

One important factor when recording videos for analysis in scatter versus fluorescence mode is to do with the nature of the light. The intensity of scattered light from a particle is related to the diameter of said particle by the sixth power, and is therefore non linear. This poses a problem when trying to record scatter from particles whose sizes differ considerably as parameter settings optimised for lower intensity can result in saturation of the camera detector but settings optimised for higher intensity particles can lead to particles of smaller sizes not being measured. In the case of liposome fusion, the use of fluorescence mode goes some way in avoiding this problem. If we assume that membranes are labelled with fluorophore at a constant density, then the amount of fluorophore on the liposome should vary linearly with the surface area. This helps to bring particles of different sizes within the dynamic range of a setting. However saturation is still possible, depending on how large the particles actually become, and therefore how much fluoroscope is present in total.

5.2.2 Determining PSDs using FTLA and raw data

Measurement of the size distribution of PCPS liposomes using FTLA made by extrusion through membranes of a nominal 400 nm pore size reveals the diameter of the resultant liposomes to be significantly smaller, with a peak diameter of 214 nm

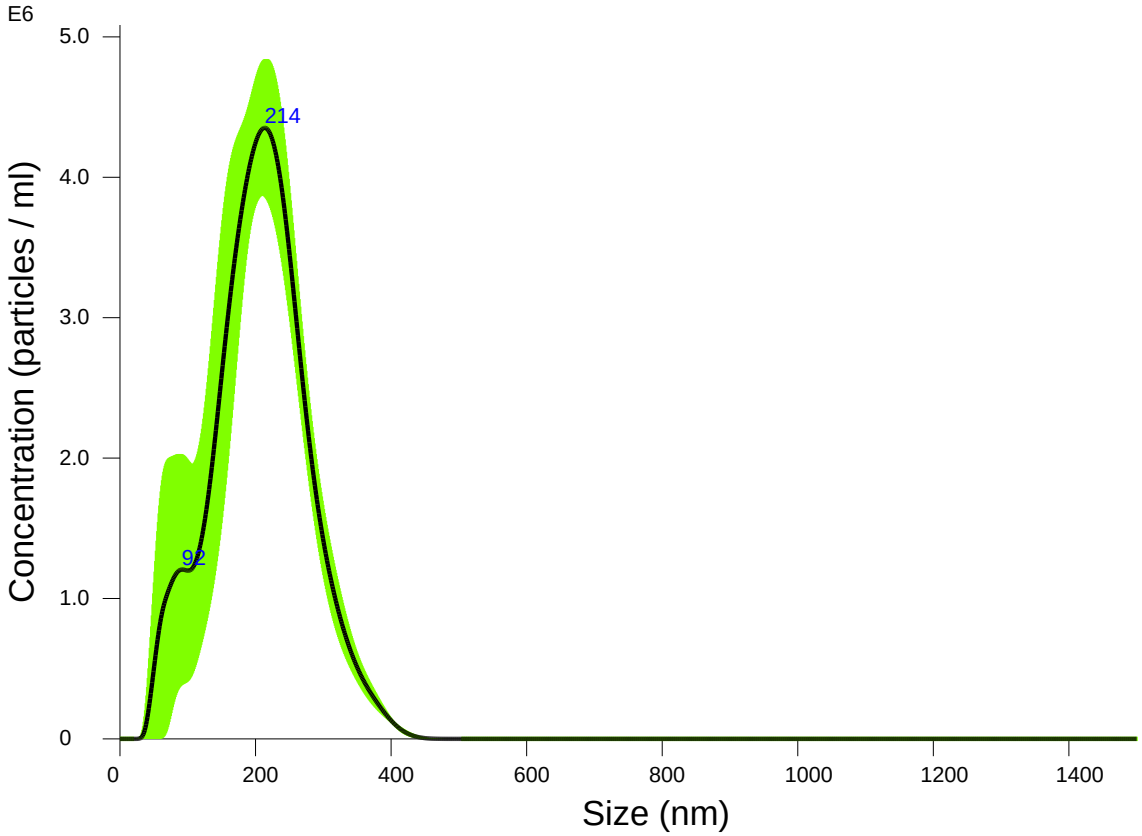

Figure 5.5. Typical size distribution of liposomes used in experiments. The size distribution is of PCPS liposomes in 20 mM HEPES, pH 7.4, extruded using a 400 nm NC filter. FTLA has been applied. The mean size of 214 nm is much lower than the nominal size of the NC filter. The green area represents +/- 1 SD (n=3).

(fig. 5.6). In addition, it is clear that the width of the liposome distribution is quite wide compared to the measurements of the fluorescent beads. Indeed, the distributions of the nominal sized 100 nm, 200 nm and 500 nm beads have a distribution width of about 100 nm, 50 nm, and 200 nm respectively; liposomes have a distribution width of almost 400 nm. In addition, FTLA representation of the liposome distribution produces a small shoulder at 92 nm. However, if we assume that the population is monodisperse and represented by a Gaussian distribution, this means there are substantial number of liposomes with sizes above and below the mean size. The distribution of the liposomes in figure 5.6 data has been plotted using binned raw data. Here the shoulder at 92 nm is no longer apparent. This emphasises how FTLA application should be used with caution.

There are two important points to be made regarding this result. The first is that the assignment of pore diameters, as being representative of the diameter of extruded

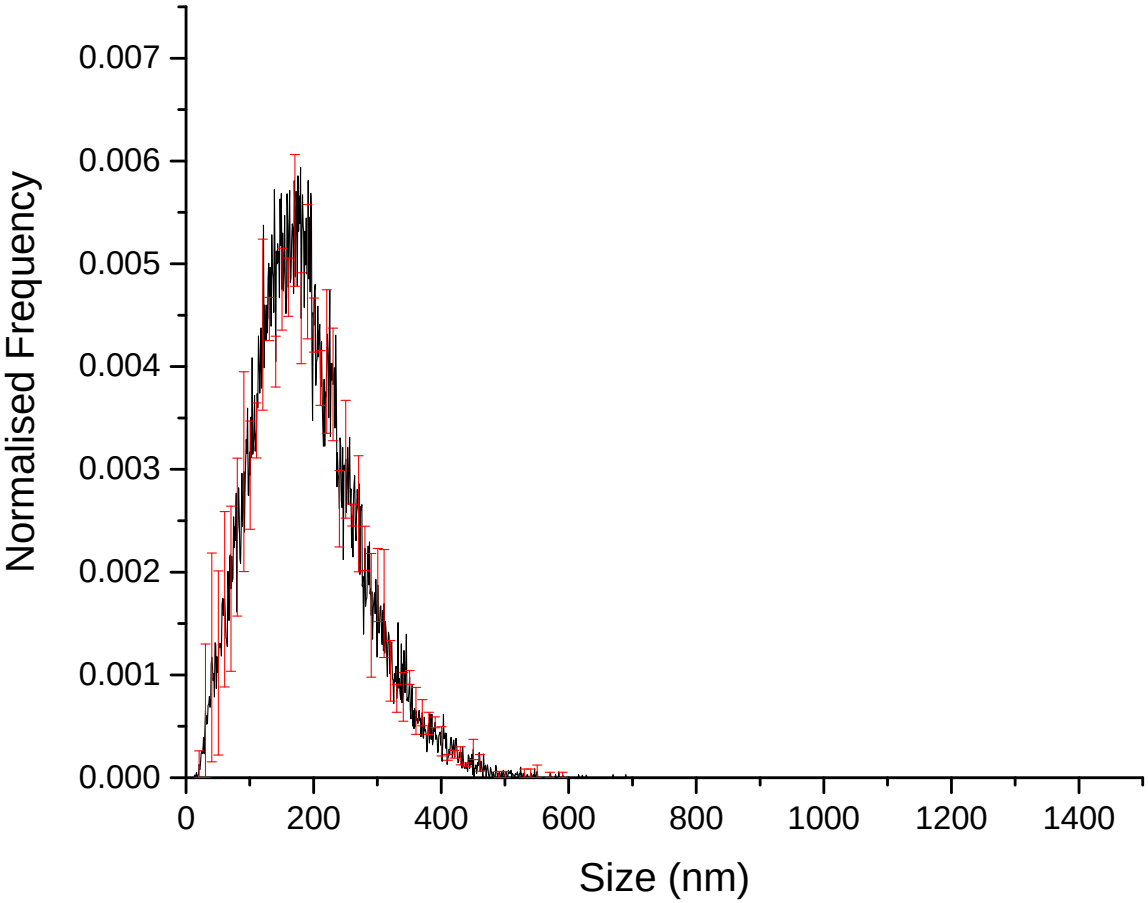

Figure 5.6. Normalised frequency distribution of a population of PCPS liposomes. Same data as in fig. 5.5 but without FTLA. One can see that the peak diameter is quite similar as data with FTLA applied, howver the shoulder at 92 nm is no longer apparent. Red error bars represent SEM (n=3).

liposomes, should be done with caution. Many studies, in which liposomes have been prepared by extrusion, use NC membranes with pore sizes of 100 nm and often this has been used as a correlate for the diameter of the liposomes. Indeed, measurement of the size distribution of liposomes prepared by extrusion of 1,2-dipalmitoyl-sn-glycero-3-phosphocholine (DPPC)/1,2-Dipalmitoyl-sn-glycero-3-phosphoserine (DPPS) lipids in solution through 100 nm NC membranes, reveals a distribution around 100 nm (Jean et al., 2016). However, many studies have used NC membranes with pore sizes of larger nominal diameter. In these cases, determination of liposome size distributions is often through DLS, known to be biased towards particles of larger sizes (Murdock et al., 2008), or through EM, in which the number of particles that can be reasonably measured is orders of magnitude lower than with NTA. The purpose of some of these studies has been to investigate the relevance and effect of membrane curvature on various peptide induced dynamics (Chong et al., 2014). In these cases, it is not difficult to imagine that the accurate (or inaccurate) sizing of liposomes can have profound consequences on conclusions drawn, particularly on the proclivity a peptide for certain curvatures, therefore accurate sizing of starting population should not seen as inconsequential. The second point is, depending on the dynamics of fusion, starting with a population of liposomes with a wide distribution of sizes may have a bearing on the conclusions drawn about the resultant distribution. In order to look at the influence of size, and by extension curvature, it is desirable to make liposomes with a narrow distribution. This is applicable both when investigating fusion between vesicles of the same size (homotypic) and that between vesicles of different sizes (heterotypic). With such wide distributions of sizes, it was not possible to experimentally determine how the size of liposomes affected fusion.

5.2.3 Effect of peptide on size distribution of liposomes

5.2.3.1 Mastoparan with PCPS

After addition of mastoparan to PCPS liposomes we can see that there are larger particles in the distribution that were not present before, consistent with fusion having

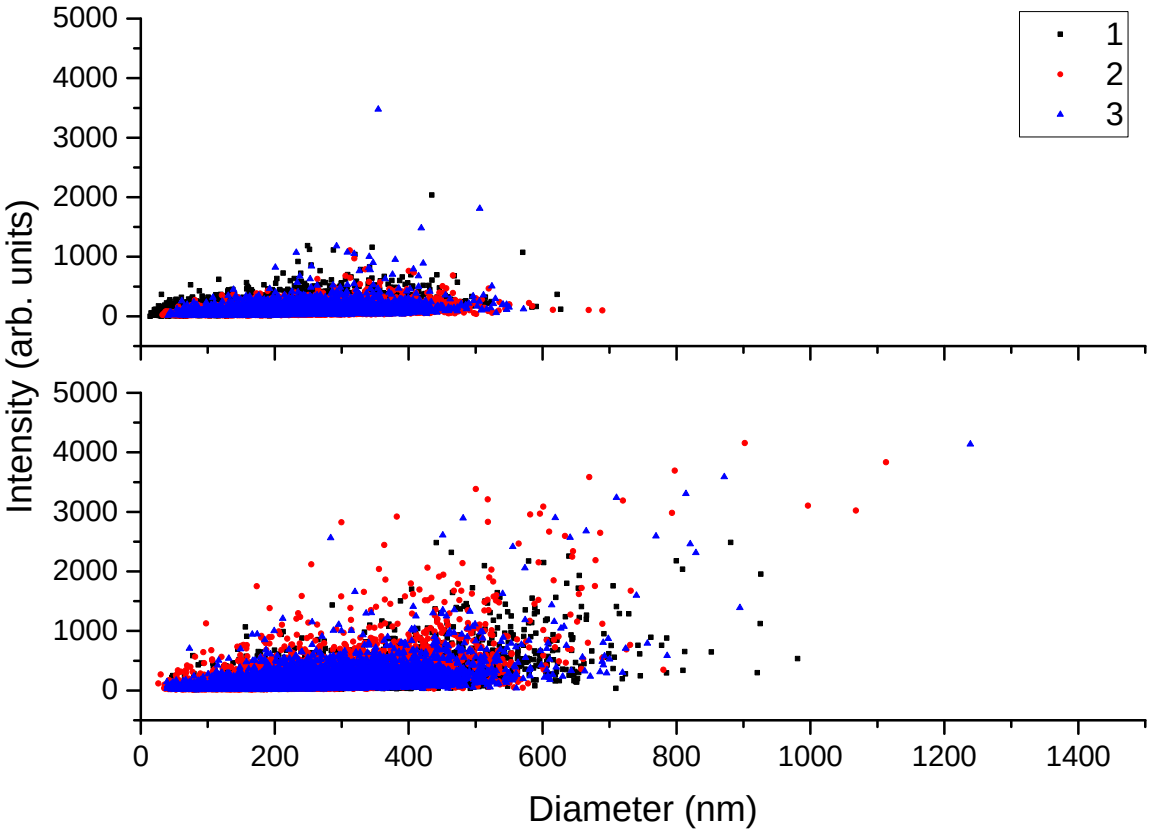

Figure 5.7. Size and intensity distrubution of liposomes with and without mastoparan. PCPS liposomes (50 μM) with (bottom panel) and without (top panel) mastoparan (25 μM) were incuabted at 37°C for 10 minutes. Samples were diluted 100 times the size distribution of particles measured. The scatter plot shows the distrubutions from 3 seperate samples for each condition.

taken place (5.7). Each of the particle distributions are calculated from a video recording of 270s (4.5 minutes).

5.2.3.2 Timecourse of lipsomes fusion with addition of hIAPP(wt)

To illustrate an increase in size over time, I added hIAPP(wt) to PCPS liposomes and measured every 30 mins (fig. 5.8). The change in size distribution is over 360 mins (6 hrs) is shown. There is clearly a decrease in the peak concentration overall. In addition, at 360 mins there is the appearance of small peaks at around 600 nm and 800 nm. However this data has had the FTLA applied. If we look at at the size distribution of particles constructed using the raw data (fig. 5.9), we see an emergence of particles of a larger size but without distinct peaks present, as seen previously. There are a couple of observations to report. Firstly, we see there is an increase in the proportion of larger particles and, secondly, there is an increased

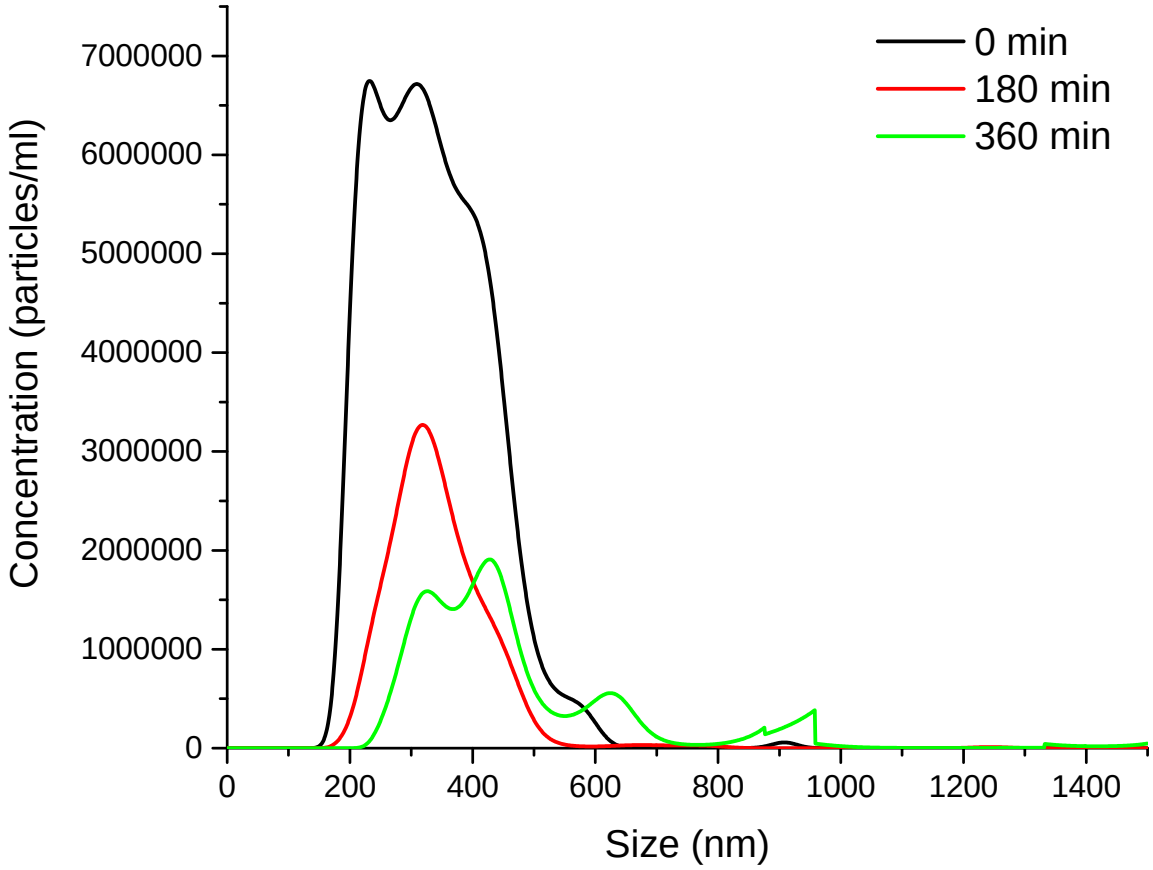

Figure 5.8. Change in size of PCPS liposomes incubated with hIAPP(wt). hIAPP(wt) (8.4 μM) was added to PCPS liposomes (50 μM). The change in PSD was measured over 6 hours. FTLA has been applied.

kurtosis of the distribution. It is possible that only the larger particles are becoming fused but in order to test this it would be necessary to produce a liposomes with a narrower size distribution. In addition the two distributions are quite different, emphasising the impact of FTLA on polydisperse PSD.

The NTA has previously been used to look at changes in size distributions, for instance, when investigating protein aggregation (Filipe et al., 2010). However in these cases, there is no 'actual' starting size distribution as the sizes of monomeric proteins are below the resolution of particle sizes that can be measured by NTA. In addition the use of the FTLA produces peaks which may not be representative of the actual distribution. Because of the changes in representation of the distribution by the application of FLTA on my data, I decided to take the particle data as is; that is to say distributions are represented by a scatter plot with each point representing a particle, with size on the x-axis and intensity on the y-axis, measured

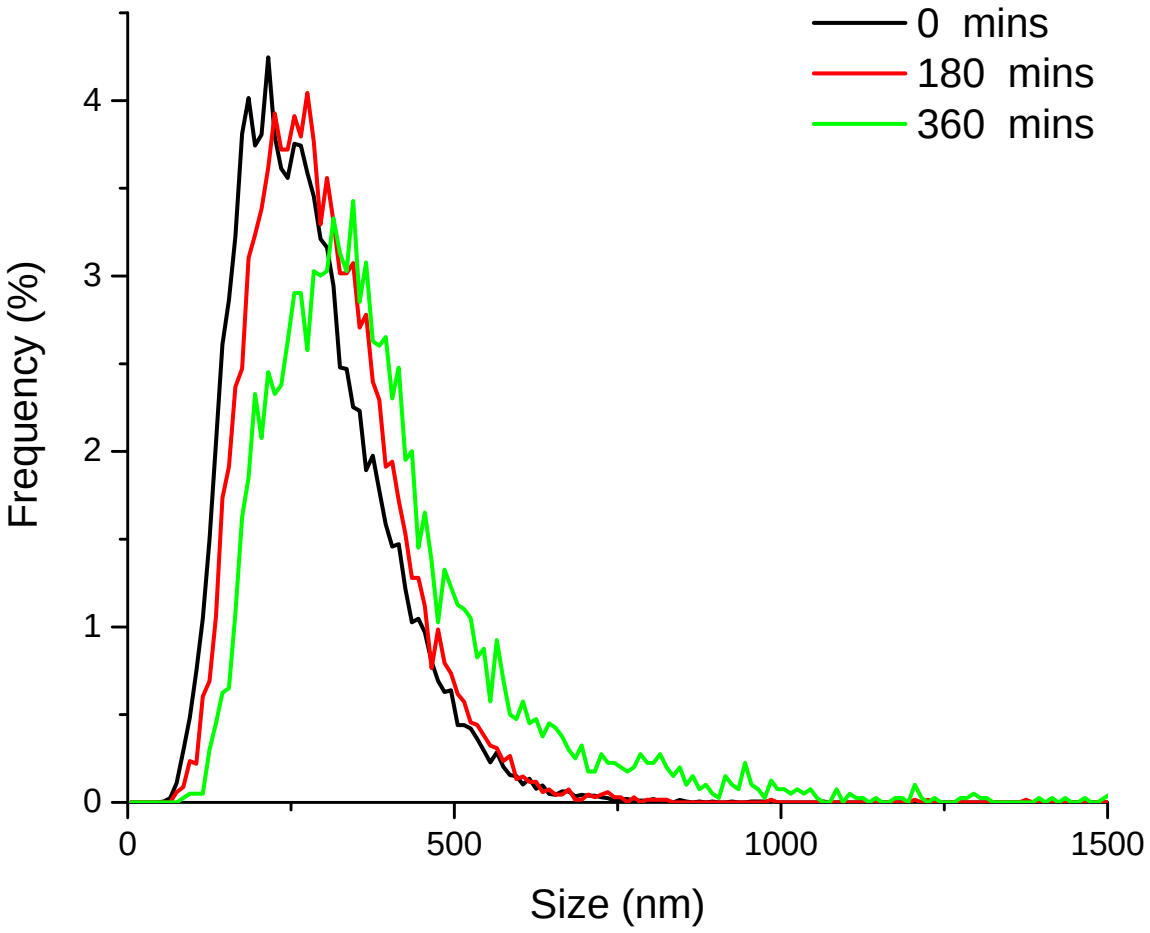

Figure 5.9. Normalised frequency distribution of PCPS liposome sizes incubated with hIAPP(wt). The graph was produced by normalising, by percentage, the number of particles within each bin (10 nm) for each timepoint

during analysis of the video.

Because I was not able to control temperature during repeated video captures, I decided to capture a single timepoint of the effect of hIAPP(wt) on fusion of PCPS liposomes after 30 minutes incubation at 37°C. This timepoint was chosen as it was still within the lag phase of amyloid fibrillization of hIAPP(wt) and enabled examine the the effect of zinc on hIAPP induced fusion of PCPS liposomes before fibrillization of peptide.

We recapitulated the experiment that had been undertaken in the lipid mixing assay, looking at the effect of zinc on the transformation of hIAPP into a fusogenic peptide. We can see that the addition of DMSO does not have a marked effect on the size distribution (fig. 5.10a). Upon addition of hIAPP(wt) alone, there are few particles of increased diameter (fig. 5.10b). Addition of zinc alone results in fusion of particles, consistent with the results from the lipid mixing assay (Chapter 4). Addition of hIAPP(wt) and zinc results in a big change in the distribution of particles. These results are consistent with zinc causing hIAPP(wt) to take on a structure that is more fusogenic than hIAPP(wt) without zinc, during the lag time before fibril formation.

5.2.3.3 The effect of hIAPP, mastoparan and zinc on liposome fusion

We next looked at the role of lipid composition on the ability of hIAPP(wt) and mastoparan to induce fusion. First, we looked at its effect on liposomes consisting of PC only (Neutral charge), again at the 30 min timepoint. The results of DMSO and DMSO + zinc on neutral liposomes has no effect (fig. 5.11, a and c). Addition hIAPP(wt) had no real effect compared to DMSO (fig. 5.11d). Surprisingly, mastoparan had a clear effect. This is in contrast to the lack of leakage by Tb-DPA assay; it is possible that mastorparan induced fusion proceeds by a different mechanism. We also looked at the effect of peptide on PS only liposomes. Mirroring the results using PC only, both DMSO and DMSO+zinc do not produce liposomes of larger sizes (fig. 5.12, a and c). Addition of mastoparan also results in large change in the size distribution (fig. 5.12b). However there is now a more noticeable

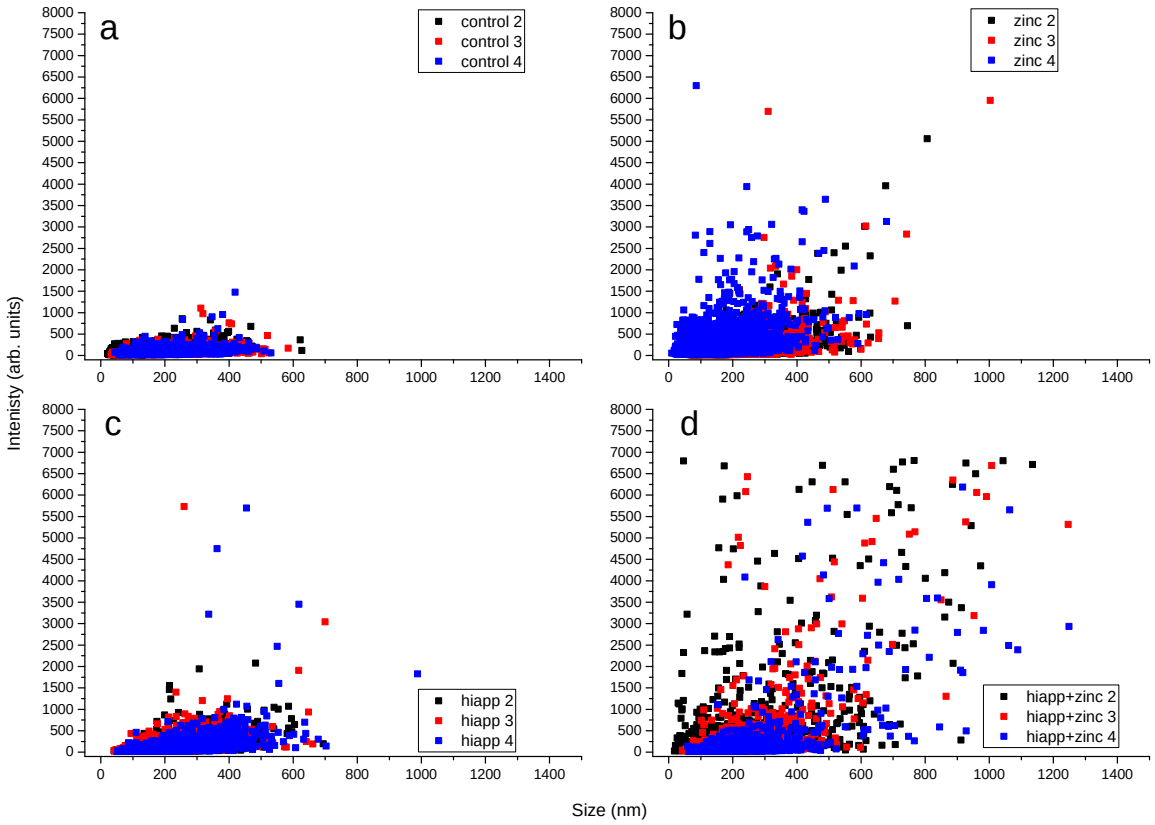

Figure 5.10. Effect of hIAPP on size of PCPS liposomes with and without zinc at 30mins. PCPS lipsomes (50 μM) had either DMSO (a), 500 (μM) zinc (b), hIAPP(wt) (4.2 μM) (c), and both hIAPP(wt) (4.2 μM) and zinc (500 μM) added. Each panel consist of 3 biological replicates (labeled 2-4) each depicteed in the scatter plot as black, red and blue. For each comparison the bilogical repeats were summed and comparison between distributions under different conditions using the Mann-Whitnney test. At the 0.05 level, the size of particles in (d) signifncatly tend to be bigger than (a). The size of partciles in (d) also significantly tend to be bigger then (b) and (c). This shows that zinc has the effect of enabling more rapid fusion of lipsomes by hIAPP(wt).

effect on size distribution of liposomes composed of PS, with the appearance of particles of both smaller and larger sizes.

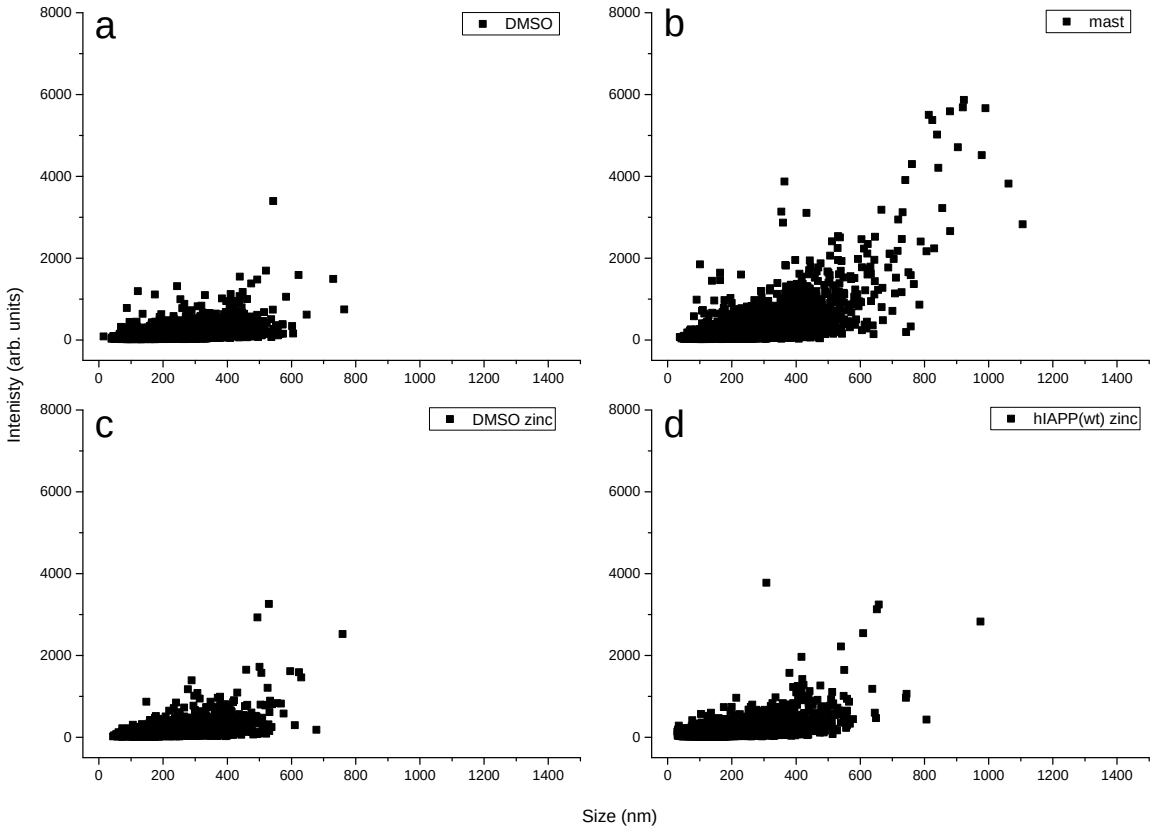

Figure 5.11. Fusion of PC liposomes by hIAPP and mastoparan. 50 μM of PC liposomes were incubated for 30 mins with DMSO (a), mastoparan (25 μM) (b), DMSO and 500 μM zinc (c), 4.2 μM hIAPP(wt) and 500 μM zinc (d). After 30 mins the samples were diluted 100 times and the particle size distributions were measured. Each scatter plot represents a single experiment.

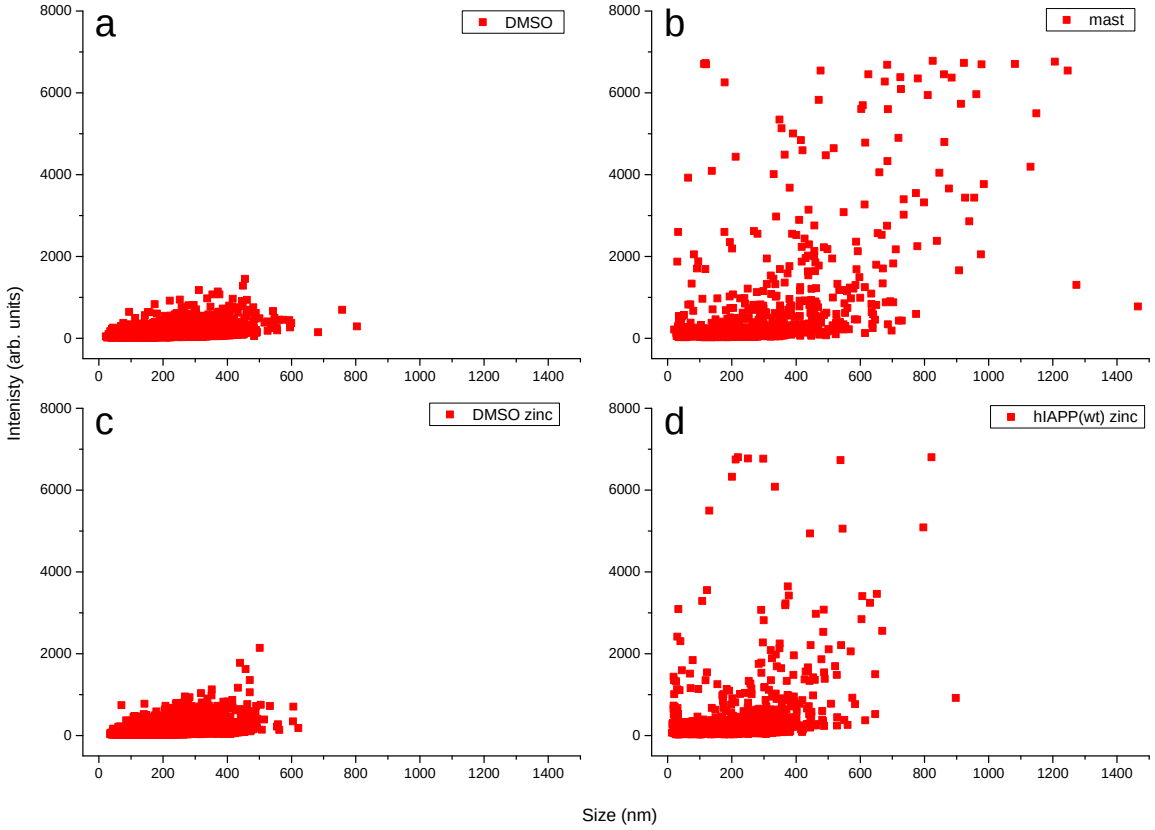

Figure 5.12. Fusion of PS lipospmes by hIAPP(wt) and mastoparan. 50 μM of PS liposomes were incubated for 30 mins with DMSO (a), mastoparan (25 μM) (b), DMSO and 500 μM zinc (c), 4.2 μM hIAPP(wt) and 500 μM zinc (d). After 30 mins the samples were diluted 100 times and the particle size distributions were meausred. Each scatter plot represents a single experiment.

5.2.4 Extending the use of NTA

We wanted to extend the use of NTA by using fluorescence based techniques used in other platforms, such as the plate reader, with the idea being to follow heterogeneous fusion between liposomes of different compositions, luminal content, and indeed sizes.

5.2.4.1 FRET

One possible utilisation of a fluorescence based approach is to extend the use of the NanoSight to the lipid mixing assay by follow the emergence of particles based on emission resulting from FRET or from dequenching of a fluorophore. The former approach is most desirable as it would allow one to follow heterologous fusion as well as homologous fusion.

The approach was to use the same fluorophore pairs as with the lipid mixing assay. By using the 488 nm laser unit to excite the donor DiO fluorophore, acceptor fluorophores DiI with in-resonance transfer range would be excited and subsequently emit fluorescence. The NanoSight microscope head was modified to insert a filter wheel between the objective and the camera. The filter wheel was inserted at the correct height in order to maintain the correct focal distance between the camera and the objective. The emission filter was selected to allow only emission from the acceptor fluorophore.

I sought to establish FRET as a valid approach by using mastoparan, which results in lipid mixing as established by the lipid mixing assay. Addition of mastoparan gave rise to a population of liposomes that were both larger and more fluorescent. To be sure that this was representative of FRET, I analysed a liposome population that contained both DiO and DiI intended as a positive control, the hypothesis being that doubly labelled liposomes should have the same distribution as singly labelled liposomes but that donor fluorescence should be higher. However, although there was no change in distribution there was also no change in fluorescence intensity. When, measuring the intensity of donor and acceptor populations separately, it became apparent that there was significant cross excitation of acceptor. This cross excitation was not apparent in

the plate reader based assay. Therefore FRET based measurements were not possible with the current NanoSight instrument setup.

5.2.4.2 Dequenching

Fluorescence dequenching was another approach considered for use with the NTA modality. This strategy involved putting a high concentration of a lipid soluble dye, r18, the fluorescence of which is quenched at high concentrations. In a plate reader based assay, lipid mixing between a liposome populations with, and without, r18 in the membranes resulted in an increase in intensity. This was an ensemble measurement and we wanted to see how this would manifest on a single particle level. We realised a potential complication with looking at dequenching using the NTA. In theory, fused particles would result in another fused particle with double the surface area. Assuming that the density of fluorophore per area unit is relatively uniform, we can use intensity per area as a measure of whether or not quenching had taken place. Fusion of liposomes containing r18 would result in an increase in intensity on a per liposome basis but intensity/area would remain constant for all sizes of liposome. On the other hand, fusion of lipsomes with r18 and lipsomes without should result in dilution in the membrane and so the intensity:area ratio for fused liposomes should be higher. Fusion of liposomes without r18 would not be visible by the NTA as they would not be fluorescent. Starting with liposomes with quenched concentrations of r18, we can set the threshold to disregard any particles above any residual fluorescence emission. By plotting intensity:area ratio against size, we should be able to see fusion between populations of lipsomes with r18 and those without. An example using this approach is shown in fig. 5.13). As expected we can see that of the four combinations of samples the only sample that gave rise to a population of particles with a higher intensity per area was from the addition of mastoparan to liposomes contain r18 at a quenched concentration and liposomes without any r18 (mast r18 + acceptor). The same combination of liposomes without mastoparan (cont r18 + acceptor) did not result in the emergence of a population with a higher intensity per area values.

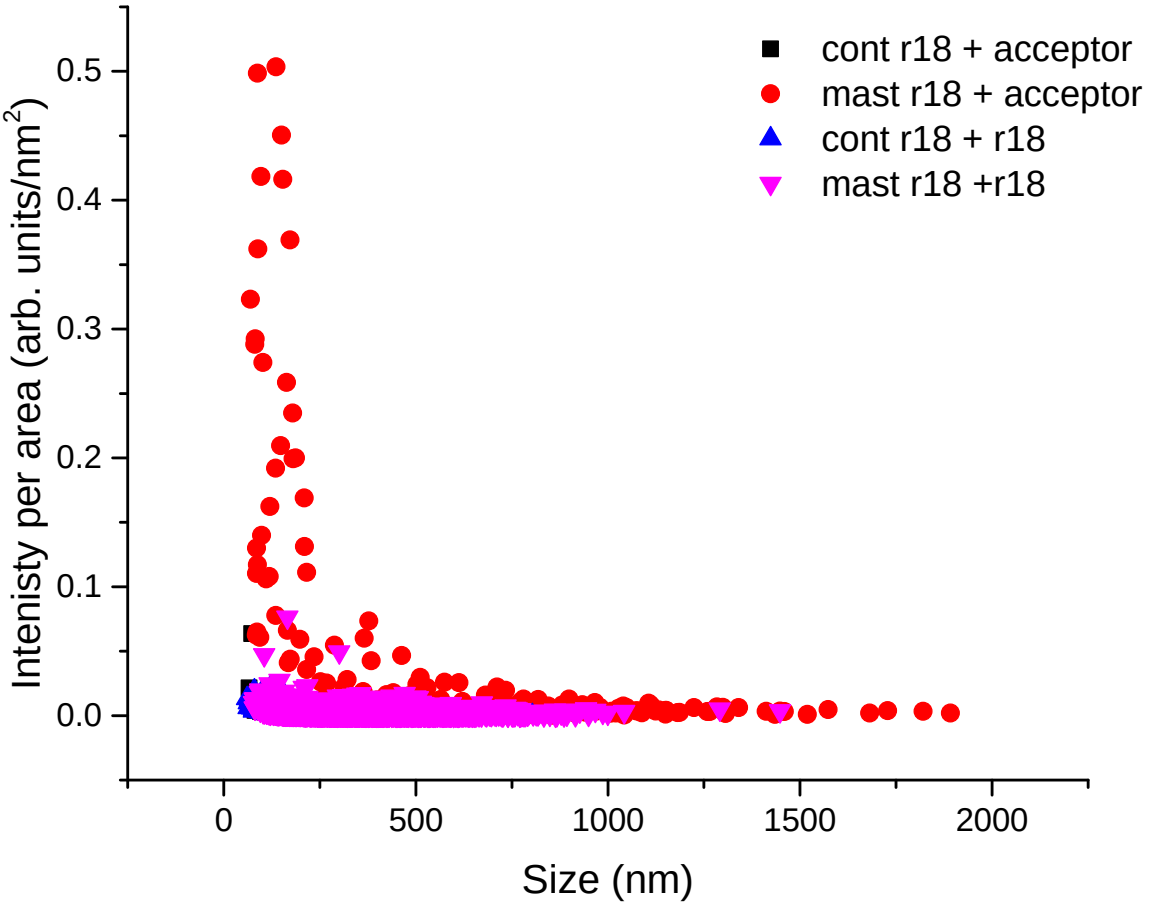

Figure 5.13. Fusion of r18 PCPS liposomes with PCPS liposomes. r18 represents 25 μM of PCPS with r18 (F:L=1:20), acceptor represents 25 μM of PCPS without r18. The prefixes cont and mast represent addition of nothing and 25 μM of mastoparan, respectively. The four samples represented in the scatter plot were incubated for 10 mins at 37°C. Subsequently the samples were diluted 100 times in 20 mM HEPES, pH 7.4 and the size distribuutions of particles were measured.

5.3 Discussion

The use of NTA is gaining ground as a technique to measure the size of particles. One of the main advantages of NTA over a technique such as DLS is the aspect of single particle counting. Given the plate reader data showing that there was lipid mixing between liposomes consisting of negatively charged lipid (PCPS) we wanted to show that there was fusion by showing an emergence of larger liposomes from a starting population of smaller liposomes. In addition we wanted to try and extend the FRET based assay utilised for lipid mixing to use in NTA. One benefit of the use of FRET in terms of analysing the amount of liposome fusion is the ability to look at heterologous fusion i.e fusion between liposomes of different lipid compositions.

I first recapitulated the results from the plate reader lipid mixing assay by adding mastoparan to PCPS liposomes and looking to see for an increase in particle size (fig. 5.7). One possible confounding factor is aggregation of liposomes and/or peptide. The presence of this may contribute to observed changes in size distribution. The use of mastoparan allows some useful control with regards to this. This peptide is not known to aggregate and I have shown that it does not form fibrils in the previous chapters. Therefore, any increase in size distribution is unlikely to be due to aggregation of the mastoparan. Having shown that lipid mixing takes place via emergence of FRET signal and that addition of mastoparan to donor and acceptor dyes in solution without lipid does not produce a signal, it is prudent to then assume that lipid mixing actually takes place and is not due to aggregated dyes. Satisfied with this, the case becomes whether liposome fusion is necessarily followed by lipid mixing and not just by aggregation.

Next I looked at the ability of IAPP(wt) to cause fusion of PCPS liposomes. As noted previously, in the results section, it was decided not to use the FTLA for the data because of the artefactual peaks created. Using normalized frequency, we see that there is and change in the distribution with the emergence of particles of a larger size and an overall shift in the peak size of liposomes (fig.5.9). Although I do not have a sample showing the size of liposomes over time without the addition of hIAPP(wt), results from the lipid mixing assay with addition of DMSO to liposomes over time do not display any lipid mixing. In addition the use of DMSO does not result in an increase in liposome size (fig. 5.10) further making it unlikely that liposomes left over the timescales measured would become fused liposomes. Additionally the expeirments using NTA are in line with in published literature. NTA was used to look at the effect of magnesium on the ability of the peptide IM30 to cause fusion of liposomes over time (Hennig et al., 2015). They show neither the time course of liposome size over time or the effect of magnesium alone on the size of lipsomes over time, despite showing that is has an effect on lipid mizing. However in my experiments I have controlled for the effect of zinc on fusion. for completion a control measurement would be useful to support the conclusions of from the NTA data presented

Given the results of the plate reader data with the use of zinc, it was rational to hypothesise that addition of zinc to hIAPP(wt) and PCPS liposomes would result in fusion much more quickly than without zinc. This appears to be the case, with the presence of large liposomes apparent much earlier when zinc is added at the same time as hIAPP(wt) (fig. 5.10). The nature of these particles is assumed to be composed of lipid. The presence of higher order aggregates of hIAPP is thought to be unlikely at this early time point since it has been shown that addition of zinc (at this concentration) does not result in fibrillization as measured by ThT assay but faster lipid mixing and the addition of zinc with hIAPP(wt) results in larger particles than zinc or hIAPP alone. It interesting to compare the effect of hIAPP(wt) on liposomes of mixed lipid composition (PCPS) to liposomes of a single composition (PC or PS). We see that the effect of hIAPP(wt), combined with zinc, on PC liposomes does not result in the same dramatic increase as with PCPS. This result is also supported by the lack of lipid mixing of PC only liposome when incubated with hIAPP(wt) (Chapter 4). However, hIAPP(wt) in the presence of zinc does seem to increase the size of PS liposomes, but again, not by the same amount as with PCPS liposomes.

There are a number of parameters that are important to consider when attributing a change in size distribution to fusion of liposomes: 1) The number of rounds of fusion in which a peptide can participate; 2) Whether the curvature of liposomes that can be fused follows a continuous or discrete distribution and whether there is a maximum or minimum difference under which fusion is permissible; 3) The starting size of liposomes (and the associated distribution; 4) The amount, and timescale, of aggregation of peptide and/or lipid; 5) The fission or breakdown of both fused and non-fused vesicles. Full modelling of such criteria is beyond the scope of this chapter as the phenomenon of lipid mixing by hIAPP(wt) has not been previously described. However, future studies would certainly benefit from incorporating such criteria to more fully understanding the dynamic of this fusion behaviour.

Chapter 6

Effect of hIAPP on the Molecular environment of lipid membranes

6.1 Introduction

In the previous chapters we described how the interaction of hIAPP with lipid membranes not only affects membrane integrity, evidenced by liposome leakage (Chapter 3), but also results in lipid mixing between membranes of liposomes (Chapter 4), and an increase in size distribution of liposomes indicative of fusion (Chapter 5). In Chapter 6 we look specifically at changes to the molecular environment of the lipid membrane resulting from interaction with IAPP peptides.

Cellular membranes are very dynamic, with appropriate spatial and temporal control of lipid and protein composition necessary for cellular processes to be carried out correctly. An important organisational aspect of membranes relates to lateral phase separation. Specifically, the formation of lipid rafts, which are predicted to be liquid ordered domains/liquid order phases are suggested to be important for processes including signal transduction (Simons and Toomre, 2000), intracellular sorting (van Meer et al., 2008) and disease pathogenesis (Taylor and Hooper, 2006).

We have seen that the interaction of hIAPP with membranes results in changes to the organisation of lipids via lipid mixing. It is therefore conceivable that changes in the order of cellular membranes, either as a direct consequence of peptide interaction, or upstream pathological changes in lipid composition, could result in defective trafficking of β-cell secretory granules to the plasma membrane. In fact the

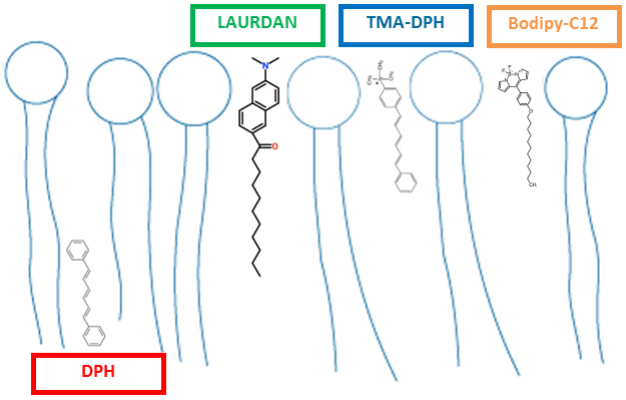

Figure 6.1. Locations of the fluorescent probes relative to lipids.

amyloid peptide α-synuclein, in an α-helical confirmation, has been proposed to possess the capacity to anneal defects in curved vesicle membranes, with the additional possibility of relevance to preventing synaptic vesicles from premature fusion (Kamp and Beyer, 2006). Thus, this precedent renders investigation of induction of changed in membrane lipid order IAPP pertinent.

6.2 Use of fluorescent probes in assessing lipid order and viscosity

There are a variety of ways to measure the order of lipid membranes. The probes that I have used in this chapter are laurdan, DPH and TMA-DPH and I will go through the mechanism by which each reports on the order of the membrane environment.

6.2.1 Measuring lipid order

6.2.1.1 Laurdan

One way of measuring membrane order is through the use of environmental sensitive fluorophores positionined in the membrane. One such fluorophore is laurdan, composed of a naphthalene ring and lauryl tail (fig. 6.1). It was first synthesised in order to measure polarity (Weber and Farris, 1979) and subsequently its use as a probe to measure lipid order in membranes was characterised by Parasassi and Krasnowska (1998); Bagatolli (2006).

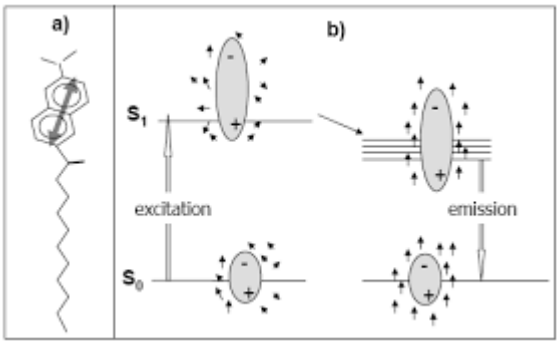

Figure 6.2. Jablonski diagram of changes in excited state of laurdan. Figure is reproduced from Sanchez and Tricerri (2007).

Due to partial charge separation between the 2-dimethylamino and the 6-carbonyl residues of laurdan, a dipole moment is present, which provides the mechanism for responding to changes in polarity. In the context of lipid membranes, the less ordered the lipids the more spaces there are between them. These spaces allow water molecules to be more dynamic around laurdan naphthalene moiety in its excited state (fig. 6.3). Excitation of the probe increases the dipole moment, resulting in surrounding dipoles, i.e. water molecules, reorienting around this new increased laurdan dipole. This reorientation of water molecules leads to a decrease in the excited state energy (fig. 6.2). When the lipid in the membrane is in a more ordered state, there is a reduction in water molecules (and associated mobility) and thus the relaxation of laurdan is not as pronounced and there is not a much of a decrease in the exited energy of the probe. In terms of the emission spectrum, since laurdan has less energy in the excited state in a less ordered membrane, it emits fluorescence of a longer wavelength and thus emission is 'red-shifted'. The converse is true in a more ordered lipid environment, with the lack of water molecules meaning the excited state is not affected, and thus the emission is of a higher energy, with a shorter, 'blue shifted' wavelength. This change is illustrated by measuring the emission spectrum of laurdan in lipid membrane at low or high temperature (fig. 6.4).

These shifts in the emission spectrum can be used to follow changes in lipid phase (or order) by use of a parametrisation called General Polarisation (GPex) (Parasassi et al., 1990):

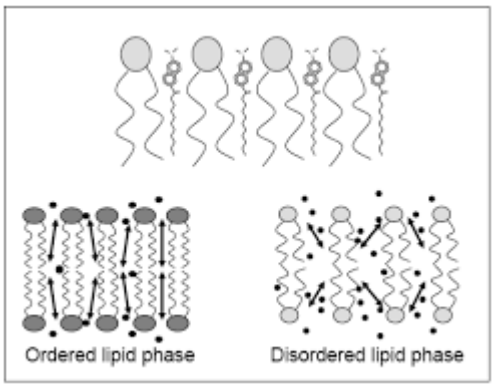

Figure 6.3. Schematic of changes to the dipole of laurdan in a lipid membrane bilayer. Black double arrows represent the dipole moment of laurdan; length of the arrows represent the size of the dipole; black dots represent water molecules. Figure is reproduced from Sanchez and Tricerri (2007).

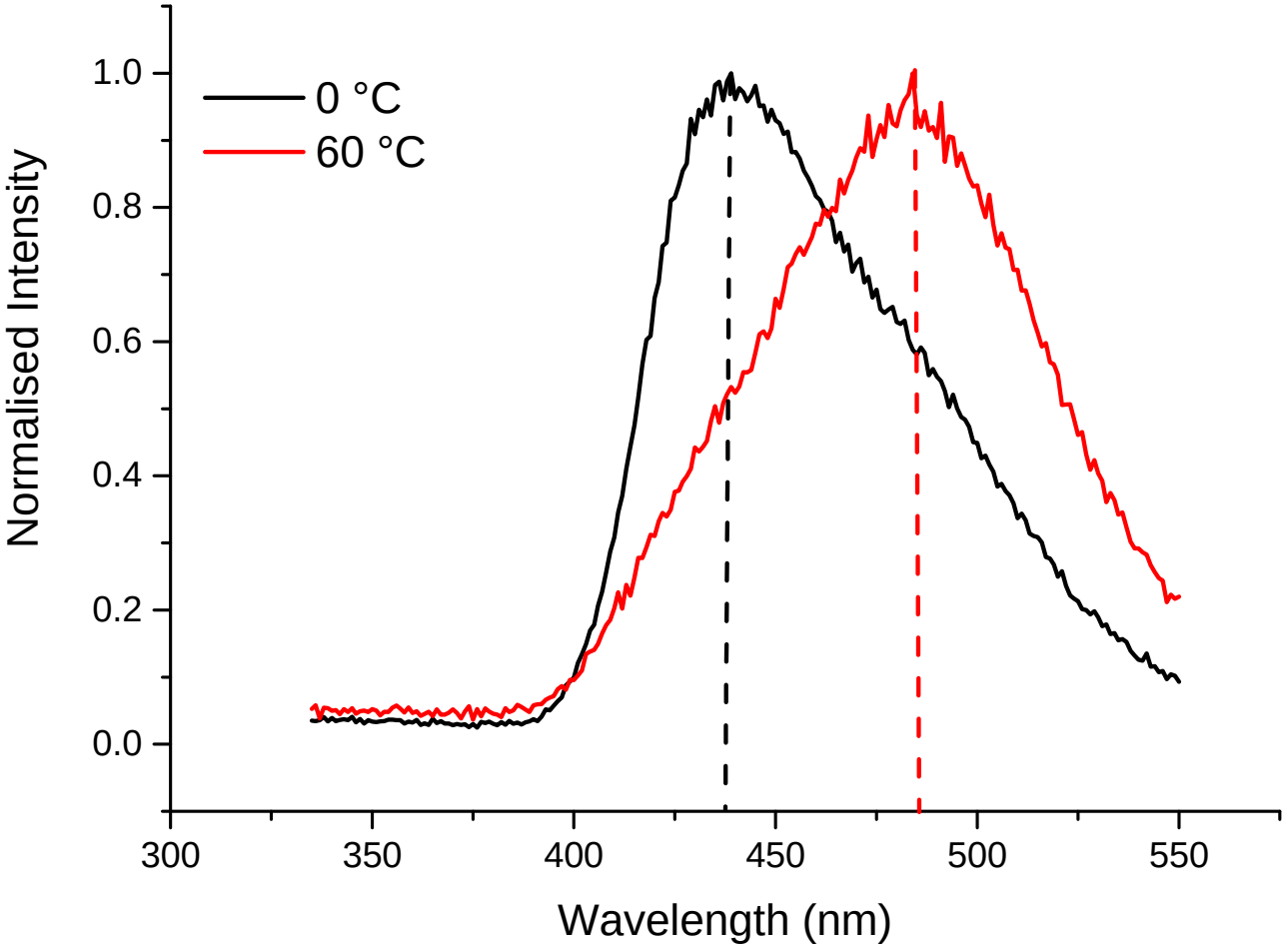

Figure 6.4. Effect of chnage in temperature on laurdan emission in PC liposomes. Fluorescence emission spectrum of laurdan excited at 360 nm; lipid:laurdan ratio, 1:400.

$$GPex(x) = \frac{I(mo) - I(md)}{I(mo) - I(md)} \tag{6.1}$$

Where x is excitation wavelength, typically around the peak excitation of 360 nm, and mo and md are the intensities of emission of laurdan at wavelengths that correspond to ordered and disordered phases, respectively. Wavelengths for mo and md are chosen to reflect the maximal peak intensities of fluorescence emission in gel (ordered) and liquid crystalline (disordered) phase, typically 440 nm and 490 nm, respectively, determined in a variety of ordered and disordered membrane compositions (Parasassi et al., 1991; Parasassi and Gratton, 1995). The corollary of this is excitation GP (GPem):

$$GPem(x) = \frac{I(xo) - I(xd)}{I(xo) - I(xd)} \tag{6.2}$$

Where m is emission wavelength, and xo and xd are the intensities at x after excitation at set xo and xd wavelengths, corresponding to ordered and disordered phases, respectively.

Typically, only GPex is measured but it is can be supplemented with measurement of GPem. GPex provides information on the mobility of water molecules that surround laurdan and as such is a measure based on the excited state laurdan (Viard et al., 1997).

On the other hand, GPem, provides information about laurdan in the ground state and is influenced by the strength of laurdan lipid interaction (Bagatolli et al., 1999). It is possible to extend the use of GPex and GPem by measuring the wavelength dependence of both functions such that several values of x and m, and GPex and

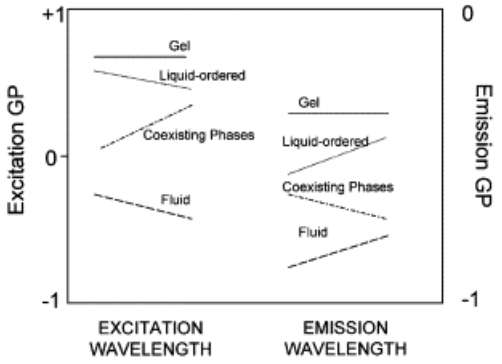

Figure 6.5. A schematic representation of the wavelength dependence of Laurdan excitation and emission GP spectra. gel (—), liquid-ordered (···), fluid (– –), and coexisting gel and fluid (– · –) phospholipid phases (Figure reproduced from Mukherjee and Chattopadhyay (2005)).

GPem are measured, respectively. Examples of wavelength dependence of GPem and GPex in various lipid order states are shown in (fig. 6.5). The change in the wavelength dependence of these parameters provides information about on aspects of phase changes in lipid membranes (Velázquez and Fernández, 2006; Mukherjee and Chattopadhyay, 2005; Bagatolli et al., 1998; Parasassi and Gratton, 1995). Thus a wealth of information can be gained from the GP functions as well as the wavelength dependence.

6.2.1.2 DPH and TMA-DPH

DPH and TMA-DPH probe also yield information about the order of lipid membranes but through changes in polarisation of the fluorescence emission. By exciting the fluorophore with polarised light and measuring the polarisation of emitted photons in orthogonal directions, one can calculate the polarisation or anisotropy. After DPH or TMA-DPH is excited it is rotates in space. The change in polarisation is determined by the degree of rotation that happens before re-emission of a photon. In an ordered membrane DPH will be less mobile. On the timescale from excitation to photon emission, DPH will not have rotated much and so the emitted photon will still be highly polarised. In a less ordered membrane, DPH will be more mobile and thus on the molecular timescale, will have moved a lot relative to when it was excited and so the degree of polarisation of emitted photons will be much lower. The addition

of TMA to DPH anchors the probe at the level of the lipid head groups, enabling information on the order of this area. DPH resides at the level of the acyl chains and so polarisation from this probe provide information about the order at the acyl chain level.

6.2.2 Measuring Viscosity

Bodipy is a probe that has been used in fluorescence microscopy for many years. Recently it was found to be a reporter of viscosity (Levitt et al., 2009; Kuimova, 2012; Zhao et al., 2016). The change to the quantum yield can be followed in response to viscosity either by measuring steady state fluorescence intensity or fluorescence lifetime. In general, intensity based measurements are more difficult because concentration, as well as viscosity will affect, the intensity. Instead, it is best to use lifetime measurements as they are independent of concentration. The mechanism by which Bodipy reports viscosity is through movement of a molecular rotor that has a twisted intramolecular charge transfer (TICT) excited state. The accessibility of the dark nonemissive TICT state is responsible for the non-radiative decay pathways in a rotor. Their radiative de-excitation pathway competes with intramolecular twisting, which leads to non-radiative deactivation of the excited state (Levitt et al., 2009).

6.3 Results

6.3.1 Membrane order

Using probes introduced previously, I have characterised the effect of hIAPP on membranes of different compositions in different environments. In keeping with earlier chapters, I have used the binary composition of PCPS at a molar ratio of PC:PS of 7:3 as a baseline for a physiologically relevant lipid composition.

The intention was to follow the kinetics of changes in the GP parameters of lipid membranes induced by IAPP and other peptides. However, it was found that serial

excitation of laurdan in liposomes resulted in an increase of both GPex and GPem values, making collecting a timecourse, with appropriate replicates, impractical. In addition, data presented in the forthcoming results section was obtained at room temperature, in contrast to data from other chapters at 37°C. Therefore investigation of the effect of IAPP on membrane order proceeded on the basis of GP data collection at a single time point, with each replicate going through only one round of excitation, therefore removing the issue of artefactual reporting of membrane order changes. For mastoparan GP data was collected for 3 time points.

A first important result, and a demonstration of the presentation of data, is from the incubation of mastoparan with PCPS liposomes. In particular, there is no change in the GPem (curve from 340 to 410 nm) and GPex (curve from 440 to 490nm) parameters and the membrane remains in the fluid phase, indicating that mastoparan does not cause changes to membrane order despite evidence of both liposomes leakage (Chapter 3) and fusion (Chapters 4 & 5) of liposomes composed of PCPS.

For IAPP the first objective was to see if there was an effect on the membrane order of liposomes with the lipid compositions used throughout the results described in this thesis. For liposomes composed of PC we see that there is essentially no effect of hIAPP or rIAPP on the order parameters of GPex and GPem at all wavelengths (fig. 6.7), suggesting that any interaction with the membrane does not affect the order of the lipid acyl chains. In contrast, incubation of negatively charged liposomes with hIAPP(wt) results in increase of both GPex and GPem at all wavelengths, consistent with the lipid bilayer becoming more ordered. Similar to the effect on a neutral membrane, rIAPP has no effect on the lipid order of PCPS membrane.

Continuing with the use of PCPS, we proceeded to look at the influence of pH on order changes induced by hIAPP(wt), producing some interesting results. At pH 7.4 there is a negative and positive correlation of GPem and GPex, respectively, with increasing wavelength. Addition of hIAPP results in the shift of both curves to higher GP values, consistent with an increase in order (fig. 6.8, left panel).

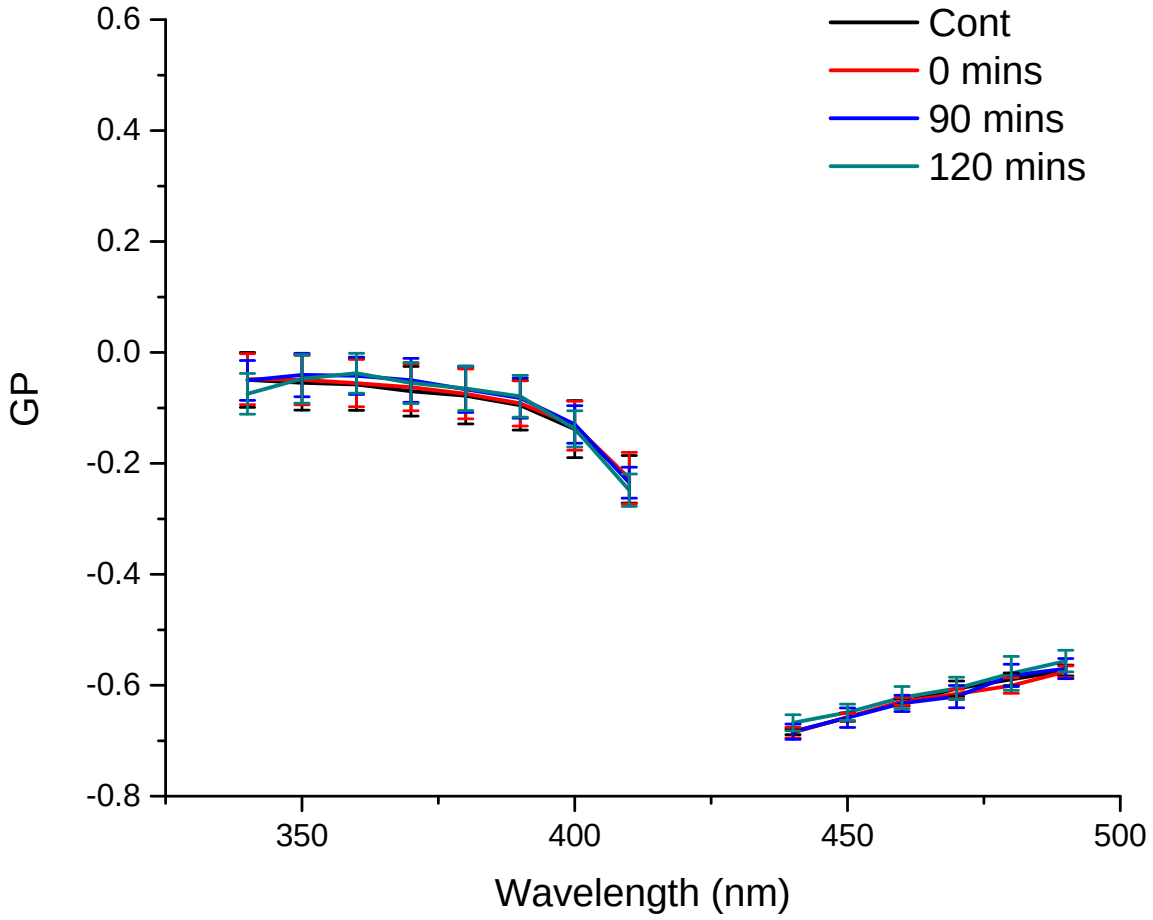

Figure 6.6. Effect of mastoparan on the lipid order of negatively charged liposome membranes. Mastoparan (25 μM) was incubated with liposomes (50 μM) composed of PC and PS (7:3 molar ratio at indicated time points. The Cont curve represents a control sample of liposomes in the same envionment but with nothing added. GPex measured from 310 to 410 nm and GPem from 440 to 490 nm. Curves represent an average of 3 replicates and error bars represent SEM (n=3).

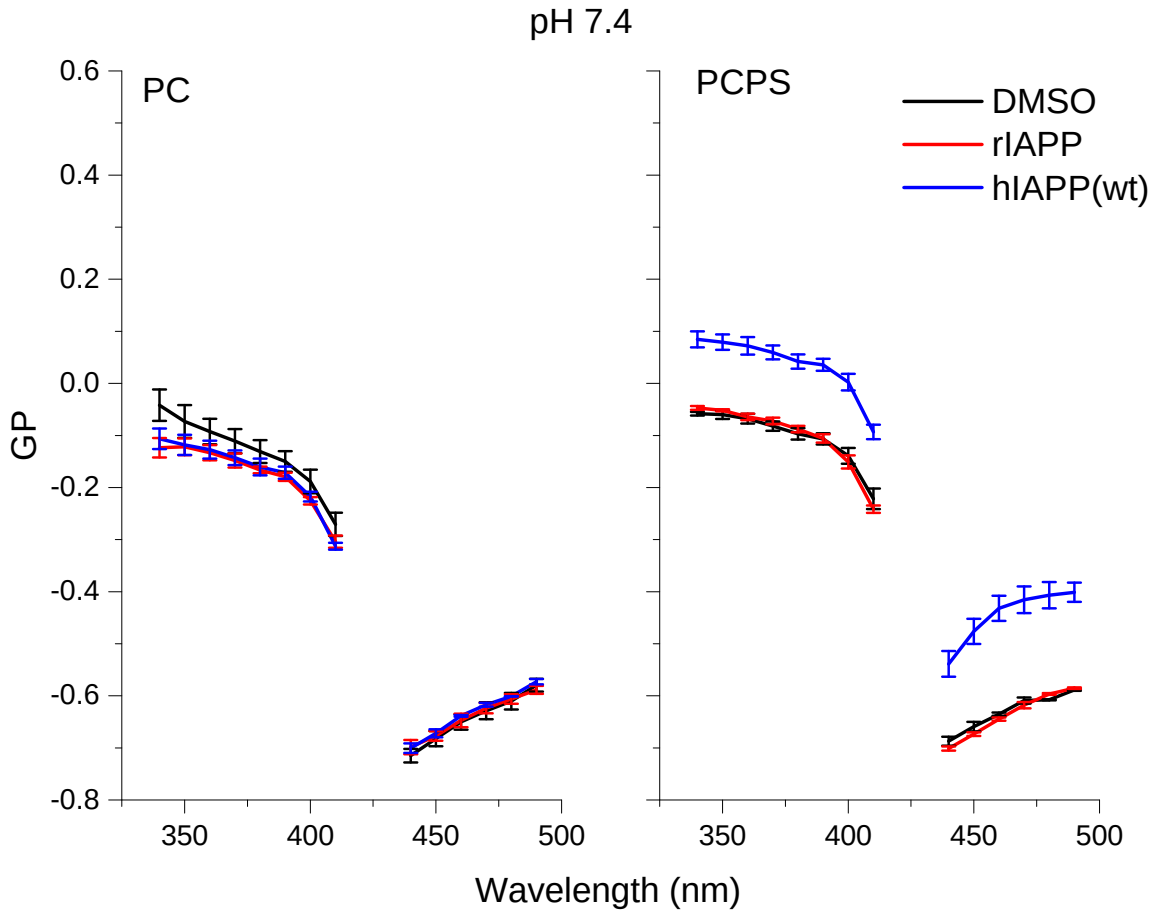

Figure 6.7. Effect of the presence of negatively charged lipids on ability of hIAPP(wt) to induce change in membrane order. hIAPP(wt) 4.2 μM was incubated with liposomes (50 μM) composed of PC or PCPS (7:3 molar ratio) at pH 7.4. DMSO curve represents data from an equivalent volume of DMSO as peptide added to a lipsomes sample. GPex measured from 310 to 410 nm and GPem from 440 to 490 nm. Curves represent an average of 3 replicates and error bars represent SEM (n=3).

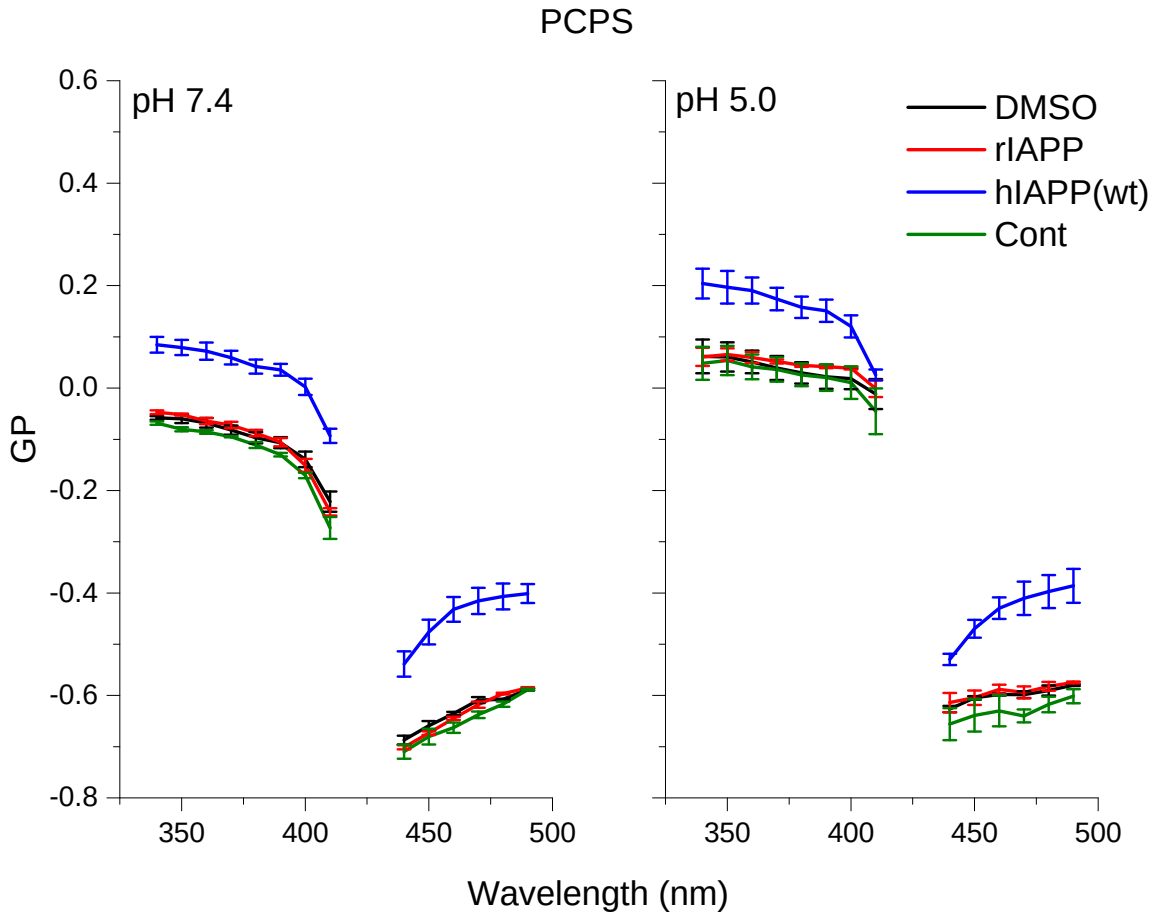

Figure 6.8. Lipid order of membranes with and without peptide is dependent on pH. hIAPP(wt) or rIAPP (4.2 μM) was incubated with liposomes (50 μM) composed of PCPS (7:3 molar ratio) at pH 7.4 or 5.0. DMSO curve represents data from an equivalent volume of DMSO as peptide added to a lipsomes sample. The Cont curve represents a control sample of liposomes in the same envionment but with nothing added. GPex is measured from 310 to 410 nm and GPem from 440 to 490 nm. Curves represent an avereage of 3 replicates and error bars represent SEM (n=3).

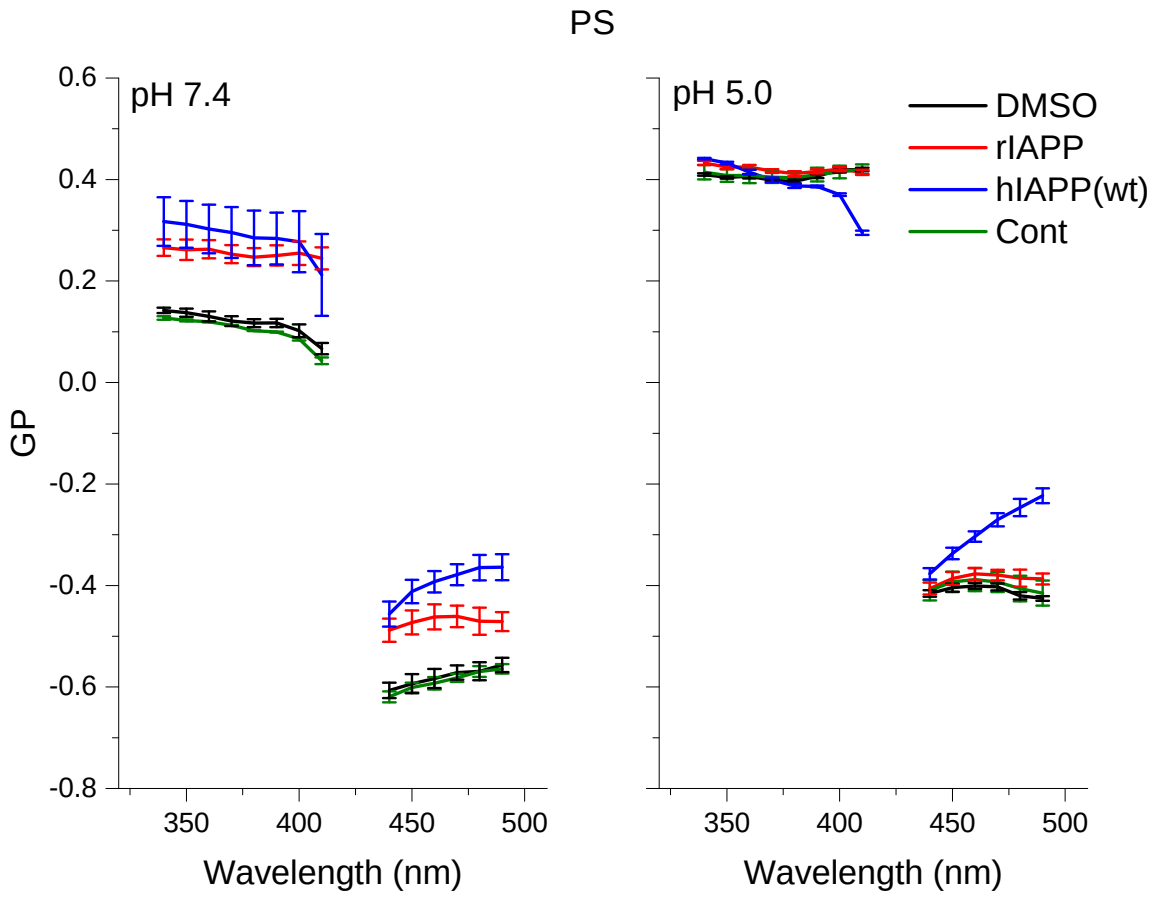

Figure 6.9. Lipid order of membranes composed solely of negatively charged lipids (PS) is increased by both hIAPP(wt) and rIAPP. hIAPP(wt) or rIAPP (4.2 μM) of was incubated with liposomes (50 μM) composed of PS at pH 7.4 or 5.0. DMSO curve represents data from an equivalent volume of DMSO as peptide added to a liposomes sample. Cont stands for liposomes in the same environment but with nothing added. GPex is measured from 310 to 410 nm and GPem from 440 to 490 nm. Curves represent an average of 3 replicates and error bars represent SEM (n=3).

Upon lowering the pH, the wavelength dependence of both GPem and GPex becomes flatter. However, the overall membrane order indicated by GPem is higher (fig. 6.8, right panel). Addition of hIAPP(wt) to liposomes at pH 5 again results in an increase of both GPem and GPex, higher than at pH 7.4, with a recapitulation of the wavelength dependence.

In the low pH environment, addition of hIAPP results in a wavelength-dependent change in the GPex and GPem curves, where the GPex (340) and GPem(490) values increase more than GPem(410) and GPex (440). At both pH 7.4 and 5.0, GPex curves are similar with and without peptide. In all cases, we see that rIAPP does not affect membrane order consistent with its role as a non-toxic peptide.

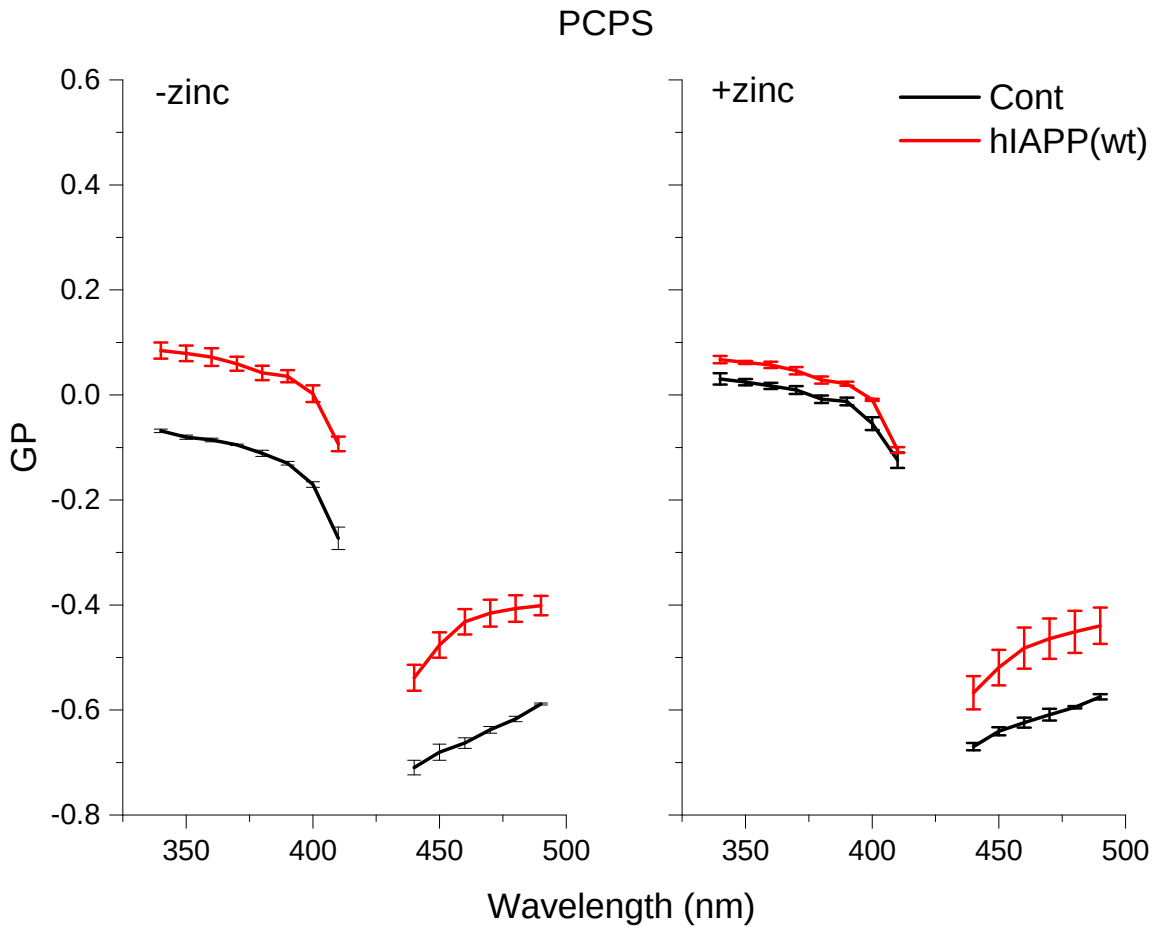

Figure 6.10. Influence of hIAPP(wt) on lipid order of negatively charged membranes PCPS in the presence of zinc. 4.2 μM of hIAPP(wt) was incubated with liposomes (50 μM) composed of PCPS (7:3 molar ratio) at pH 7.4. DMSO curve represents addition of an equivalent volume of DMSO as peptide added to lipsome samples. Cont represents liposomes in the same environment but with nothing added. GPex is measured from 310 to 410 nm and GPem from 440 to 490 nm. Curves represent an average of 3 replicates and error bars represent SEM (n=3).

Use of the non-physiological, unary composition of negatively charged PS to look at IAPP interaction shows interesting differences compared to the more physiological PCPS composition (fig. 6.9). Of particular interest is that both hIAPP and rIAPP result in an increase of membrane order. Additionally, in comparison to PCPS and PC compositions, PS has a higher overall membrane order than PC and PCPS composition at both pH 7.4 and 5.0, indicated by the GPem and GPex curve values being higher overall. In contrast to PCPS, the baseline GPem and GPex curves of PS have higher values at pH 7.4 than at pH 5.0.

We looked at the effect zinc had on how hIAPP affected the order parameters (fig. 6.10. Interestingly, the addition of zinc had an effect not dissimilar to that of pH on

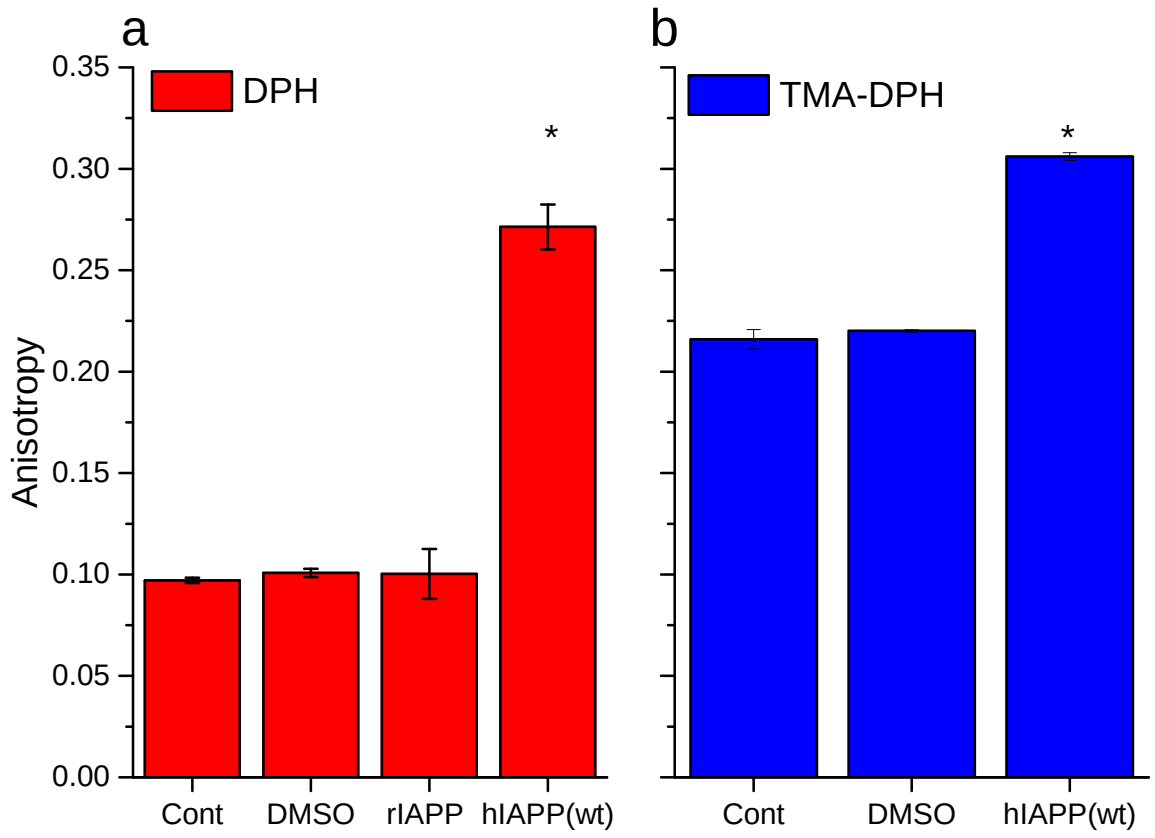

Figure 6.11. hIAPP increases the lipid order of membranes in the acyl chain region and at the level of the polar heads. Liposomes 50 μM with either DPH (a) or TMA-DPH (b) were incubated with 4.2 μM of peptide. Curves represent an avereage of 3 replicates and error bars represent SEM (n=3).

negatively charged lipid. Again the GPem curve before addition of peptide is shifted towards higher values; however there is not as much change in the GPex. Incubation of hIAPP does not result in any significant additional increase in order of either GPem or GPex. An increase in zinc and and increase in pH have the common effect of neutralising negative charge at the membrane.

Finally we looked at differences in the order of acyl chain region compared to the polar head region (fig. 6.11). DPH and TMA-DPH report membrane order I the same way but locations of the probe in the membrane is different, TMA is cationic preventing its incorporation in the acyl region. Thus the two probes report on the order of different parts of the membrane. As we can see the anisotropy reported by DPH of PCPS is lower than reported by TMA-DPH consistent with the polar head region being more order than the polar head region, which makes sense since there are more degrees of freedom in the acyl region. Addition of rIAPP to PCPS with DPH

results in a large increase in anisotropy consistent with an increase in order at the acyl chain region. The changes in the order of the acyl region, are mirrored by TMA-DPH which reports an increase in order upon incubation with hIAPP. Consistent with laurdan results DMSO has no significant effect on order at either the polar head region or at the acyl chain region.

6.3.2 Membrane viscosity

The importance of maintaining different viscosities in different parts of the cell is receiving more attention. Recently in our lab the ability of hIAPP to form a gel has been investigated, as well as the kinetics of viscosity changes during elation (Jean et al., 2016). The possibility was raised that hIAPP could form a gel at the bilayer resulting in changes in how the membrane responds, resulting in a change from physiological to pathological behaviour. Viscosity of membranes has been measured using Fluorescence Correlation Spectroscopy (FCS) by following various membrane probes in the membrane (Chiantia et al., 2009). Viscosity of, and at, the membrane can be followed using Bodipy. Levitt et al. were amongst the first people to characterise Bodipy as a viscosity probe (Levitt et al., 2009). They produced two meso-substituted fluorophores based on the boron-dipyrrin (BODIPY) structure with hydrophobic. These probes have hydrophobic additions, such as C12, that enable partition into lipid membranes. Others have since explored other variants with the purpose of targeting this probe to particular places in the cell for example the mitochondria (Zhao et al., 2016). These methods have involved making changes to the structure such that its ability to move to different membranes is restricted or that it targets membranes based on electron potential. An alternative is target the membrane by tagging proteins that are known to be in the membrane. One such methodology is SNAP tag. This is based on the use of human DNA repair protein O6-alkylguanine-DNA-alkyltransferase (hAGT) to covalently attach the probe to the protein. For this to work the protein of interest needs to be expressed with hAGT include at the end of the sequence and the probe to be covalently attached needs to have the benzylguanine attached.

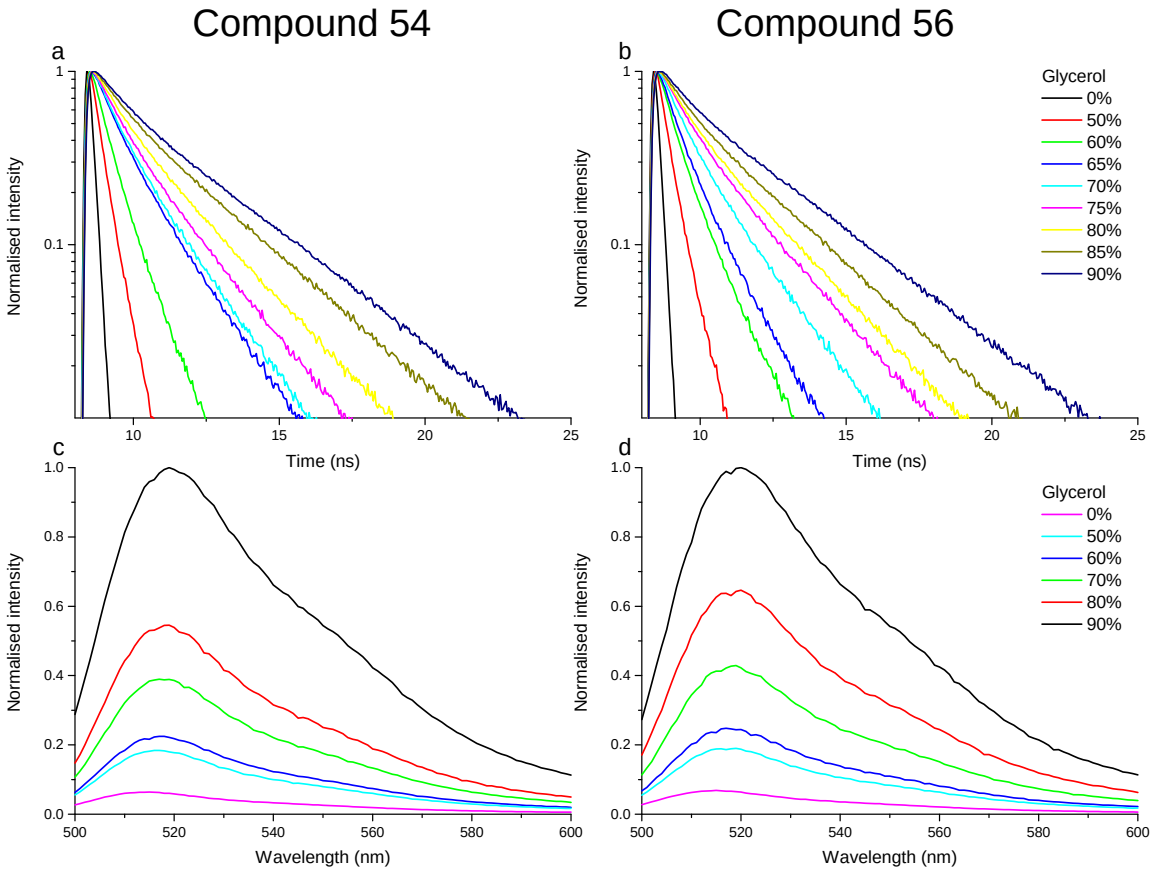

Figure 6.12. Viscosity responsiveness of intermediates measured via fluorescence intensity and lifetime. Intermediate compounds 54 and 56 along the synthesis pathway to Bodipy-SNAP were tested for preserved response to viscosity. 15 μM of each compound was tested in a series of indicated glycerol percentages in dH_2O at ambient temperatures using both fluorescence lifetime (a and b) and intensity (c and d)

In collaboration with chemistry, the Bodipy-C12 probe was adapted to a SNAP tag version. C-12 and the SNAP tag version of Bodipy was synthesised in the lab of Prof. Tim Donohue (Niall Moon). There were 2 aims: 1) synthesise Bodipy-C12 to use in initial experimentation and 2) Make a functional Bodipy-SNAP that maintained responsive to viscosity. In order to ensure that adaptation of the Bodipy probe to a SNAP tag version did not affect its characteristics as viscosity sensor, the intermediates along the synthesis pathway were tested for preservation of viscosity response. Compounds 54 and 56 were tested to check that benzyl and phenyl attachments did not interfere with the desired function as molecular rotors (fig. 6.12). Before use, both Bodipy-C12 and Bodipy-SNAP were tested for response to viscosity via both lifetime and steady state measurements (fig. 6.13).

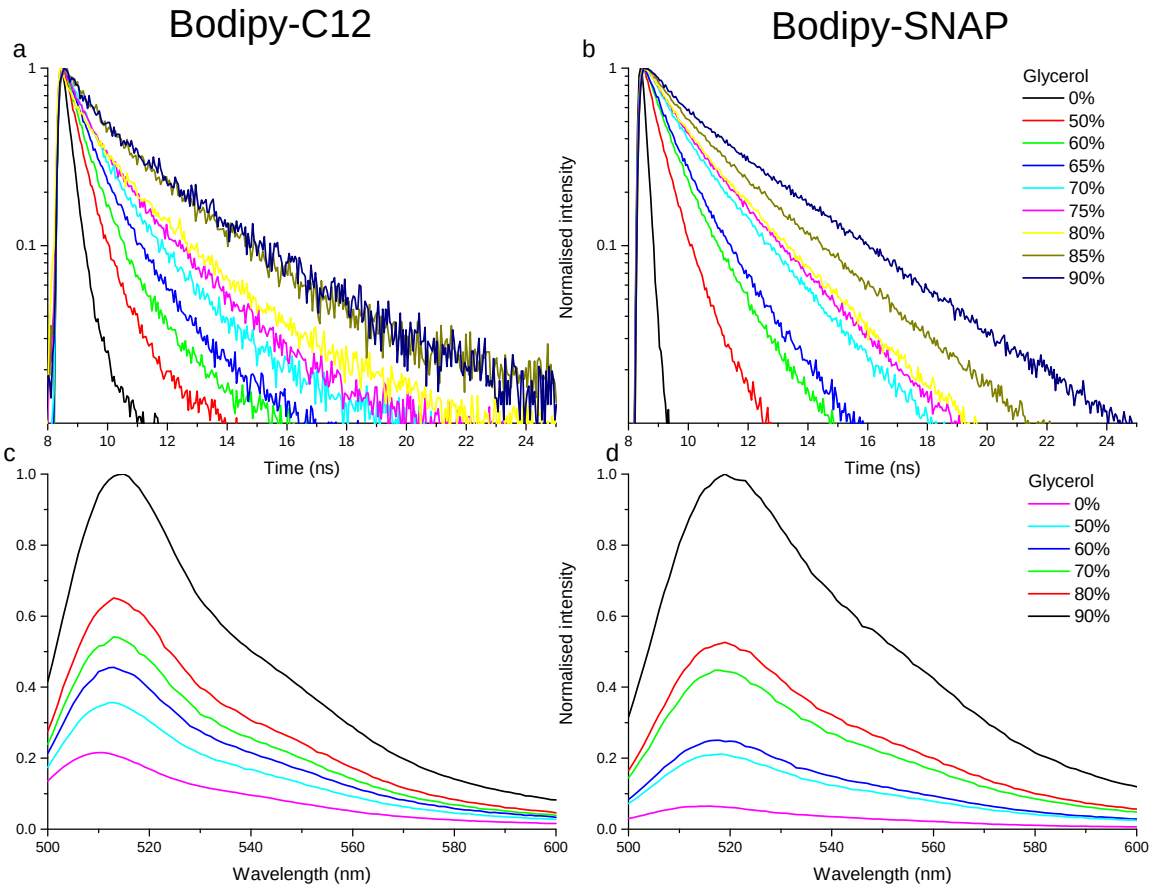

Figure 6.13. Viscosity responsiveness of Bodipy-C12 and Bodipy-SNAP. Bodipy-C12 and Bodipy-SNAP were tested for preserved response to viscosity. 15 μM of each compound was tested in a series of indicated glycerol percentages in dH_2O at ambient temperatures using both fluorescence lifetime (a and b) and intensity (c and d).

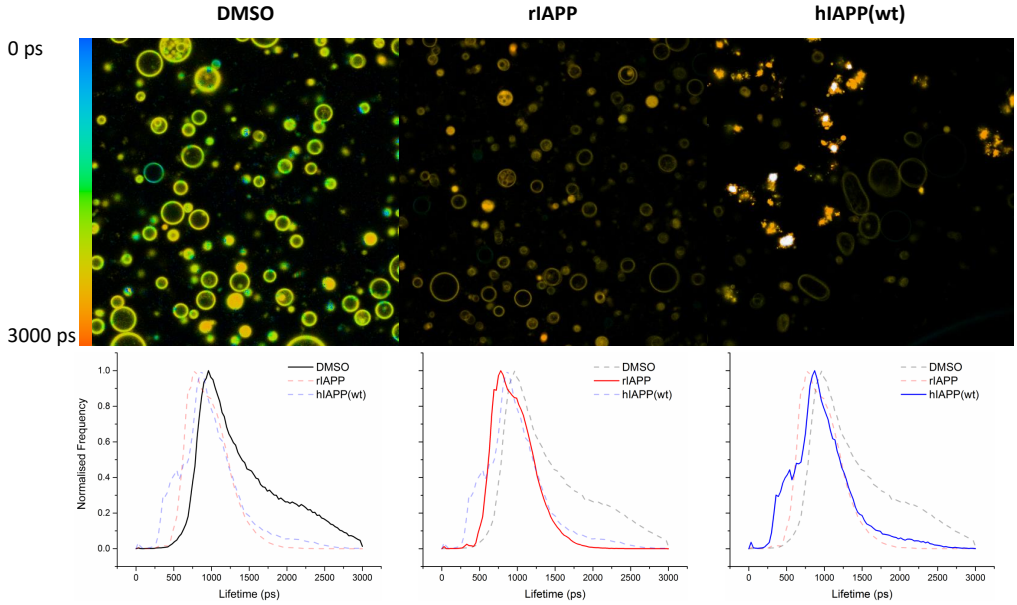

Figure 6.14. Effect of IAPP on membrane viscosity of PCPS GUVs. GUVs were incbated with DMSO, rIAPP or hIAPP(wt) for 1 hour. Images (60X magnification) of lipsomes in each condition is shown on the top row. The bottom row shows a normalised histogram of lifetimes for each condition (solid line) together with histograms from the other conditions (dashed line). The rainbow colour bar represents the lifetime of Bodipy-SNAP in picoseconds (ps) with longer lifetimes representing higher viscosity.

I used Bodipy-C12 in GUVs and LUVs to look at a 3 hour time point after addition of hIAPP(wt). A relative high F:L ratio (1:20) was used in order to more easily measure any changes to viscosity of the membrane. Shown in figure 6.14 are representative images of GUVs incubated with DMSO, rIAPP or hIAPP. Although I have shown throughout the thesis that DMSO does not affect read outs of the other assays, GUVs are larger and therefore differ in terms of curvature. The tension of such surfaces may be affected differently and so I wanted to rule out any vesiculation DMSO was included as a control. Looking at the associated histograms of pixels with certain lifetimes we can see that addition of both rIAPP and hIAPP results in a shift from higher lifetimes to lower lifetimes. It is important to remember that the GUVs are made with 300 mM sucrose in the internal volume. For microscopy a volume of these GUVs are added to 100 mM salt solution (The GUVs are able to maintain integrity despite this mismatch in osmolality). However, the internal viscosities will differ as even at the same concentration, sucrose is more viscous than NaCl.

Therefore internal and external leaflets of the membrane will differ in viscosity. At the level of magnification and resolution of a confocal microscopy it is not possible to resolve such a difference. However there is clearly a decrease in viscosity of the environment which Bodipy is experiencing. It is likely that the presence of sucrose in the luminal volume has an effect on the reported viscosity. Interestingly, although incubation with rIAPP does not seem to result in a loss of integrity (lack of aggregate lipids) there is a decrease in fluorescence lifetime, consistent with a decrease in viscosity. GUVs incubated with hIAPP shows presence of lipid aggregates. This is reflected in the accompanying histogram distribution of lifetimes, by an appearance of a shoulder at lower lifetimes. It is possible that due to loss of membrane integrity the sucrose that was once luminal is diluted into the bulk. The organisation of the lipids may now be such that sucrose is excluding from accessing Bodipy, contributing this shoulder of lower viscosity.

I also looked at Bodipy-C12 in live cells (fig. 6.15 and fig. 6.16). In fig. 6.15 cells were incubated in cygel. Cygel has the property of being liquid at 4°C but becomes a gel when warmed above 23°C. Interestingly although the temperature at which the cells were imaged meant that cygel is in a gel form, the lifetime of Bodipy in the plasma membrane is lower than intracellularly. This suggests that cygel may act as a gel on a macroscopic level but at a microscopic level a Bodipy responds in a different way. To illustrate the proof of concept of concept of targeting Bodipy-SNAP, HeLa cells were transfected with a plasmid expressing a SNAP tagable version of a Nup protein. As can bee seen in fig. 6.16 there is a clear attachment of Bodipy-SNAP to the nuclear membrane.

6.4 Discussion

The effect that amyloid peptides have on lipid order has been previously investigated; Aβ (Hicks et al., 2008; Ashley et al., 2006; Yip et al., 2002; Waschuk et al., 2001; Kremer et al., 2001), α-synuclein (Kamp and Beyer, 2006), β2-microglobulin (Sheynis et al., 2013) and lysozyme (Melo et al., 2014; Kastorna et al., 2012), and most recently

hIAPP (Pilkington et al., 2016), have all been investigated for their ability to affect order using laurdan based measurements. These studies range from looking at the order of membranes in the context of live cells, plasma and or organelle isolated membranes, and LUVs and GUVs. Not surprisingly, the conclusions drawn from these studies can be separated into ones that looked at order of live cell membranes or of isolated/synthetic generated mimetic membranes. In general an increase in lipid order is seen when adding amyloid peptides to membrane mimetics, however experiments using live cells are likely to yield different results as cell membranes are dynamic and more complex in composition. Indeed investigation of the effect of IAPP on lipid order in live cells demonstrated a decrease in membrane order (Pilkington et al., 2016) in contrast to my work using LUVs which showed an increase in membrane order. The results from my experiments are in agreement with others that have used membrane mimetics to investigate effect of Aβ on membrane (Kremer et al., 2001). In agreement with data produced form my experiments using laurdan, changes in DPH anisotropy indicate that interaction of IAPP with the lipid membrane results in changes in the lipid head group environment, consistent with either an increase in lipid order or an increase in water penetration at the interfacial region.

Other factors may contribute to differences in how amyloid effects membrane order. Initial membrane order has be shown to differ due to geometry of the bilayer, with planar surfaces being less ordered than curved surfaces (Yip et al., 2002). Yip et al. show that Aβ is able to increase the GP of membrane in both gel (planar) and liquid crystalline (liposome) phases. However others have demonstrated an inability of Aβ to effect fluidity of lipid membranes in a gel phase (Kremer et al., 2001). Khemtémourian et al. (2011) look at the effect of hIAPP on membrane order using NMR. They posit that their results are consistent with either 1. Reduction in vesicle size producing a heterogeneous size distribution or 2. Perturbation of lipid acyl chain order and lipid dynamics. Khemtemourian et al. support 1. based on DLS size distribution of liposomes becoming smaller (Khemtémourian et al., 2011). The results of Khemtermourian et al. contrast with the results from my experiments using laurdan. The main difference is that they use NMR spectroscopy to measure lipid

order. In addition the way IAPP is added to lipid differs; IAPP peptide was added to lipid in chloroform solution, with multilamellar liposomes subsequently formed for experimentation.

The results regarding the effect of pH and hIAPP(wt) on lipid order of PCPS are summarised in figure 6.17 and reveal interesting aspects of IAPP order induction. Using figure 6.5 as a reference for changes to membrane order, we can see that decrease in pH results in the loss of wavelength dependence consistent with the lipids in the membrane becoming a more ordered gel phase. Subsequent addition of hIAPP results in an increase of order but with a wavelength dependence.

When the environment remains at a neutral pH, addition of hIAPP again increases lipid order but the phase is still consistent with a liquid like environment. Changes in GPex(410) and GPem(440) without changes in GPex(340) and GPem(490) indicate that only those laurdan molecules in a more restricted (gel-like) micro-environments are affected (Kremer et al., 2001). In the data I am reporting, the opposite trend is apparent with an increase in GPex(340) and GPem(410) without associated increase in GPex(410) and GPem(440) indicating that only molecules in a less restricted (liquid-like) environment are effected.

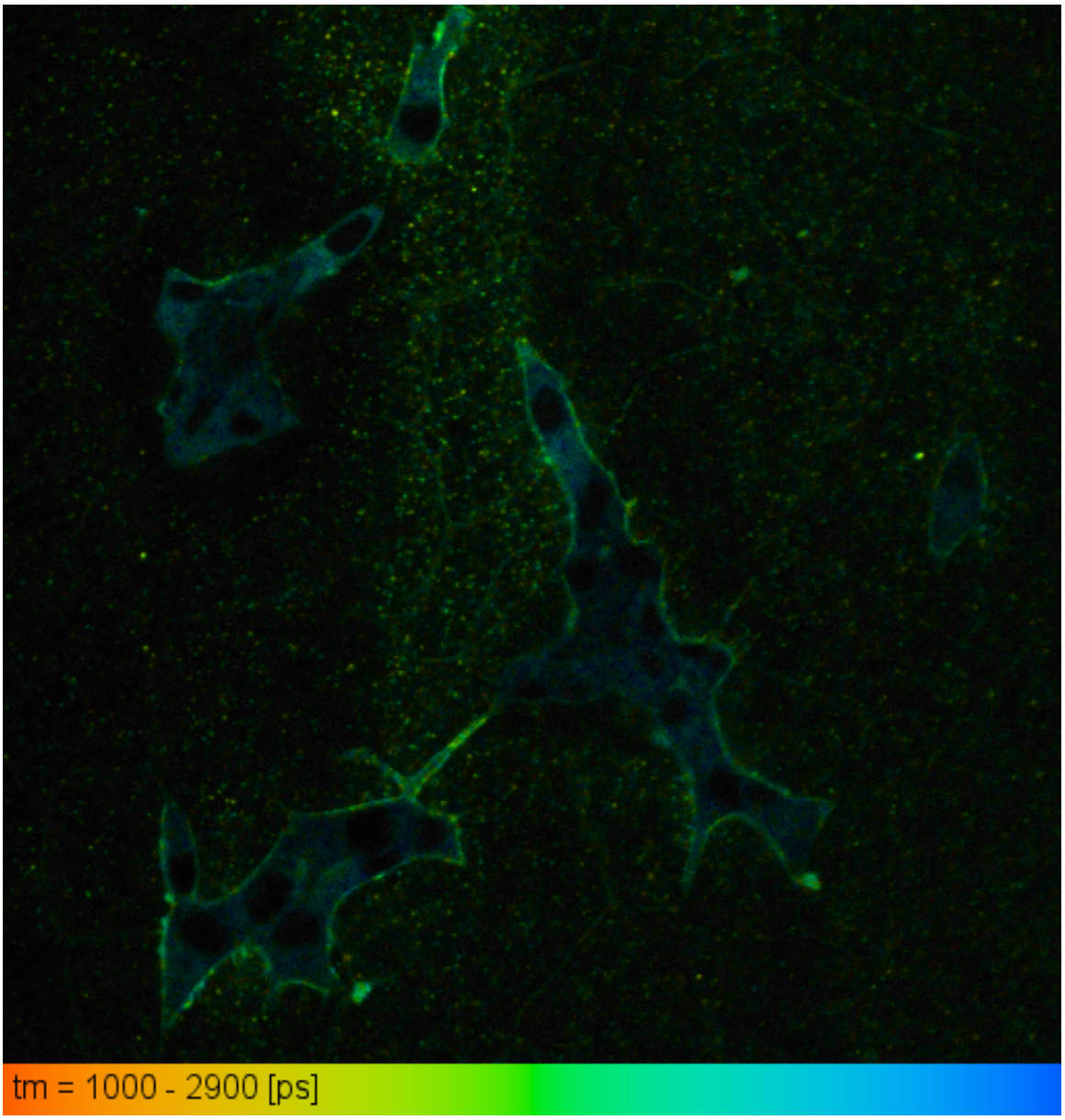

Figure 6.15. INS1e cells with Bodipy-C12 in membranes after application of viscosity altering cygel. Cells were incubated with 15 μM of Bodipy-C12. The rainbow colour bar represents the lifetime of Bodipy-SNAP in picoseconds (ps) with longer lifetimes correlating with higher viscosity. Image was obtained using a 60X Objective.

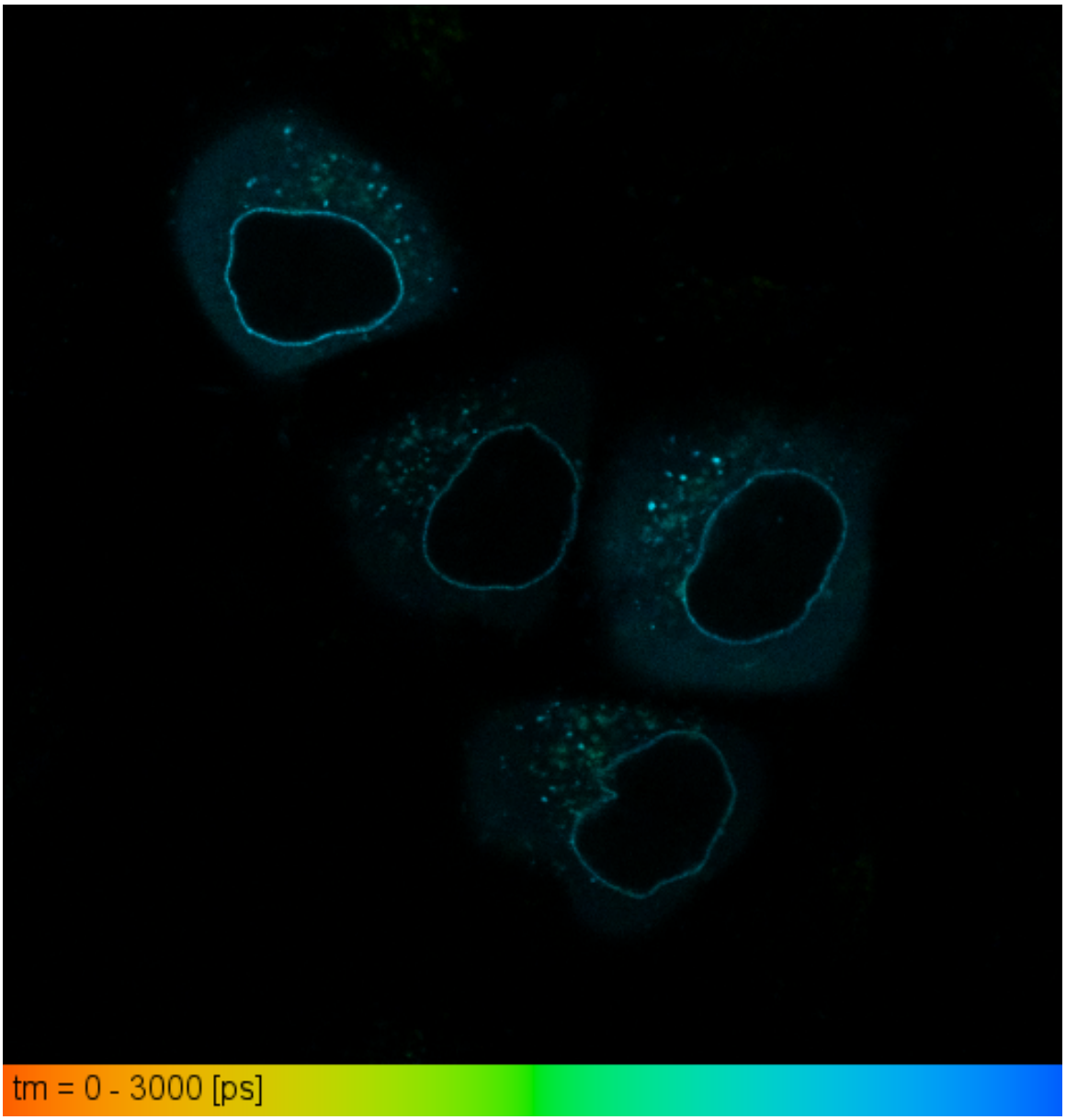

Figure 6.16. HeLa cells with Bodipy-SNAP attached to Nup complex in the nuclear membrane. The rainbow colour bar represents the lifetime of Bodipy-SNAP in picoseconds (ps) with longest lifetimes correlating with higher viscosity. Image was obtained using a 100X Objective. Sample prepared, and image obtained, by Alex Foley (Vaux Group, Sir William Dunn School of Pathology).

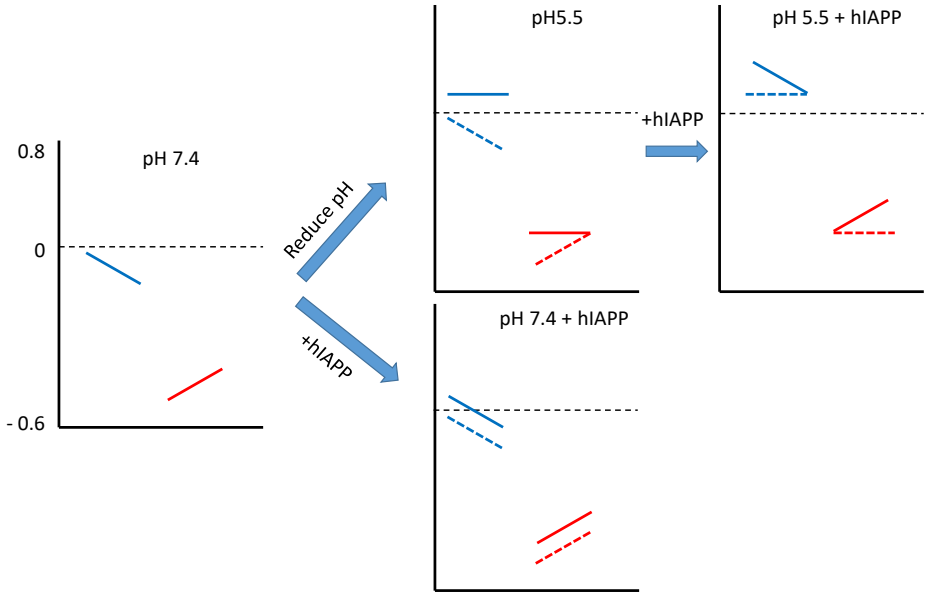

Figure 6.17. Changes to GP wavelength dependence with pH.

Chapter 7

Discussion

7.1 Summary of results

The results of this thesis are the culmination of efforts to decipher the structural changes imparted on hIAPP and lipid membranes due to their interaction. Attention was paid to how this interaction can be modified by the physiological environment of the granule. The desire was to shed light on how the modulation of this environment might result in the pathology of T2D. hIAPPs toxic effect on cells is clear from the literature and experiments establishing IAPP interaction with cellular membrane mimetics have shown how lipid composition can affect the way IAPP fibrillizes. Although these systems are highly reductionist, they are extremely valuable in that they afford high control and repeatability, and as such have provided a basis for new insights to possible mechanisms of membrane mediated toxicty of hIAPP.

Surprisingly, I have found that neutral PC liposomes, in a high ionic environment, were able to accelerate the fibrillization of hIAPP without undergoing loss of integrity due to hIAPP interaction. Additionally, inclusion of negatively charged lipid, PS, resulted in liposomes that were capable of undergoing lipid mixing. Most notably this lipid mixing behaviour is accelerated by the presence of zinc, speculated to be through an intermediate consistent with non-amyloid structure. In contrast, a high ionic strength environment slows down lipid mixing whilst also slowing fibrillization.

The kinetics strongly suggest the existence of different pathways of lipid mixing by hIAPP.

The novel phenomenon of hIAPP-induced lipid mixing of PCPS liposomes was investigated further by NTA and proved to be successful in confirming fusion. It is a powerful technique, enabling the measurement of the diameter of many particles, in the order of thousands, without any special treatment of the sample e.g. addition of fluorescent probes. However, liposomes were made with fluorecent probes in order to avoid non linear light scattering as partciles increased in diamtere. In line with a fusogenic role, incubation of hIAPP with liposomes led to an increase in size distribution of liposomes. In addition fusion of liposomes was accelerated with the addition of zinc. The hope was to extend the use of NTA using FRET and dequenching approaches to characterise fusion between liposomes of the same lipid composition (homotypic) and of different compositions (heterotypic). Although a FRET based approach was ultimately not feasable due to cross excition of the acceptor, fluorescence dequenching experiments using r18 showed promise and minor adaptations to hardware and data analysis are expected to make measurement of FRET relatively simple.

Changes to membrane order induced by interaction with IAPP have been investigated for the first time using the probe laurdan. It has been demonstrated that the order of lipids in neutral liposomes (PC), at low ionic strength, is not affected by either rIAPP or hIAPP, consistent with other measures of interaction. The investigation of lipid order of liposomes composed of PCPS shows that interaction of hIAPP decreases fluidity (increases order) whilst rIAPP has no effect. However, membranes of liposomes composed solely of negatively charged lipid (PS) became more ordered in the presence of both hIAPP and rIAPP. This raises the possibility that membrane charge, combined with lipid order, are important determinants of IAPP-membrane interaction and is not just associated with an ability of IAPP to form amyloid. Additionally, pH has a differential effect on lipid order, with low pH increasing baseline order of both PS and PCPS liposomes and alters the way hIAPP increases order of PCPS liposome membranes.

In addition to the above some interesting results regarding hIAPP variants were generated. I showed that an addition of a single tryptophan (hIAPP(W38)) significantly reduces the rate and amount of fibrillization as well as the amount of leakage from PCPS liposomes. However, we confirmed that a substitution with tryptophan, hIAPP(Y37W), had no effect on either fibrillization or capacity to induce leakage.

7.2 Inferences from the results

In the context of the pancreatic islet, there are many factors, both in the milieu of the secretory granule and cytoplasm in the secretory beta cell and extracellular matrix, that may be relevant to the pathological perturbation of hIAPP and membrane structure. The effects of many of them on the structure of IAPP in non-lipid environments have been addressed in the literature. However it is beyond the scope of this thesis to explore all of them in regards to their effect on peptide-lipid interaction and structure. Using simple compositions, we have gone some way to addressing the role of the physiological relevant cation zinc in changes to peptide and membrane following their interaction. Zinc at a concentration that accelerates lipid mixing of PCPS membranes prevents burial of the hIAPP C-terminal region and fibrillization. Prevention of C-terminal burial may allow hIAPP to form oligomers that are better able to induce curvature. The effect of zinc on liposome leakage could not be assessed, due to its interference with the Tb-DPA assay, but we know from the experiments in buffer without zinc and NaCl that leakage of PCPS liposmes precedes lipid mixing. This poses the question- What structures might be involved in these different process and is there interconversion?

Work looking at IAPP-induced leakage of DOPG liposomes by rIAPP and hIAPP found that leakage was inconsistent with a detergent or carpet mechanism. Instead the data supported an all-or-none mechanism, from a non-amyloid and non-β sheet structure, postulated to be pore of toroidal, barrel or chaotic (Last et al., 2011). As fusion of membranes induced by peptides often proceeds through pore formation

(Gilbert, 2016), it is of interest to see what effect zinc would have on the structure of IAPP peptides that cause fusion. Would there be change in the α-helical structure and would oligomers become "off pathway" β sheet?. A lack of increase in ThT fluorescence does not necessarily reflect a lack of β sheet. Indeed, it has been demonstrated that binding of ThT requires the stacking of at least 4-5 beta sheet monomers. Of course CD measurements would go some way to addressing these questions and given more time it would be an avenue which I would want to pursue.

A high ionic strength environment increases the lag phase of hIAPP(wt) induced lipid mixing, which correlates with an increase in lag phase of fibrillization. Again, results from tryptophan burial experiments indicate that a high ionic strength environment prevents burial of the C-terminus into the membrane. However, this seems not to impact subsequent fibrillization. From lipid order measurements it is clear that pH has a differential ability to effect membrane order, dependent on a combination of lipid charge and interacting peptide (hIAPP or rIAPP). Low pH has been shown to inhibit hIAPP fibrillization, as well as increase the lag time, which correlates with reduction in liposome leakage (Khemtémourian et al., 2011). Using solid state NMR Khemetemourian et al. also show that hIAPP(1-19) has the capacity to disorder the acyl chain (Khemtémourian et al., 2010). However, using NMR, it was shown with Aβ incorporated in liposomes increased the acyl chain order (Lau et al., 2007). There is data supporting the concept that neutralisation is amongst one of the last things to happen during fusion (Hutton, 1982), suggesting that a maintenance of a low pH is important up until the last moment. Although hIAPP increases order of PCPS at both pH 5.0 and 7.4, the order at pH 5.5 is consistent with a liquid ordered phase whereas at pH 7.4 it remains in a fluid phase. Such a difference may be of importance in the granule. The results from the membrane order experiments are from end timepoints, but the kinetics of order change would be of great interest. A further question that this research opens up is whether IAPP initially behaves like mastoparan, inserting into membrane without affecting lipid order, undergoing a sudden switch in confirmation now able to effect order; or is there a gradual increase order, correlating with other features of membrane interaction like leakage and fusion.

The use of NTA enabled the detection of the size distribution through single particle measurement and the complexities of interpreting this distribution in terms of fusion is discussed in chapter 5. One can envisage not only wanting to measure homotypic fusion but also heterotypic fusion; in this case, a number of parameters are of interest, including different lipid compositions, diameters of liposomes or content of the luminal volume. However, if one wanted to do this using NTA on a single particle level, FRET based measurements would be ideally placed to enable this. However, recording the desired emissions to follow FRET are complicated due to the presence of only one camera to record fluorescence emission. The instrument could be set up for FRET based measurements simply by the addition of a dichroic mirror enabling splitting of the signal and a second camera to record the fluoresce. Simultaneous recording of both channels would provide the necessary emission intensities and tracking of particles could be done using either of the channels. Since the algorithms for intensity calculation are proprietary, in order to compare intensities, the generated pixel coordinates and particle tracks could be used to find intensities per particle, frame by frame, using a script. A ratio of intensities per particle would then give a FRET value.

The kinetics of the changes of various measures of membrane and peptide structure in physiological environments would provide a picture of causative and consequential effects of their interaction. The data presented is a mixture of kinetic and dynamic data, using lipid compositions, to maximise the breadth of phenomena studied.

7.3 Future work

The experiments presented within this thesis pave the way for further research to understand important determinants for IAPP induced fusion of liposomes. In particular, the secondary structure content of hIAPP conformations that can cause lipid mixing has not been fully elucidated. Although we confirmed by CD that all three hIAPP variants (wt, w38 and Y37W) could form elements of β-sheet structure in solution, consistent with fibrillization, the secondary structure of fusogenic IAPP

conformations could not be determined. In chapter 4 I showed that zinc could be used to block fibrillization whilst accelerating lipid mixing. It is possible that zinc stabilizes α-helical structure or permits formation of oligomers with β sheet structure but stops these oligomers from assembling into structures capable of binding ThT. One difficulty with using CD to examine the changes in secondary structure is the strict criteria for selection of solvents. If one wants to make recordings in the UV range the solvent needs to have low ultraviolet (UV) absorption and the main buffer used in this thesis for assays contained HEPES which absorbs in the UV range. In addition DMSO is also known to absorb in the UV range and thus reducing its concentration in a sample is recommended. Therefore when measuring CD spectra of IAPP I used a peptide from a stock dissolved in HFIP and incubated in phosphate buffer, all of which are compatible with obtaining CD spectra. This allowed me to know that the hIAPP peptides could all form beta sheet structure consistent with the ThT data. Ideally, I would have liked to compare the secondary structure of IAPP with and without zinc and correlate this with fusion. However, to compare the kinetics of fibrillization, lipid mixing and secondary structure, it would have been necessary to use the same buffers and solvents. Since the buffer and stock preparations used in ThT and fusion assays were not compatible with acquisition of secondary structure by CD this was not possible. For future experiments in this area one could use phosphate buffer and HFIP for all assays. However as has already been noted, the kinetics of fibrillization can be altered by many factors including pH, buffer composition, salt and lipid composition and one cannot predict the effect. In addition use of HFIP is known to effect the order of lipid membranes and thus use of it in the lipid mixing assay may produce unexpected results.

One interesting way to pursue the important structural elements of fusogenic hIAPP might be to use the mutant hIAPP(L12N/N14L). This double mutation is conservative with respect to formation of parallel, in register, β sheet stacking. However it is not conservative with respect to α-helical propensity has reduced α-helical content (Magzoub and Miranker, 2012). One can imagine that if fusion

was due to an on pathway, beta-sheet oligomeric species, hIAPP(L12N/N14L) would still be able to cause fusion as this peptide is still able to form fibrils which I have shown correlate with fusion. However, if it was the case that an α-helical oligomeric species was necessary for fusion one might see a lack of fusion but formation of ThT positive fibrils.

One experiment that would be of interest to undertake would be that involving the use of both the fluorescent properties of trytophan, in hIAPP(Y37W) and laurdan. FRET between trytophan and laurdan has been used previously to gain low resolution structural information of the position of acetylcholine receptor in lipid bilayers (Antollini et al., 1996). In addition, by selectively exciting laurdan molecules that were close to tryptophan residues or exciting laurdan directly, at different temperatures, it was possible to gain information about vicinal lipid order around tryptophan as compared to the bulk membrane. The data described in this paper was gathered using steady state intensity measurents requiring a lot of control measurments resulting in a complicated protocol in order to correctly measure FRET and different GP values (Antollini and Barrantes, 2007). One way to circumvent such control measurements is to move from the steady state domain to the life time domain as measurement of lifetime of a probe does not depend on its concentration. Thus both the lifetimes of tryptophan with and without laurdan, would be easier to retrive. At the time the original work was done with acetylcholine receptor (1996) the use of a pulsed UV source, which is necessary to gain lifteime information of trytophan, was not as wide spread but is now becoming more mainstream and thus would definitely be a useful avenue to pursue.

The relevance of this work to the pathology of T2D would be strengthened by establishing aspects of it in cellular models. As highlighted previously, the use of synthetic membrane mimetics are highly reductionist. Although the use of the types and ratios of lipid used in this thesis are in line published research literature, there are aspects of cellular lipid complexity that have not been investigated in relation to the phenomena described in this thesis.

In terms of lipids, ternary systems using Phosphatidylethanolamine (PE) (Sciacca et al., 2012) and cholesterol (Cho et al., 2009; Cao et al., 2013) have been shown to modulate IAPP folding and the extent of membrane perturbation. Of course the use of lipids derived from cells is a step closer to full physiological relevance however discrepancies have arisen. Use of giant plasma membrane vesicles (GPMVs) derived from COS-1 cell membranes apparently inhibits fibrillization of hIAPP, despite binding to the membrane (Schlamadinger and Miranker, 2014). This is in contrast to another study where GUVs formed of lipids extracted from INS-1 cells accelerated fibrillization and resulted in membrane perturbation (Seeliger et al., 2012). Differences in the type of cells, and their condition, from which the lipid was isolated, as well as the experimental method for vesicle preparation may explain these differences. In any case, a key factor is a lack of cellular dynamics, and by extension a dynamic membrane. Endogenously and exogenous IAPP cause toxicity to cells, and apart from the membrane perturbation hypothesis, IAPP is thought to induce toxicity through other routes as described in Chapter 1. It is possible that induction of such processes might have an effect on membrane composition contributing to a diversification of toxicity by IAPP interaction with membrane. Recently absolute amounts and proportions of lipids in plasma, secretory granule and mitochondrial membranes from Ins-1 pancreatic β cells was published (MacDonald et al., 2015). In addition, the proportions of a variety of lipids in these organelles was found to undergo changes in response to glucose. This demonstrates the importance of the use of dynamic membranes when assessing the membrane-mediated toxicity of IAPP. Although absolute control of lipid composition is not possible in live cells, some control of cholesterol content in various cell compartments has been modulated by addition and removal (Wang et al., 2000; Bogan et al., 2012).

Translating the kind of measurements done in liposome-based systems to a live cell context is possible, but it can be complicated. We have started in this vein with the creation of a SNAP tag version of the molecular rotor for the investigation of viscosity changes and have demonstrated targeting to a nuclear membrane protein. Targeting

of the probe to any part of the cell that has proteins is theoretically possible and one can envisage a secretory granule with Bodipy-SNAP bound, in turn, to proteins on the luminal and cytosolic sides of the membrane. In addition, measuring viscosity of the mitochondrial membranes and compartments would be of interest since hIAPP has been shown to associate with them and induce toxicity.

In conclusion, my novel finding is that hIAPP is capable of fusion and that this can be separated into different kinetic regimes using zinc and NaCl. I was able to further confirm fusion using NTA and show that liposomes increased in size with addition of hIAPP and was modulated by zince. It will be of particular interest to investigate the role of unwanted fusion in the granule, or indeed if it has a dual physiological role that is beneficial to the cell in other contexts.

References

Abedini, A. and Raleigh, D. P. Destabilization of human IAPP amyloid fibrils by proline mutations outside of the putative amyloidogenic domain: Is there a critical amyloidogenic domain in human IAPP? *Journal of Molecular Biology*, 355(2): 274–281, 2006.

Abedini, A. and Raleigh, D. P. A role for helical intermediates in amyloid formation by natively unfolded polypeptides? *Physical Biology*, 6(1):015005, feb 2009.

Ahronheim, J. H. The nature of the hyaline material in the pancreatic islands in diabetes mellitus. *The American journal of pathology*, 19(5):873, 1943.

Aitken, J. F., Loomes, K. M., Scott, D. W., Reddy, S., Phillips, A. R. J., Prijic, G., Fernando, C., Zhang, S., Broadhurst, R., L'Huillier, P., and Cooper, G. J. S. Tetracycline treatment retards the onset and slows the progression of diabetes in human amylin/islet amyloid polypeptide transgenic mice. *Diabetes*, 59(1):161–171, 2010.

Akter, R., Cao, P., Noor, H., Ridgway, Z., Tu, L. H., Wang, H., Wong, A. G., Zhang, X., Abedini, A., Schmidt, A. M., and Raleigh, D. P. Islet Amyloid Polypeptide: Structure, Function, and Pathophysiology. *Journal of Diabetes Research*, 2016, 2016.

Anguiano, M., Nowak, R. J., and Lansbury, P. T. Protofibrillar islet amyloid polypeptide permeabilizes synthetic vesicles by a pore-like mechanism that may be relevant to type II diabetes. *Biochemistry*, 41(38):11338–11343, 2002.

Antollini, S. S., Soto, M. a., Bonini de Romanelli, I., Gutiérrez-Merino, C., Sotomayor, P., and Barrantes, F. J. Physical state of bulk and protein-associated lipid in nicotinic acetylcholine receptor-rich membrane studied by laurdan generalized polarization and fluorescence energy transfer. *Biophysical journal*, 70(3):1275–84, mar 1996.

Antollini, S. S. and Barrantes, F. J. Laurdan studies of membrane lipid-nicotinic acetylcholine receptor protein interactions. *Methods in molecular biology (Clifton, N.J.)*, 400(2):531–42, jan 2007.

Apostolidou, M., Jayasinghe, S. a., and Langen, R. Structure of alpha-helical membrane-bound human islet amyloid polypeptide and its implications for membrane-mediated misfolding. *The Journal of biological chemistry*, 283(25): 17205–10, jun 2008.

Arbuzova, A. and Schwarz, G. Pore-forming action of mastoparan peptides on liposomes: a quantitative analysis. *Biochimica et biophysica acta*, 1420(1-2):139–52, aug 1999.

Ashburn, T. T. and Lansbury, P. T. Interspecies sequence variations affect the kinetics and thermodynamics of amyloid formation: peptide models of pancreatic amyloid. *Journal of the American Chemical Society*, 115(23):11012–11013, 1993.

Ashley, R. H., Harroun, T. a., Hauss, T., Breen, K. C., and Bradshaw, J. P. Autoinsertion of soluble oligomers of Alzheimer's Abeta(1-42) peptide into cholesterol-containing membranes is accompanied by relocation of the sterol towards the bilayer surface. *BMC structural biology*, 6:21, jan 2006.

Bagatolli, L. a., Gratton, E., and Fidelio, G. D. Water dynamics in glycosphingolipid aggregates studied by LAURDAN fluorescence. *Biophysical journal*, 75(1):331–41, jul 1998.

Bagatolli, L. a., Parasassi, T., Fidelio, G. D., and Gratton, E. A model for the interaction of 6-lauroyl-2-(N,N-dimethylamino)naphthalene with lipid

environments: implications for spectral properties. *Photochemistry and photobiology*, 70(4):557–64, oct 1999.

Bagatolli, L. a. To see or not to see: lateral organization of biological membranes and fluorescence microscopy. *Biochimica et biophysica acta*, 1758(10):1541–56, oct 2006.

Bai, J. Z., Saafi, E. L., Zhang, S., and Cooper, G. J. Role of Ca2+ in apoptosis evoked by human amylin in pancreatic islet beta-cells. *Biochem J*, 343 Pt 1:53–61, 1999.

Baumgart, T., Hunt, G., Farkas, E. R., Webb, W. W., and Feigenson, G. W. Fluorescence probe partitioning between Lo/Ld phases in lipid membranes. *Biochimica et Biophysica Acta (BBA) - Biomembranes*, 1768(9):2182–2194, sep 2007.

Bernhardt, N. A., Berhanu, W. M., and Hansmann, U. H. E. Mutations and Seeding of Amylin Fibril-Like Oligomers. *The Journal of Physical Chemistry B*, 117(50): 16076–16085, dec 2013.

Betsholtz, C., Christmansson, L., Engström, U., Rorsman, F., Svensson, V., Johnson, K. H., and Westermark, P. Sequence divergence in a specific region of islet amyloid polypeptide (IAPP) explains differences in islet amyloid formation between species. *FEBS Letters*, 251(1-2):261–264, 1989.

Biancalana, M. and Koide, S. Molecular mechanism of Thioflavin-T binding to amyloid fibrils. *Biochimica et Biophysica Acta - Proteins and Proteomics*, 1804 (7):1405–1412, 2010.

Bogan, J. S., Xu, Y., and Hao, M. Cholesterol accumulation increases insulin granule size and impairs membrane trafficking. *Traffic (Copenhagen, Denmark)*, 13(11): 1466–80, nov 2012.

Bram, Y., Frydman-Marom, A., Yanai, I., Gilead, S., Shaltiel-Karyo, R., Amdursky, N., and Gazit, E. Apoptosis induced by islet amyloid polypeptide soluble oligomers is neutralized by diabetes-associated specific antibodies. *Scientific reports*, 4(Dm): 4267, jan 2014.

Braun, A. R., Sevcsik, E., Chin, P., Rhoades, E., Tristram-Nagle, S., and Sachs, J. N. α-Synuclein Induces Both Positive Mean Curvature and Negative Gaussian Curvature in Membranes. *Journal of the American Chemical Society*, 134(5):2613–2620, feb 2012.

Brender, J. R., Hartman, K., Nanga, R. P. R., Popovych, N., de la Salud Bea, R., Vivekanandan, S., Marsh, E. N. G., and Ramamoorthy, A. Role of zinc in human islet amyloid polypeptide aggregation. *Journal of the American Chemical Society*, 132(26):8973–83, jul 2010.

Brender, J. R., Lee, E. L., Hartman, K., Wong, P. T., Ramamoorthy, A., Steel, D. G., and Gafni, A. Biphasic effects of insulin on islet amyloid polypeptide membrane disruption. *Biophysical journal*, 100(3):685–92, feb 2011.

Brender, J. R., Heyl, D. L., Samisetti, S., Kotler, S. A., Osborne, J. M., Pesaru, R. R., and Ramamoorthy, A. Membrane disordering is not sufficient for membrane permeabilization by islet amyloid polypeptide: studies of IAPP(2029) fragments. *Physical Chemistry Chemical Physics*, 15(23):8908, jun 2013.

Buchanan, L. E., Dunkelberger, E. B., Tran, H. Q., Cheng, P.-N. P.-N. N., Chiu, C.-C. C.-C., Cao, P., Raleigh, D. P., de Pablo, J. J., Nowick, J. S., and Zanni, M. T. Mechanism of IAPP amyloid fibril formation involves an intermediate with a transient β-sheet. *Proceedings of the National Academy of Sciences of the United States of America*, 110(48):1–6, nov 2013.

Butler, A. E., Janson, J., Bonner-Weir, S., Ritzel, R., Rizza, R. A., and Butler, P. C. Beta-cell deficit and increased beta-cell apoptosis in humans with type 2 diabetes. *Diabetes*, 52(1):102–10, jan 2003a.

Butler, A. E., Janson, J., Soeller, W. C., and Butler, P. C. Increased Beta -Cell Apoptosis Prevents Adaptive Increase in Beta -Cell Mass in Mouse Model of Type 2 Diabetes. *Diabetes*, 52(September):2304–2314, 2003b.

Caillon, L., Lequin, O., and Khemtémourian, L. Evaluation of membrane models and their composition for islet amyloid polypeptide-membrane aggregation. *Biochimica et Biophysica Acta - Biomembranes*, 1828(9):2091–2098, may 2013.

Cao, P., Tu, L.-h., Abedini, A., Levsh, O., Akter, R., Patsalo, V., Schmidt, A. M., and Raleigh, D. P. Sensitivity of Amyloid Formation by Human Islet Amyloid Polypeptide to Mutations at Residue 20. *Journal of Molecular Biology*, 421(2-3): 282–295, aug 2012.

Cao, P., Marek, P., Noor, H., Patsalo, V., Tu, L.-H., Wang, H., Abedini, A., and Raleigh, D. P. Islet amyloid: from fundamental biophysics to mechanisms of cytotoxicity. *FEBS letters*, 587(8):1106–18, apr 2013.

Carr, B. and Wright, M. *Nanoparticle Tracking Analysis - A Review of Applications and Usage 2010-2012*, volume 44. 2013.

Castellani, R. J., Lee, H.-g., Siedlak, S. L., Nunomura, A., Hayashi, T., Nakamura, M., Zhu, X., Perry, G., and Smith, M. A. Reexamining Alzheimer's disease: evidence for a protective role for amyloid-beta protein precursor and amyloid-beta. *Journal of Alzheimer's disease : JAD*, 18(2):447–52, 2009.

Cernea, S. and Dobreanu, M. Diabetes and beta cell function: from mechanisms to evaluation and clinical implications. *Biochemia Medica*, 23(3):266–280, 2013.

Chargé, S. B., de Koning, E. J., and Clark, a. Effect of pH and insulin on fibrillogenesis of islet amyloid polypeptide in vitro. *Biochemistry*, 34(44):14588–93, nov 1995.

Chiantia, S., Ries, J., and Schwille, P. Fluorescence correlation spectroscopy in membrane structure elucidation. *Biochim. Biophys. Acta*, 1788(1):225–233, 2009.

Cho, W.-J., Trikha, S., and Jeremic, A. M. Cholesterol regulates assembly of human islet amyloid polypeptide on model membranes. *Journal of molecular biology*, 393 (3):765–75, oct 2009.

Choi, B.-K., Choi, M.-G., Kim, J.-Y., Yang, Y., Lai, Y., Kweon, D.-H., Lee, N. K., and Shin, Y.-K. Large α-synuclein oligomers inhibit neuronal SNARE-mediated vesicle docking. *Proceedings of the National Academy of Sciences of the United States of America*, 110(10):4087–92, 2013.

Chong, S. S. Y., Taneva, S. G., Lee, J. M. C., and Cornell, R. B. The curvature sensitivity of a membrane-binding amphipathic helix can be modulated by the charge on a flanking region. *Biochemistry*, 53(3):450–61, jan 2014.

Clark, A., Wells, C. A., Buley, I. D., Cruickshank, J. K., Vanhegan, R. I., Matthews, D. R., Cooper, G. J., Holman, R. R., and Turner, R. C. Islet amyloid, increased A-cells, reduced B-cells and exocrine fibrosis: quantitative changes in the pancreas in type 2 diabetes. *Diabetes research (Edinburgh, Scotland)*, 9(4):151–9, dec 1988.

Cohen, A. S. Amyloidosis. In Glenner, G. G., Osserman, E. F., Benditt, E. P., Calkins, E., Cohen, A. S., and Zucker-Franklin, D., editors, *Amyloidosis*, pages 3–19. Springer US, Boston, MA, 1986.

Cooper, G. J., Willis, a. C., Clark, A., Turner, R. C., Sim, R. B., and Reid, K. B. Purification and characterization of a peptide from amyloid-rich pancreases of type 2 diabetic patients. *Proceedings of the National Academy of Sciences*, 84(23):8628–8632, dec 1987.

Cypionka, A., Stein, A., Hernandez, J. M., Hippchen, H., Jahn, R., and Walla, P. J. Discrimination between docking and fusion of liposomes reconstituted with neuronal SNARE-proteins using FCS. *Proceedings of the National Academy of Sciences*, 106(44):18575–18580, nov 2009.

de Planque, M. R., Raussens, V., Contera, S. A., Rijkers, D. T., Liskamp, R. M., Ruysschaert, J.-M., Ryan, J. F., Separovic, F., and Watts, A. β-Sheet Structured

β-Amyloid(1-40) Perturbs Phosphatidylcholine Model Membranes. *Journal of Molecular Biology*, 368(4):982–997, may 2007.

Dupiereux, I., Zorzi, W., Lins, L., Brasseur, R., Colson, P., Heinen, E., and Elmoualij, B. Interaction of the 106-126 prion peptide with lipid membranes and potential implication for neurotoxicity. *Biochemical and Biophysical Research Communications*, 331(4):894–901, 2005.

Eisert, R., Felau, L., and Brown, L. R. Methods for enhancing the accuracy and reproducibility of Congo red and thioflavin T assays. *Analytical Biochemistry*, 353 (1):144–146, jun 2006.

Emdin, S. O., Dodson, G. G., Cutfield, J. M., and Cutfield, S. M. Role of zinc in insulin biosynthesis. *Diabetologia*, 19(3):174–182, sep 1980.

Engel, A. and Walter, P. Membrane lysis during biological membrane fusion: collateral damage by misregulated fusion machines. *The Journal of Cell Biology*, 183(2):181–186, 2008.

Engel, M. F. M., Khemtémourian, L., Kleijer, C. C., Meeldijk, H. J. D., Jacobs, J., Verkleij, A. J., de Kruijff, B., Killian, J. A., and Höppener, J. W. M. Membrane damage by human islet amyloid polypeptide through fibril growth at the membrane. *Proceedings of the National Academy of Sciences of the United States of America*, 105(16):6033–8, apr 2008.

Fantini, J., Carlus, D., and Yahi, N. The fusogenic tilted peptide (67-78) of α-synuclein is a cholesterol binding domain. *Biochimica et biophysica acta*, 1808(10): 2343–51, oct 2011.

Filipe, V., Hawe, A., and Jiskoot, W. Critical evaluation of nanoparticle tracking analysis (NTA) by NanoSight for the measurement of nanoparticles and protein aggregates. *Pharmaceutical Research*, 27(5):796–810, 2010.

Foster, M. C., Leapman, R. D., Li, M. X., and Atwater, I. Elemental composition of secretory granules in pancreatic islets of Langerhans. *Biophysical journal*, 64(2): 525–32, feb 1993.

Fraley, R., Wilschut, J., Duzgunes, N., Smith, C., and Papahadjopoulos, D. Studies on the mechanism of membrane fusion: role of phosphate in promoting calcium ion induced fusion of phospholipid vesicles. *Biochemistry*, 19(26):6021–6029, dec 1980.

Fricker, L. D. Carboxypeptidase E. In *Handbook of Proteolytic Enzymes*, volume 1, pages 840–844. Elsevier, oct 2004.

Furuta, M., Yano, H., Zhou, A., Rouille, Y., Holst, J. J., Carroll, R., Ravazzola, M., Orci, L., Furuta, H., and Steiner, D. F. Defective prohormone processing and altered pancreatic islet morphology in mice lacking active SPC2. *Proceedings of the National Academy of Sciences*, 94(13):6646–6651, jun 1997.

Gabrys, C. M., Qiang, W., Sun, Y., Xie, L., Schmick, S. D., and Weliky, D. P. Solid-State Nuclear Magnetic Resonance Measurements of HIV Fusion Peptide 13 CO to Lipid 31 P Proximities Support Similar Partially Inserted Membrane Locations of the α Helical and β Sheet Peptide Structures. *The Journal of Physical Chemistry A*, 117(39):9848–9859, oct 2013.

Gebre-Medhin, S., Mulder, H., Pekny, M., Westermark, G., Törnell, J., Westermark, P., Sundler, F., Ahrén, B., and Betsholtz, C. Increased insulin secretion and glucose tolerance in mice lacking islet amyloid polypeptide (amylin). *Biochemical and biophysical research communications*, 250(2):271–7, sep 1998.

Giehm, L. and Otzen, D. E. Strategies to increase the reproducibility of protein fibrillization in plate reader assays. *Analytical Biochemistry*, 400(2):270–281, may 2010.

Gilbert, R. J. C. Protein-lipid interactions and non-lamellar lipidic structures in membrane pore formation and membrane fusion. *Biochimica et Biophysica Acta - Biomembranes*, 1858(3):487–499, 2016.

Gilead, S. and Gazit, E. The Role of the 1420 Domain of the Islet Amyloid Polypeptide in Amyloid Formation. *Experimental Diabetes Research*, 2008:1–8, 2008.

Grage, S. L., Afonin, S., Grüne, M., and Ulrich, A. S. Interaction of the fusogenic peptide B18 in its amyloid-state with lipid membranes studied by solid state NMR. *Chemistry and physics of lipids*, 132(1):65–77, nov 2004.

Green, J., Goldsbury, C., Mini, T., Sunderji, S., Frey, P., Kistler, J., Cooper, G., and Aebi, U. Full-length rat amylin forms fibrils following substitution of single residues from human amylin. *Journal of Molecular Biology*, 326(02):1147–1156, 2003.

Gregory, S. M., Cavenaugh, A., Journigan, V., Pokorny, A., and Almeida, P. F. F. A quantitative model for the all-or-none permeabilization of phospholipid vesicles by the antimicrobial peptide cecropin A. *Biophysical journal*, 94(5):1667–80, mar 2008.

GRODSKY, G. M. and SCHMID-FORMBY, F. Kinetic and Quantitative Relationships between Insulinc Release and 65 Zn Efflux from Perifused Islets*. *Endocrinology*, 117(2):704–710, aug 1985.

Gurlo, T., Ryazantsev, S., Huang, C.-j., Yeh, M. W., Reber, H. a., Hines, O. J., O'Brien, T. D., Glabe, C. G., and Butler, P. C. Evidence for proteotoxicity in beta cells in type 2 diabetes: toxic islet amyloid polypeptide oligomers form intracellularly in the secretory pathway. *The American journal of pathology*, 176 (2):861–9, feb 2010.

Hay, D. L., Chen, S., Lutz, T. A., Parkes, D. G., and Roth, J. D. Amylin : Pharmacology , Physiology , and Clinical Potential. (July):564–600, 2015.

Hayden, M. R. Islet amyloid, metabolic syndrome, and the natural progressive history of type 2 diabetes mellitus. *Journal of the Pancreas*, 3(5):126–138, 2002.

Hebda, J. a. and Miranker, A. D. The interplay of catalysis and toxicity by amyloid intermediates on lipid bilayers: insights from type II diabetes. *Annual review of biophysics*, 38:125–52, jan 2009.

Hennig, R., Heidrich, J., Saur, M., Schmüser, L., Roeters, S. J., Hellmann, N., Woutersen, S., Bonn, M., Weidner, T., Markl, J., and Schneider, D. IM30 triggers membrane fusion in cyanobacteria and chloroplasts. *Nature communications*, 6 (May):7018, 2015.

Hicks, J. B., Lai, Y., Sheng, W., Yang, X., Zhu, D., Sun, G. Y., and Lee, J. C.-M. Amyloid-beta peptide induces temporal membrane biphasic changes in astrocytes through cytosolic phospholipase A2. *Biochimica et biophysica acta*, 1778(11):2512–9, nov 2008.

Hiddinga, H. J. and Eberhardt, N. L. Intracellular amyloidogenesis by human islet amyloid polypeptide induces apoptosis in COS-1 cells. *The American journal of pathology*, 154(4):1077–88, apr 1999.

Higham, C. E., Hull, R. L., Lawrie, L., Shennan, K. I., Morris, J. F., Birch, N. P., Docherty, K., and Clark, A. Processing of synthetic pro-islet amyloid polypeptide (proIAPP) 'amylin' by recombinant prohormone convertase enzymes, PC2 and PC3, in vitro. *European journal of biochemistry / FEBS*, 267(16):4998–5004, aug 2000.

Höppener, J. W., Ahrén, B., Lips, C. J., Epstein, F. H., Höppener, J. W., Ahrén, B., and Lips, C. J. Islet Amyloid and Type 2 Diabetes Mellitus. *New England Journal of Medicine*, 343(6):411–419, aug 2000.

Hori, Y., Demura, M., Iwadate, M., Ulrich, A. S., Niidome, T., Aoyagi, H., and Asakura, T. Interaction of mastoparan with membranes studied by 1H-NMR spectroscopy in detergent micelles and by solid-state 2H-NMR and 15N-NMR spectroscopy in oriented lipid bilayers. *European Journal of Biochemistry*, 268 (2):302–309, 2001.

Howard, C. F. Longitudinal studies on the development of diabetes in individual Macaca nigra. *Diabetologia*, 29(5):301–6, may 1986.

Huang, C.-J., Haataja, L., Gurlo, T., Butler, A. E., Wu, X., Soeller, W. C., and Butler, P. C. Induction of endoplasmic reticulum stress-induced beta-cell apoptosis and accumulation of polyubiquitinated proteins by human islet amyloid polypeptide. *American journal of physiology. Endocrinology and metabolism*, 293: E1656–E1662, 2007a.

Huang, C.-j., Lin, C.-y., Haataja, L., and Gurlo, T. High expression rates of human islet amyloid polypeptide induce endoplasmic reticulum stressmediated β-cell apoptosis, a characteristic of humans with type 2 but not type 1 diabetes. *Diabetes*, 56(August 2007):2016–2027, 2007b.

Huang, C. J., Gurlo, T., Haataja, L., Costes, S., Daval, M., Ryazantsev, S., Wu, X., Butler, A. E., and Butler, P. C. Calcium-activated calpain-2 is a mediator of beta cell dysfunction and apoptosis in type 2 diabetes. *Journal of Biological Chemistry*, 285(1):339–348, 2010.

Hudson, S. A., Ecroyd, H., Kee, T. W., and Carver, J. A. The thioflavin T fluorescence assay for amyloid fibril detection can be biased by the presence of exogenous compounds. *FEBS Journal*, 276(20):5960–5972, oct 2009.

Hutton, J. C. The internal pH and membrane potential of the insulin-secretory granule. *The Biochemical journal*, 204(1):171–8, apr 1982.

Hutton, J. C. Insulin secretory granule biogenesis and the proinsulin-processing endopeptidases. *Diabetologia*, 37(S2):S48–S56, sep 1994.

Hutton, M. The effects of environmental lead exposure and in vitro zinc on tissue δ-aminolevulinic acid dehydratase in urban pigeons. *Comparative Biochemistry and Physiology Part C: Comparative Pharmacology*, 74(2):441–446, jan 1983.

Iannuzzi, C., Maritato, R., Irace, G., and Sirangelo, I. Misfolding and Amyloid Aggregation of Apomyoglobin. *International Journal of Molecular Sciences*, 14(7): 14287–14300, jul 2013.

Invernizzi, G., Papaleo, E., Sabate, R., and Ventura, S. Protein aggregation: Mechanisms and functional consequences. *International Journal of Biochemistry and Cell Biology*, 44(9):1541–1554, 2012.

Jack, L., Boseman, L., and Vinicor, F. Aging Americans and diabetes. A public health and clinical response. *Geriatrics*, 59(4):14–7, apr 2004.

Janson, J., Ashley, R. H., Harrison, D., McIntyre, S., and Butler, P. C. The mechanism of islet amyloid polypeptide toxicity is membrane disruption by intermediate-sized toxic amyloid particles. *Diabetes*, 48(3):491–8, mar 1999.

Jayasinghe, S. a. and Langen, R. Lipid membranes modulate the structure of islet amyloid polypeptide. *Biochemistry*, 44(36):12113–9, sep 2005.

Jean, L., Lee, C. F., Hodder, P., Hawkins, N., and Vaux, D. J. Dynamics of the formation of a hydrogel by a pathogenic amyloid peptide: islet amyloid polypeptide. *Scientific Reports*, In prepara(April):1–10, 2016.

Jeong, H. R. and An, S. S. A. Causative factors for formation of toxic islet amyloid polypeptide oligomer in type 2 diabetes mellitus. *Clinical interventions in aging*, 10:1873–9, nov 2015.

Jiang, P., Li, W., Shea, J. E., and Mu, Y. Resveratrol inhibits the formation of multiple-layered ??-sheet oligomers of the human islet amyloid polypeptide segment 22-27. *Biophysical Journal*, 100(6):1550–1558, 2011.

Johnson, K. H., O'Brien, T. D., Hayden, D. W., Jordan, K., Ghobrial, H. K., Mahoney, W. C., and Westermark, P. Immunolocalization of islet amyloid polypeptide (IAPP) in pancreatic beta cells by means of peroxidase-antiperoxidase (PAP) and protein A-gold techniques. *The American journal of pathology*, 130(1): 1–8, jan 1988.

Johnson, K. H., Jordan, K., O'Brien, T. D., Murtaugh, M. P., Wernstedt, C., Betsholtz, C., and Westermark, P. *Factors Affecting Diabetogenesis and*

Amyloidogenesis are Provided by Studies of IAPP in the Dog and Cat, pages 445–448. Springer Netherlands, Dordrecht, 1991.

Kahn, S. E. The relative contributions of insulin resistance and beta-cell dysfunction to the pathophysiology of Type 2 diabetes. *Diabetologia*, 46:3–19, 2003.

Kamp, F. and Beyer, K. Binding of -Synuclein Affects the Lipid Packing in Bilayers of Small Vesicles. *Journal of Biological Chemistry*, 281(14):9251–9259, apr 2006.

Kapurniotu, A., Bernhagen, J., Greenfield, N., Al-Abed, Y., Teichberg, S., Frank, R. W., Voelter, W., and Bucala, R. Contribution of advanced glycosylation to the amyloidogenicity of islet and amyloid polypeptide. *European Journal of Biochemistry*, 251(1-2):208–216, 1998.

Kastorna, A., Trusova, V., Gorbenko, G., and Kinnunen, P. Membrane effects of lysozyme amyloid fibrils. *Chemistry and physics of lipids*, 165(3):331–7, apr 2012.

Kaufmann, J. E., Irminger, J. C., Mungall, J., and Halban, P. A. Proinsulin conversion in GH3 cells after coexpression of human proinsulin with the endoproteases PC2 and/or PC3. *Diabetes*, 46(6):978–82, jun 1997.

Kayed, R., Sokolov, Y., Edmonds, B., McIntire, T. M., Milton, S. C., Hall, J. E., and Glabe, C. G. Permeabilization of lipid bilayers is a common conformation-dependent activity of soluble amyloid oligomers in protein misfolding diseases. *The Journal of biological chemistry*, 279(45):46363–6, nov 2004.

Kegulian, N. C., Sankhagowit, S., Apostolidou, M., Jayasinghe, S. A., Malmstadt, N., Butler, P. C., and Langen, R. Membrane Curvature-sensing and Curvature-inducing Activity of Islet Amyloid Polypeptide and Its Implications for Membrane Disruption. *Journal of Biological Chemistry*, 290(43):25782–25793, oct 2015.

Khemtémourian, L., Lahoz Casarramona, G., Suylen, D. P. L., Hackeng, T. M., Meeldijk, J. D., de Kruijff, B., Höppener, J. W. M., and Killian, J. A. Impaired processing of human pro-islet amyloid polypeptide is not a causative factor for fibril formation or membrane damage in vitro. *Biochemistry*, 48(46):10918–25, nov 2009.

Khemtémourian, L., Engel, M. F. M., Liskamp, R. M. J., Höppener, J. W. M., and Killian, J. A. The N-terminal fragment of human islet amyloid polypeptide is non-fibrillogenic in the presence of membranes and does not cause leakage of bilayers of physiologically relevant lipid composition. *Biochimica et biophysica acta*, 1798(9): 1805–11, sep 2010.

Khemtémourian, L., Doménech, E., Doux, J. P. F., Koorengevel, M. C., and Killian, J. A. Low pH acts as inhibitor of membrane damage induced by human islet amyloid polypeptide. *Journal of the American Chemical Society*, 133(39):15598–604, oct 2011.

Kinnunen, P. K. J., Domanov, Y. A., Mattila, J.-P., and Varis, T. Formation of / tubules by and temporin B on supported. *Soft matter*, 11(47):9188–9200, 2015.

Klöppel, G., Löhr, M., Habich, K., Oberholzer, M., and Heitz, P. U. Islet pathology and the pathogenesis of type 1 and type 2 diabetes mellitus revisited., 1985.

Knight, J. D. and Miranker, A. D. Phospholipid catalysis of diabetic amyloid assembly. *Journal of molecular biology*, 341(5):1175–87, aug 2004.

Knight, J. D., Hebda, J. A., and Miranker, A. D. Conserved and cooperative assembly of membrane-bound alpha-helical states of islet amyloid polypeptide. *Biochemistry*, 45(31):9496–508, aug 2006.

Konarkowska, B., Aitken, J. F., Kistler, J., Zhang, S., and Cooper, G. J. S. The aggregation potential of human amylin determines its cytotoxicity towards islet beta-cells. *The FEBS journal*, 273(15):3614–24, aug 2006.

Koo, B. W., Hebda, J. A., and Miranker, A. D. Amide inequivalence in the fibrillar assembly of islet amyloid polypeptide. *Protein engineering design selection PEDS*, 21(3):147–154, 2008.

Kremer, J. J., Sklansky, D. J., and Murphy, R. M. Profile of Changes in Lipid Bilayer Structure Caused by β-Amyloid Peptide . *Biochemistry*, 40(29):8563–8571, jul 2001.

Kuimova, M. K. Mapping viscosity in cells using molecular rotors. *Physical Chemistry Chemical Physics*, 14(37):12671, 2012.

Kyoung, M., Zhang, Y., Diao, J., Chu, S., and Brunger, A. T. Studying calcium-triggered vesicle fusion in a single vesicle-vesicle content and lipid-mixing system. *Nature protocols*, 8(1):1–16, jan 2013.

Lai, Y., Kim, S., Varkey, J., Lou, X., Song, J. K., Diao, J., Langen, R., and Shin, Y. K. Nonaggregated α-synuclein influences snare-dependent vesicle docking via membrane binding. *Biochemistry*, 2014.

Landreh, M., Alvelius, G., Willander, H., Stukenborg, J.-B., Söder, O., Johansson, J., and Jörnvall, H. Insulin solubility transitions by pH-dependent interactions with proinsulin C-peptide. *The FEBS journal*, 279(24):4589–97, dec 2012.

Larson, J. L. and Miranker, A. D. The Mechanism of Insulin Action on Islet Amyloid Polypeptide Fiber Formation. *Journal of Molecular Biology*, 335(1):221–231, jan 2004.

Last, N. B., Rhoades, E., and Miranker, A. D. Evolution of Membrane Leakage by Pre-Amyloidogenic Oligomers of Islet Amyloid Polypeptide. *Biophysical Journal*, 100(3):350a, feb 2011.

Last, N. B., Schlamadinger, D. E., and Miranker, A. D. A common landscape for membrane-active peptides. *Protein science : a publication of the Protein Society*, 22(7):870–82, jul 2013.

Lau, T. L., Gehman, J. D., Wade, J. D., Perez, K., Masters, C. L., Barnham, K. J., and Separovic, F. Membrane interactions and the effect of metal ions of the amyloidogenic fragment A??(25-35) in comparison to A??(1-42). *Biochimica et Biophysica Acta - Biomembranes*, 1768(10):2400–2408, 2007.

Leahy, J. L. Pathogenesis of Type 2 Diabetes Mellitus. *Archives of Medical Research*, 36(3):197–209, may 2005.

Lee, H.-G., Casadesus, G., Zhu, X., Takeda, A., Perry, G., and Smith, M. A. Challenging the amyloid cascade hypothesis: senile plaques and amyloid-beta as protective adaptations to Alzheimer disease. *Annals of the New York Academy of Sciences*, 1019(1):1–4, jun 2004.

Lee, S. C., Hashim, Y., Li, J. K. Y., Ko, G. T. C., Critchley, J. A. J. H., Cockram, C. S., and Chan, J. C. N. The islet amyloid polypeptide (amylin) gene S20G mutation in Chinese subjects: Evidence for associations with type 2 diabetes and cholesterol levels. *Clinical Endocrinology*, 54(4):541–546, 2001.

Leite, N., Aufderhorst-Roberts, A., Palma, M., Connell, S., Neto, J., and Beales, P. PE and PS Lipids Synergistically Enhance Membrane Poration by a Peptide with Anticancer Properties. *Biophysical Journal*, 109(5):936–947, 2015.

Levitt, J. a., Kuimova, M. K., Yahioglu, G., Chung, P. H., Suhling, K., and Phillips, D. Membrane-bound molecular rotors measure viscosity in live cells via fluorescence lifetime imaging. *Journal of Physical Chemistry C*, 113:11634–11642, 2009.

Li, Y. V. Zinc and insulin in pancreatic beta-cells. *Endocrine*, 45(2):178–189, mar 2014.

Lillioja, S., Mott, D. M., Howard, B. V., Bennett, P. H., Yki-Järvinen, H., Freymond, D., Nyomba, B. L., Zurlo, F., Swinburn, B., and Bogardus, C. Impaired glucose tolerance as a disorder of insulin action. Longitudinal and cross-sectional studies in Pima Indians. *The New England Journal of Medicine*, 318(19):1217–1225, 1988.

Lim, Y.-A., Rhein, V., Baysang, G., Meier, F., Poljak, A., Raftery, M. J., Guilhaus, M., Ittner, L. M., Eckert, A., and Götz, J. Abeta and human amylin share a common toxicity pathway via mitochondrial dysfunction. *Proteomics*, 10(8):1621–33, apr 2010.

Lin, C.-Y., Gurlo, T., Haataja, L., Hsueh, W. a., and Butler, P. C. Activation of peroxisome proliferator-activated receptor-gamma by rosiglitazone protects human islet cells against human islet amyloid polypeptide toxicity by a

phosphatidylinositol 3'-kinase-dependent pathway. *The Journal of clinical endocrinology and metabolism*, 90(12):6678–86, 2005.

Lorenzo, a., Razzaboni, B., Weir, G. C., and Yankner, B. a. Pancreatic islet cell toxicity of amylin associated with type-2 diabetes mellitus. *Nature*, 368(6473): 756–760, 1994.

Loura, L. Interaction of peptides with binary phospholipid membranes: application of fluorescence methodologies. *Chemistry and Physics of Lipids*, 122(1-2):77–96, jan 2003.

Loura, L. M. S. and Prieto, M. FRET in Membrane Biophysics: An Overview. *Frontiers in physiology*, 2(November):82, jan 2011.

Luca, S., Yau, W.-M. M., Leapman, R., and Tycko, R. Peptide conformation and supramolecular organization in amylin fibrils: Constraints from solid-state NMR. *Biochemistry*, 46(47):13505–13522, nov 2007.

Lukinius, A., Wilander, E., Westermark, G. T., Engstrm, U., and Westermark, P. Co-localization of islet amyloid polypeptide and insulin in the B cell secretory granules of the human pancreatic islets. *Diabetologia*, 32(4):240–244, apr 1989.

Maas, S. L., de Vrij, J., van der Vlist, E. J., Geragousian, B., van Bloois, L., Mastrobattista, E., Schiffelers, R. M., Wauben, M. H., Broekman, M. L., and Nolte-'t Hoen, E. N. Possibilities and limitations of current technologies for quantification of biological extracellular vesicles and synthetic mimics. *Journal of Controlled Release*, 200:87–96, feb 2015.

MacArthur, D. L., de Koning, E. J., Verbeek, J. S., Morris, J. F., and Clark, A. Amyloid fibril formation is progressive and correlates with beta-cell secretion in transgenic mouse isolated islets. *Diabetologia*, 42(10):1219–27, oct 1999.

MacDonald, M. J., Ade, L., Ntambi, J. M., Ansari, I.-U. H., and Stoker, S. W. Characterization of Phospholipids in Insulin Secretory Granules and Mitochondria

in Pancreatic Beta Cells and Their Changes with Glucose Stimulation. *Journal of Biological Chemistry*, 290(17):11075–11092, apr 2015.

MacDonald, R. C., MacDonald, R. I., Menco, B. P. M., Takeshita, K., Subbarao, N. K., and Hu, L. R. Small-volume extrusion apparatus for preparation of large, unilamellar vesicles. *Biochimica et Biophysica Acta - Biomembranes*, 1061(2):297–303, 1991.

Magzoub, M. and Miranker, A. D. Concentration-dependent transitions govern the subcellular localization of islet amyloid polypeptide. *FASEB journal : official publication of the Federation of American Societies for Experimental Biology*, 26 (3):1228–38, mar 2012.

Marek, P., Gupta, R., and Raleigh, D. P. The fluorescent amino acid p-cyanophenylalanine provides an intrinsic probe of amyloid formation. *ChemBioChem*, 9(9):1372–1374, 2008.

Marek, P., Mukherjee, S., Zanni, M. T., and Raleigh, D. P. Residue-specific, real-time characterization of lag-phase species and fibril growth during amyloid formation: A combined fluorescence and IR study of p-cyanophenylalanine analogs of islet amyloid polypeptide. *Journal of Molecular Biology*, 400(4):878–888, 2010.

Marek, P. J., Patsalo, V., Green, D. F., and Raleigh, D. P. Ionic strength effects on amyloid formation by amylin are a complicated interplay among Debye screening, ion selectivity, and Hofmeister effects. *Biochemistry*, 51(43):8478–90, oct 2012.

Markuszewski, R. Structure , fluorescence , and chelating properties of Calcein. pages 16–18, 1976.

Marsden, H. R., Tomatsu, I., and Kros, A. Model systems for membrane fusion. *Chemical Society reviews*, 40:1572–1585, 2011.

Martin, B. C., Warram, J. H., Krolewski, A. S., Bergman, R. N., Soeldner, J. S., and Kahn, C. R. Role of glucose and insulin resistance in development of type 2

diabetes mellitus: results of a 25-year follow-up study. *Lancet (London, England)*, 340(8825):925–9, 1992.

Marzban, L., Trigo-Gonzalez, G., Zhu, X., Rhodes, C. J., Halban, P. A., Steiner, D. F., and Verchere, C. B. Role of beta-cell prohormone convertase (PC)1/3 in processing of pro-islet amyloid polypeptide. *Diabetes*, 53(1):141–8, jan 2004.

Marzban, L., Soukhatcheva, G., and Verchere, C. B. Role of carboxypeptidase E in processing of pro-islet amyloid polypeptide in {beta}-cells. *Endocrinology*, 146(4): 1808–17, may 2005a.

Marzban, L., Trigo-Gonzalez, G., and Verchere, C. B. Processing of pro-islet amyloid polypeptide in the constitutive and regulated secretory pathways of beta cells. *Molecular endocrinology (Baltimore, Md.)*, 19(8):2154–63, aug 2005b.

Mattson, M. P. and Goodman, Y. Different amyloidogenic peptides share a similar mechanism of neurotoxicity involving reactive oxygen species and calcium. *Brain Research*, 676(1):219–224, 1995.

Matveyenko, A. V. and Butler, P. C. Beta-cell deficit due to increased apoptosis in the human islet amyloid polypeptide transgenic (HIP) rat recapitulates the metabolic defects present in type 2 diabetes. *Diabetes*, 55(7):2106–14, jul 2006.

Mazor, Y., Gilead, S., Benhar, I., and Gazit, E. Identification and characterization of a novel molecular-recognition and self-assembly domain within the islet amyloid polypeptide. *Journal of Molecular Biology*, 322(5):1013–1024, 2002.

Meier, J. J., Kayed, R., Lin, C.-Y., Gurlo, T., Haataja, L., Jayasinghe, S., Langen, R., Glabe, C. G., and Butler, P. C. Inhibition of human IAPP fibril formation does not prevent beta-cell death: evidence for distinct actions of oligomers and fibrils of human IAPP. *American journal of physiology. Endocrinology and metabolism*, 291 (6):E1317–24, dec 2006.

Melo, A. M., Loura, L. M. S., Fernandes, F., Villalaín, J., Prieto, M., and Coutinho, A. Electrostatically driven lipidlysozyme mixed fibers display a multilamellar structure without amyloid features. *Soft Matter*, 10(6):840, 2014.

Michael, J., Carroll, R., Swift, H. H., and Steiner, D. F. Studies on the molecular organization of rat insulin secretory granules. *The Journal of biological chemistry*, 262(34):16531–16535, dec 1987.

Milardi, D., Sciacca, M. F. M., Pappalardo, M., Grasso, D. M., and La Rosa, C. The role of aromatic side-chains in amyloid growth and membrane interaction of the islet amyloid polypeptide fragment LANFLVH. *European biophysics journal : EBJ*, 40(1):1–12, jan 2011.

Mirzabekov, T. A., Lin, M. C., and Kagan, B. L. Pore formation by the cytotoxic islet amyloid peptide amylin. *Journal of Biological Chemistry*, 271(4):1988–1992, 1996.

Moens, P. D. J., Helms, M. K., and Jameson, D. M. Detection of tryptophan to tryptophan energy transfer in proteins. *The protein journal*, 23(1):79–83, jan 2004.

Morita, S., Sakagashira, S., Ueyama, M., Shimajiri, Y., Furuta, M., and Sanke, T. Progressive deterioration of insulin secretion in Japanese type 2 diabetic patients in comparison with those who carry the S20G mutation of the islet amyloid polypeptide gene: A long-term follow-up study. *Journal of Diabetes Investigation*, 2(4):287–292, aug 2011.

Muff, R., Born, W., and Fischer, J. A. Calcitonin, calcitonin gene-related peptide, adrenomedullin and amylin: Homologous peptides, separate receptors and overlapping biological actions, 1995.

Mukherjee, S. and Chattopadhyay, A. Monitoring the organization and dynamics of bovine hippocampal membranes utilizing Laurdan generalized polarization. *Biochimica et biophysica acta*, 1714(1):43–55, aug 2005.

Murdock, R. C., Braydich-Stolle, L., Schrand, A. M., Schlager, J. J., and Hussain, S. M. Characterization of Nanomaterial Dispersion in Solution Prior to In Vitro Exposure Using Dynamic Light Scattering Technique. *Toxicological Sciences*, 101 (2):239–253, feb 2008.

Nedumpully-Govindan, P. and Ding, F. Inhibition of IAPP aggregation by insulin depends on the insulin oligomeric state regulated by zinc ion concentration. *Scientific Reports*, 5:8240, 2015.

Nilsson, M. R. and Raleigh, D. P. Analysis of amylin cleavage products provides new insights into the amyloidogenic region of human amylin. *Journal of molecular biology*, 294(5):1375–85, 1999.

Njus, D., Kelley, P. M., and Harnadek, G. J. Bioenergetics of secretory vesicles. *BBA Reviews On Bioenergetics*, 853(3-4):237–265, 1986.

O'Brien, T. D., Hayden, D. W., Johnson, K. H., and Fletcher, T. F. Immunohistochemical morphometry of pancreatic endocrine cells in diabetic, normoglycaemic glucose-intolerant and normal cats. *Journal of Comparative Pathology*, 96(4):357–369, 1986.

Opie, E. L. ON THE RELATION OF CHRONIC INTERSTITIAL PANCREATITIS TO THE ISLANDS OF LANGERHANS AND TO DIABETES MELUTUS. *Journal of Experimental Medicine*, 5(4):397–428, jan 1901.

Paasonen, L., Laaksonen, T., Johans, C., Yliperttula, M., Kontturi, K., and Urtti, A. Gold nanoparticles enable selective light-induced contents release from liposomes. *Journal of Controlled Release*, 122:86–93, 2007.

Padrick, S. B. and Miranker, A. D. Islet amyloid polypeptide: identification of long-range contacts and local order on the fibrillogenesis pathway. *Journal of Molecular Biology*, 308(4):783–794, may 2001.

Parasassi, T., De Stasio, G., D'Ubaldo, a., and Gratton, E. Phase fluctuation in phospholipid membranes revealed by Laurdan fluorescence. *Biophysical journal*, 57 (6):1179–86, jun 1990.

Parasassi, T., De Stasio, G., Ravagnan, G., Rusch, R. M., and Gratton, E. Quantitation of lipid phases in phospholipid vesicles by the generalized polarization of Laurdan fluorescence. *Biophysical journal*, 60(1):179–89, jul 1991.

Parasassi, T. and Gratton, E. Membrane lipid domains and dynamics as detected by Laurdan fluorescence. *Journal of Fluorescence*, 5(1):59–69, mar 1995.

Parasassi, T. and Krasnowska, E. Laurdan and Prodan as polarity-sensitive fluorescent membrane probes. *... of fluorescence*, 8(4):365–373, 1998.

Park, S., Ahuja, M., Kim, M. S., Brailoiu, G. C., Jha, A., Zeng, M., Baydyuk, M., Wu, L.-G., Wassif, C. A., Porter, F. D., Zerfas, P. M., Eckhaus, M. A., Brailoiu, E., Shin, D. M., Muallem, S., S., P., M., A., M.S., K., G.C., B., A., J., M., Z., M., B., L.-G., W., C.A., W., F.D., P., P.M., Z., M.A., E., E., B., D.M., S., and S., M. Fusion of lysosomes with secretory organelles leads to uncontrolled exocytosis in the lysosomal storage disease mucolipidosis type IV. *EMBO Reports*, 17(2):266–278, 2016.

Parlati, F., Weber, T., McNew, J. A., Westermann, B., Sollner, T. H., and Rothman, J. E. Rapid and efficient fusion of phospholipid vesicles by the alpha -helical core of a SNARE complex in the absence of an N-terminal regulatory domain. *Proceedings of the National Academy of Sciences*, 96(22):12565–12570, oct 1999.

Paulsson, J. F. and Westermark, G. T. Aberrant processing of human proislet amyloid polypeptide results in increased amyloid formation. *Diabetes*, 54(7):2117–25, jul 2005.

Pawar, A. P., DuBay, K. F., Zurdo, J., Chiti, F., Vendruscolo, M., and Dobson, C. M. Prediction of "aggregation-prone" and "aggregation- susceptible" regions in proteins associated with neurodegenerative diseases. *Journal of Molecular Biology*, 350(2):379–392, 2005.

Pilkington, E. H., Gurzov, E. N., Kakinen, A., Litwak, S. A., Stanley, W. J., Davis, T. P., and Ke, P. C. Pancreatic β-Cell Membrane Fluidity and Toxicity Induced by Human Islet Amyloid Polypeptide Species. *Scientific Reports*, 6(November 2015): 21274, 2016.

Pillot, T., Lins, L., Goethals, M., Vanloo, B., Baert, J., Vandekerckhove, J., Rosseneu, M., and Brasseur, R. The 118-135 peptide of the human prion protein forms amyloid fibrils and induces liposome fusion. *Journal of molecular biology*, 274(3):381–93, dec 1997.

Poitout, V. and Robertson, R. P. Minireview: Secondary ??-cell failure in type 2 diabetes - A convergence of glucotoxicity and lipotoxicity, 2002.

Popa, S. and Mot, M. Beta-Cell Function and Failure in Type 2 Diabetes. In Masuo, K., editor, *Type 2 Diabetes*. InTech, jun 2013.

Porte, D. Clinical importance of insulin secretion and its interaction with insulin resistance in the treatment of type 2 diabetes mellitus and its complications. *Diabetes/metabolism research and reviews*, 17(3):181–8, 2001.

Prentki, M. and Nolan, C. J. Islet β-cell failure in type 2 diabetes. *The Journal of Clinical Investigation*, 116(7):1802–1812, 2006.

Prentki, M., Joly, E., El-Assaad, W., and Roduit, R. Malonyl-CoA signaling, lipid partitioning, and glucolipotoxicity: role in beta-cell adaptation and failure in the etiology of diabetes. *Diabetes*, 51 Suppl 3(SUPPL. 3):S405–13, dec 2002.

Qian, Z., Jia, Y., and Wei, G. Binding Orientations and Lipid Interactions of Human Amylin at Zwitterionic and Anionic Lipid Bilayers. *Journal of Diabetes Research*, 2016:1–13, 2016.

Qiang, W., Sun, Y., and Weliky, D. P. A strong correlation between fusogenicity and membrane insertion depth of the HIV fusion peptide. *Proceedings of the National Academy of Sciences of the United States of America*, 106(36):15314–9, 2009.

Reiffen, F. U. and Gratzl, M. Ca2+ binding to chromaffin vesicle matrix proteins: effect of pH, Mg2+, and ionic strength. *Biochemistry*, 25(15):4402–6, jul 1986.

Ritzel, R. A., Meier, J. J., Lin, C. Y., Veldhuis, J. D., and Butler, P. C. Human islet amyloid polypeptide oligomers disrupt cell coupling, induce apoptosis, and impair insulin secretion in isolated human islets. *Diabetes*, 56(1):65–71, 2007.

Robertson, J. L. We choose to go to the membrane. *Proceedings of the National Academy of Sciences of the United States of America*, 108(25):10027–8, jun 2011.

Sakagashira, S., Hiddinga, H. J., Tateishi, K., Sanke, T., Hanabusa, T., Nanjo, K., and Eberhardt, N. L. S20G mutant amylin exhibits increased in vitro amyloidogenicity and increased intracellular cytotoxicity compared to wild-type amylin. *The American journal of pathology*, 157(6):2101–9, dec 2000.

Sakagashira, S. Sanke, T. Hanabusa, T. Shimomura, H. O. S. Missense Mutation of Amylin Gener (S20G) in Japanese NIDDM Patients. *Journal of Chemical Information and Modeling*, 53(9):1689–1699, dec 2013.

Salamekh, S., Brender, J. R., Hyung, S.-J., Nanga, R. P. R., Vivekanandan, S., Ruotolo, B. T., and Ramamoorthy, A. A two-site mechanism for the inhibition of IAPP amyloidogenesis by zinc. *Journal of molecular biology*, 410(2):294–306, jul 2011.

Sanchez, S. and Tricerri, M. Laurdan generalized polarization: from cuvette to microscope. *Modern Research and ...*, pages 1007–1014, 2007.

Saveyn, H., De Baets, B., Thas, O., Hole, P., Smith, J., and Van der Meeren, P. Accurate particle size distribution determination by nanoparticle tracking analysis based on 2-D Brownian dynamics simulation. *Journal of Colloid and Interface Science*, 352(2):593–600, 2010.

Scheltens, P., Blennow, K., Breteler, M. M. B., de Strooper, B., Frisoni, G. B., Salloway, S., and Van der Flier, W. M. Alzheimer's disease. *The Lancet*, 388 (10043):505–517, jul 2016.

Schier, F. Letter to the Editor. *Journal of Pediatric Surgery*, 45(2):464, feb 2010.

Schlamadinger, D. E. and Miranker, A. D. Fiber-dependent and -independent toxicity of islet amyloid polypeptide. *Biophysical journal*, 107(11):2559–66, dec 2014.

Schubert, D., Behl, C., Lesley, R., Brack, A., Dargusch, R., Sagara, Y., and Kimura, H. Amyloid peptides are toxic via a common oxidative mechanism. *Proc Natl Acad Sci U S A*, 92(6):1989–1993, 1995.

Sciacca, M. F. M., Kotler, S. a., Brender, J. R., Chen, J., Lee, D.-k., and Ramamoorthy, A. Two-step mechanism of membrane disruption by Aβ through membrane fragmentation and pore formation. *Biophysical journal*, 103(4):702–10, aug 2012.

Sciacca, M. F. M., Milardi, D., Messina, G. M. L., Marletta, G., Brender, J. R., Ramamoorthy, A., and La Rosa, C. Cations as switches of amyloid-mediated membrane disruption mechanisms: calcium and IAPP. *Biophysical journal*, 104 (1):173–84, jan 2013.

Scrocchi, L. A., Ha, K., Chen, Y., Wu, L., Wang, F., and Fraser, P. E. Identification of minimal peptide sequences in the (8-20) domain of human islet amyloid polypeptide involved in fibrillogenesis. *Journal of Structural Biology*, 141(3):218–227, 2003.

Seeliger, J., Weise, K., Opitz, N., and Winter, R. The effect of Aβ on IAPP aggregation in the presence of an isolated β-cell membrane. *Journal of molecular biology*, 421(2-3):348–63, aug 2012.

Sheynis, T., Friediger, A., Xue, W.-F., Hellewell, A. L., Tipping, K. W., Hewitt, E. W., Radford, S. E., and Jelinek, R. Aggregation modulators interfere with membrane interactions of β2-microglobulin fibrils. *Biophysical journal*, 105(3):745–55, aug 2013.

Simons, K. and Toomre, D. Lipid rafts and signal transduction. *Nature reviews. Molecular cell biology*, 1(1):31–9, oct 2000.

Sipe, J. D. and Cohen, A. S. Review: History of the Amyloid Fibril. *Journal of Structural Biology*, 130(2-3):88–98, 2000.

Sipe, J. D., Benson, M. D., Buxbaum, J. N., Ikeda, S.-i., Merlini, G., Saraiva, M. J. M., and Westermark, P. Nomenclature 2014: Amyloid fibril proteins and clinical classification of the amyloidosis. *Amyloid*, 21(4):221–224, 2014.

Skeby, K. K., Andersen, O. J., Pogorelov, T. V., Tajkhorshid, E., and Schiøtt, B. Conformational Dynamics of the Human Islet Amyloid Polypeptide in a Membrane Environment: Toward the Aggregation Prone Form. *Biochemistry*, 55(13):2031–2042, apr 2016.

Sladek, R., Rocheleau, G., Rung, J., Dina, C., Shen, L., Serre, D., Boutin, P., Vincent, D., Belisle, A., Hadjadj, S., Balkau, B., Heude, B., Charpentier, G., Hudson, T. J., Montpetit, A., Pshezhetsky, A. V., Prentki, M., Posner, B. I., Balding, D. J., Meyre, D., Polychronakos, C., and Froguel, P. A genome-wide association study identifies novel risk loci for type 2 diabetes. *Nature*, 445(7130):881–885, feb 2007.

Smith, P. E. S., Brender, J. R., and Ramamoorthy, A. Induction of negative curvature as a mechanism of cell toxicity by amyloidogenic peptides: the case of islet amyloid polypeptide. *Journal of the American Chemical Society*, 131(12):4470–8, apr 2009.

Soeller, W. C., Janson, J., Hart, S. E., Parker, J. C., Carty, M. D., Stevenson, R. W., Kreutter, D. K., and Butler, P. C. Islet amyloid-associated diabetes in obese A(vy)/a mice expressing human islet amyloid polypeptide. *Diabetes*, 47(5): 743–50, may 1998.

Sokolov, Y., Kozak, J. A., Kayed, R., Chanturiya, A., Glabe, C., and Hall, J. E. Soluble amyloid oligomers increase bilayer conductance by altering dielectric structure. *The Journal of general physiology*, 128(6):637–47, dec 2006.

Sparr, E., Engel, M. F. M., Sakharov, D. V., Sprong, M., Jacobs, J., De Kruijff, B., Höppener, J. W. M., and Antoinette Killian, J. Islet amyloid polypeptide-induced membrane leakage involves uptake of lipids by forming amyloid fibers. *FEBS Letters*, 577(1-2):117–120, 2004.

Tartaglia, G. G., Cavalli, A., Pellarin, R., and Caflisch, A. Prediction of Aggregation Rate and Aggregation-Prone Segments in Polypeptide Sequences. *Protein science : a publication of the Protein Society*, 14(10):2723–34, 2005.

Taylor, D. R. and Hooper, N. M. The prion protein and lipid rafts. *Molecular membrane biology*, 23(1):89–99, 2006.

Tomasello, M. F., Sinopoli, A., and Pappalardo, G. On the Environmental Factors Affecting the Structural and Cytotoxic Properties of IAPP Peptides. *Journal of Diabetes Research*, 2015:1–15, 2015.

Tomiyama, T., Kaneko, H., Kataoka, K. I., Asano, S., and Endo, N. Rifampicin inhibits the toxicity of pre-aggregated amyloid peptides by binding to peptide fibrils and preventing amyloid-cell interaction. *The Biochemical journal*, 322 (Pt 3:859–65, 1997.

Tu, L.-H. and Raleigh, D. P. Role of Aromatic Interactions in Amyloid Formation by Islet Amyloid Polypeptide. *Biochemistry*, 52(2):333–342, jan 2013.

Tu, L.-H., Serrano, A. L., Zanni, M. T., and Raleigh, D. P. Mutational analysis of preamyloid intermediates: the role of his-tyr interactions in islet amyloid formation. *Biophysical journal*, 106(7):1520–7, apr 2014.

Ulrich, a. S., Tichelaar, W., Förster, G., Zschörnig, O., Weinkauf, S., and Meyer, H. W. Ultrastructural characterization of peptide-induced membrane fusion and peptide self-assembly in the lipid bilayer. *Biophysical journal*, 77(2):829–41, 1999.

Vaiana, S. M., Best, R. B., Yau, W.-M., Eaton, W. a., and Hofrichter, J. Evidence for a partially structured state of the amylin monomer. *Biophysical journal*, 97(11): 2948–57, dec 2009.

van der Pol, E., Coumans, F. A. W., Grootemaat, A. E., Gardiner, C., Sargent, I. L., Harrison, P., Sturk, A., van Leeuwen, T. G., and Nieuwland, R. Particle size distribution of exosomes and microvesicles determined by transmission electron

microscopy, flow cytometry, nanoparticle tracking analysis, and resistive pulse sensing. *Journal of Thrombosis and Haemostasis*, 12(7):1182–1192, jul 2014.

van Meer, G., Voelker, D. R., and Feigenson, G. W. Membrane lipids: where they are and how they behave. *Nature reviews. Molecular cell biology*, 9(2):112–24, feb 2008.

Varkey, J., Isas, J. M., Mizuno, N., Jensen, M. B., Bhatia, V. K., Jao, C. C., Petrlova, J., Voss, J. C., Stamou, D. G., Steven, A. C., and Langen, R. Membrane Curvature Induction and Tubulation Are Common Features of Synucleins and Apolipoproteins. *Journal of Biological Chemistry*, 285(42):32486–32493, oct 2010.

Velázquez, J. B. and Fernández, M. S. GPS, the slope of Laurdan generalized polarization spectra, in the study of phospholipid lateral organization and Escherichia coli lipid phases. *Archives of biochemistry and biophysics*, 455(2):163–74, dec 2006.

Vestergaard, M. C., Morita, M., Hamada, T., and Takagi, M. Membrane fusion and vesicular transformation induced by Alzheimer's amyloid beta. *Biochimica et biophysica acta*, 1828(4):1314–21, apr 2013.

Viard, M., Gallay, J., Vincent, M., Meyer, O., Robert, B., and Paternostre, M. Laurdan solvatochromism: solvent dielectric relaxation and intramolecular excited-state reaction. *Biophysical journal*, 73(4):2221–34, oct 1997.

Wajchenberg, B. L. β-Cell Failure in Diabetes and Preservation by Clinical Treatment. *Endocrine Reviews*, 28(2):187–218, apr 2007.

Wang, J., Xu, J., Finnerty, J., Furuta, M., Steiner, D. F., and Verchere, C. B. The prohormone convertase enzyme 2 (PC2) is essential for processing pro-islet amyloid polypeptide at the NH2-terminal cleavage site. *Diabetes*, 50(3):534–539, mar 2001.

Wang, L., Lei, L., Li, Y., Wang, L., and Li, F. A hIAPP-derived all-d-amino-acid inhibits hIAPP fibrillation efficiently at membrane surface by targeting α-helical oligomeric intermediates. *FEBS letters*, 588(6):884–91, mar 2014.

Wang, Y., Thiele, C., and Huttner, W. B. Cholesterol is required for the formation of regulated and constitutive secretory vesicles from the trans-Golgi network. *Traffic (Copenhagen, Denmark)*, 1(12):952–62, dec 2000.

Waschuk, S. a., Elton, E. a., Darabie, a. a., Fraser, P. E., and McLaurin, J. a. Cellular membrane composition defines A beta-lipid interactions. *The Journal of biological chemistry*, 276(36):33561–8, sep 2001.

Weber, G. and Farris, F. J. Synthesis and spectral properties of a hydrophobic fluorescent probe: 6-propionyl-2-(dimethylamino)naphthalene. *Biochemistry*, 18 (14):3075–8, jul 1979.

Wei, L., Jiang, P., Xu, W., Li, H., Zhang, H., Yan, L., Chan-Park, M. B., Liu, X. W., Tang, K., Mu, Y., and Pervushin, K. The molecular basis of distinct aggregation pathways of islet amyloid polypeptide. *Journal of Biological Chemistry*, 286(8): 6291–6300, 2011.

Westermark, G. T., Christmanson, L., Terenghi, G., Permerth, J., Betsholtz, C., Larsson, J., Polak, J. M., and Westermark, P. Islet amyloid polypeptide: demonstration of mRNA in human pancreatic islets by in situ hybridization in islets with and without amyloid deposits. *Diabetologia*, 36(4):323–8, apr 1993.

Westermark, P., Wernstedt, C., Wilander, E., Hayden, D. W., O'Brien, T. D., and Johnson, K. H. Amyloid fibrils in human insulinoma and islets of Langerhans of the diabetic cat are derived from a neuropeptide-like protein also present in normal islet cells. *Proceedings of the National Academy of Sciences*, 84(11):3881–3885, jun 1987a.

Westermark, P., Wilander, E., Westermark, G. T., and Johnson, K. H. Islet amyloid polypeptide-like immunoreactivity in the islet B cells of Type 2 (non-insulin-dependent) diabetic and non-diabetic individuals. *Diabetologia*, 30(11):887–892, 1987b.

Westermark, P., Engström, U., Johnson, K. H., Westermark, G. T., and Betsholtz, C. Islet amyloid polypeptide: pinpointing amino acid residues linked to amyloid fibril formation. *Proceedings of the National Academy of Sciences of the United States of America*, 87(13):5036–40, jul 1990.

Westermark, P. Fine structure of islets of Langerhans in insular amyloidosis. *Virchows Archiv Abteilung A Pathologische Anatomie*, 359(1):1–18, 1973.

Westermark, P. Amyloid and polypeptide hormones: What is their interrelationship? *Amyloid*, 1(1):47–60, 1994.

Westermark, P. Amyloid in the islets of Langerhans: thoughts and some historical aspects. *Upsala journal of medical sciences*, 116(2):81–9, may 2011.

Westermark, P., Andersson, A., and Westermark, G. T. Islet amyloid polypeptide, islet amyloid, and diabetes mellitus. *Physiological reviews*, 91(3):795–826, jul 2011.

Westphal, C. H. and Chandra, S. S. Monomeric Synucleins Generate Membrane Curvature. *Journal of Biological Chemistry*, 288(3):1829–1840, jan 2013.

Whiles, J. a., Brasseur, R., Glover, K. J., Melacini, G., Komives, E. a., and Vold, R. R. Orientation and effects of mastoparan X on phospholipid bicelles. *Biophysical journal*, 80(1):280–293, 2001.

Williams, T. L., Johnson, B. R. G., Urbanc, B., Jenkins, a. T. a., Connell, S. D. a., and Serpell, L. C. Aβ42 oligomers, but not fibrils, simultaneously bind to and cause damage to ganglioside-containing lipid membranes. *The Biochemical journal*, 439 (1):67–77, oct 2011.

Williamson, J. a. and Miranker, A. D. Direct detection of transient a-helical states in islet amyloid polypeptide. *Protein Science*, 16:110–117, 2007.

Williamson, J. a., Loria, J. P., and Miranker, A. D. Helix stabilization precedes aqueous and bilayer-catalyzed fiber formation in islet amyloid polypeptide. *Journal of molecular biology*, 393(2):383–96, oct 2009.

Wilschut, J., Düzgüne, N., Fraley, R., and Papahadjopoulos, D. Studies on the mechanism of membrane fusion: kinetics of calcium ion induced fusion of phosphatidylserine vesicles followed by a new assay for mixing of aqueous vesicle contents. *Biochemistry*, 19(26):6011–6021, 1980.

Wiltzius, J. J. W., Sievers, S. A., Sawaya, M. R., and Eisenberg, D. Atomic structures of IAPP (amylin) fusions suggest a mechanism for fibrillation and the role of insulin in the process. *Protein science : a publication of the Protein Society*, 18(7):1521–30, jul 2009.

Wiltzius, J. J., Sievers, S. a., Sawaya, M. R., Cascio, D., Popov, D., Riekel, C., and Eisenberg, D. Atomic structure of the cross-β spine of islet amyloid polypeptide (amylin). *Protein Science*, 17(9):1467–1474, sep 2008.

Wimley, W. C. and White, S. H. Determining the membrane topology of peptides by fluorescence quenching. *Biochemistry*, 39(1):161–70, jan 2000.

Yandek, L. E., Pokorny, A., and Almeida, P. F. F. Wasp mastoparans follow the same mechanism as the cell-penetrating peptide transportan 10. *Biochemistry*, 48 (30):7342–51, aug 2009.

Yip, C. M., Darabie, A. a., and McLaurin, J. Abeta42-peptide assembly on lipid bilayers. *Journal of molecular biology*, 318(1):97–107, apr 2002.

Yonemoto, I. T., Kroon, G. J. A., Dyson, H. J., Balch, W. E., and Kelly, J. W. Amylin proprotein processing generates progressively more amyloidogenic peptides that initially sample the helical state. *Biochemistry*, 47(37):9900–10, sep 2008.

Yoon, T.-y., Okumus, B., Zhang, F., Shin, Y.-k., and Ha, T. Multiple intermediates in SNARE-induced membrane fusion. *Proceedings of the National Academy of Sciences of the United States of America*, 103(52):19731–19736, 2006.

Zeggini, E., Weedon, M. N., Lindgren, C. M., Frayling, T. M., Elliott, K. S., Lango, H., Timpson, N. J., Perry, J. R. B., Rayner, N. W., Freathy, R. M., Barrett, J. C., Shields, B., Morris, A. P., Ellard, S., Groves, C. J., Harries, L. W., Marchini,

J. L., Owen, K. R., Knight, B., Cardon, L. R., Walker, M., Hitman, G. a., Morris, A. D., Doney, A. S. F., Burton, P. R., Clayton, D. G., Craddock, N., Deloukas, P., Duncanson, A., Kwiatkowski, D. P., Ouwehand, W. H., Samani, N. J., Todd, J. A., Donnelly, P., Davison, D., Easton, D., Evans, D., Leung, H.-T., Spencer, C. C. A., Tobin, M. D., Attwood, A. P., Boorman, J. P., Cant, B., Everson, U., Hussey, J. M., Jolley, J. D., Knight, A. S., Koch, K., Meech, E., Nutland, S., Prowse, C. V., Stevens, H. E., Taylor, N. C., Walters, G. R., Walker, N. M., Watkins, N. A., Winzer, T., Jones, R. W., McArdle, W. L., Ring, S. M., Strachan, D. P., Pembrey, M., Breen, G., St. Clair, D., Caesar, S., Gordon-Smith, K., Jones, L., Fraser, C., Green, E. K., Grozeva, D., Hamshere, M. L., Holmans, P. A., Jones, I. R., Kirov, G., Moskvina, V., Nikolov, I., O'Donovan, M. C., Owen, M. J., Collier, D. A., Elkin, A., Farmer, A., Williamson, R., McGuffin, P., Young, A. H., Ferrier, I. N., Ball, S. G., Balmforth, A. J., Barrett, J. H., Bishop, D. T., Iles, M. M., Maqbool, A., Yuldasheva, N., Hall, A. S., Braund, P. S., Dixon, R. J., Mangino, M., Stevens, S., Thompson, J. R., Bredin, F., Tremelling, M., Parkes, M., Drummond, H., Lees, C. W., Nimmo, E. R., Satsangi, J., Fisher, S. A., Forbes, A., Lewis, C. M., Onnie, C. M., Prescott, N. J., Sanderson, J., Mathew, C. G., Barbour, J., Mohiuddin, M. K., Todhunter, C. E., Mansfield, J. C., Ahmad, T., Cummings, F. R., Jewell, D. P., Webster, J., Brown, M. J., Lathrop, G. M., Connell, J., Dominiczak, A., Braga Marcano, C. A., Burke, B., Dobson, R., Gungadoo, J., Lee, K. L., Munroe, P. B., Newhouse, S. J., Onipinla, A., Wallace, C., Xue, M., Caulfield, M., Farrall, M., Barton, A., Bruce, I. N., Donovan, H., Eyre, S., Gilbert, P. D., Hider, S. L., Hinks, A. M., John, S. L., Potter, C., Silman, A. J., Symmons, D. P. M., Thomson, W., Worthington, J., Dunger, D. B., Widmer, B., Newport, M., Sirugo, G., Lyons, E., Vannberg, F., Hill, A. V. S., Bradbury, L. A., Farrar, C., Pointon, J. J., Wordsworth, P., Brown, M. A., Franklyn, J. A., Heward, J. M., Simmonds, M. J., Gough, S. C. L., Seal, S., Stratton, M. R., Rahman, N., Ban, M., Goris, A., Sawcer, S. J., Compston, A., Conway, D., Jallow, M., Rockett, K. A., Bumpstead, S. J., Chaney, A., Downes, K., Ghori, M. J. R., Gwilliam, R., Hunt, S. E., Inouye, M., Keniry, A., King, E., McGinnis, R., Potter, S., Ravindrarajah, R.,

Whittaker, P., Widden, C., Withers, D., Cardin, N. J., Ferreira, T., Pereira-Gale, J., Hallgrimsdottir, I. B., Howie, B. N., Su, Z., Teo, Y. Y., Vukcevic, D., Bentley, D., Compston, A., Ouwehand, N. J., Samani, M. R., Isaacs, J. D., Morgan, A. W., Wilson, G. D., Ardern-Jones, A., Berg, J., Brady, A., Bradshaw, N., Brewer, C., Brice, G., Bullman, B., Campbell, J., Castle, B., Cetnarsryj, R., Chapman, C., Chu, C., Coates, N., Cole, T., Davidson, R., Donaldson, A., Dorkins, H., Douglas, F., Eccles, D., Eeles, R., Elmslie, F., Evans, D. G., Goff, S., Goodman, S., Goudie, D., Gray, J., Greenhalgh, L., Gregory, H., Hodgson, S. V., Homfray, T., Houlston, R. S., Izatt, L., Jackson, L., Jeffers, L., Johnson-Roffey, V., Kavalier, F., Kirk, C., Lalloo, F., Langman, C., Locke, I., Longmuir, M., Mackay, J., Magee, A., Mansour, S., Miedzybrodzka, Z., Miller, J., Morrison, P., Murday, V., Paterson, J., Pichert, G., Porteous, M., Rahman, N., Rogers, M., Rowe, S., Shanley, S., Saggar, A., Scott, G., Side, L., Snadden, L., Steel, M., Thomas, M., Thomas, S., McCarthy, M. I., and Hattersley, A. T. Replication of Genome-Wide Association Signals in UK Samples Reveals Risk Loci for Type 2 Diabetes. *Science*, 316(5829):1336–1341, jun 2007.

Zhang, S., Liu, J., MacGibbon, G., Dragunow, M., and Cooper, G. J. S. Increased expression and activation of c-Jun contributes to human amylin-induced apoptosis in pancreatic islet ??-cells. *Journal of Molecular Biology*, 324(2):271–285, 2002.

Zhao, M., Zhu, Y., Su, J., Geng, Q., Tian, X., Zhang, J., Zhou, H., Zhang, S., Wu, J., and Tian, Y. A water-soluble two-photon fluorescence chemosensor for ratiometric imaging of mitochondrial viscosity in living cells. *Journal of Materials Chemistry B*, 4(35):5907–5912, 2016.

Zhu, X., Orci, L., Carroll, R., Norrbom, C., Ravazzola, M., and Steiner, D. F. Severe block in processing of proinsulin to insulin accompanied by elevation of des-64,65 proinsulin intermediates in islets of mice lacking prohormone convertase 1/3. *Proceedings of the National Academy of Sciences of the United States of America*, 99(16):10299–304, aug 2002.

Zick, M. and Wickner, W. T. A distinct tethering step is vital for vacuole membrane fusion. *eLife*, 3:e03251, 2014.

Zimmet, P., Alberti, K. G. M. M., and Shaw, J. Global and societal implications of the diabetes epidemic. *Nature*, 414(6865):782–787, dec 2001.

Zucchi, P. C. and Zick, M. Membrane fusion catalyzed by a Rab, SNAREs, and SNARE chaperones is accompanied by enhanced permeability to small molecules and by lysis. *Molecular Biology of the Cell*, 22:4635–4646, 2011.